Everest Advances in Science and Technology (EAST) Vol. 2, No. 1, 2026
ISSN: 3102-0410 (Print), 3102-0429 (Online)
DOI: 10.3126/east.v2i1.98504

A Construction Technology Adaptations in Composite RCC–Pre-Engineered Residential Building: A Case Study from Kathmandu Valley

ADITYA SHAH[1], NITESH SHRESTHA[2*]

Abstract. The devastating earthquake that highly affected Nepal in April of 2015 raised awareness of the country's building practices and escalated the transition to a modern, resilient building system, especially in the rapidly growing housing settlements of Kathmandu. In this meantime, the efficiency and structural merit of RCC–Pre-Engineered Building (PEB) construction have drawn a lot of attention from different societies; but fewer studies and research have responded to practical on-site adaptations in urban zones. This case study focusses on a three and half story residential building of height 12 meters in total, that integrates a hybrid RCC-steel structural building. RCC beam and columns, a mid-bay PEB beam, composite slabs, integrated footings with anchor bolts, and lift pit make up the structure modern and incorporating urban amenities. The implementation of pulley-based erection techniques supported by RCC columns permitted the safe and effective lifting of heavy fabricated PEB beams after observations showed that typical crane mobilization was difficult to mobilize. These technique—pulley systems, integration of RCC and PEB members, and optimized detailing—systematically addressed site limits while withstanding structural integrity. The research focus that these methods are repeatable and context-specific, connecting theoretical design with real-world practical implementation and providing clear information about resilient building construction in countries like Nepal where developing physical infrastructure industries are growing rapidly and possible area for generating employment which leads to uplift developing economies and businesses.

Keywords: Construction technology adaptation; Composite structures; RCC–PEB integration; Erection methods; Composite slab; Urban construction

[1],[2] Everest Engineering College, Lalitpur, Nepal
E-mail: nitesh.shrestha@eemc.edu.np
* Corresponding author

Manuscript received: 12 March 2026; Revised: 16 June 2026; Accepted: 18 July 2026.

1. INTRODUCTION

The structural composition of RCC–PEB structures are growing structural preferences due to their capability to combine the stability of reinforced cement concrete (RCC) with the modular efficiency of pre engineered buildings (PEB). While design and analysis of such systems are well reviewed in literature, there is limited academic reporting on how construction technologies are executed to site constraints in practice. This research presents a case study from Kathmandu Valley, where a composite RCC–PEB building was constructed under restricted site conditions. The structure elevates to 12 m with three and a half stories, withstanding by RCC columns — 500 × 500 mm on the left side and 600 × 600 mm on the right side of building respectively— with an on-site fabricated PEB steel section in the midbay. At the top floor, 2 ISMC 300 columns were installed above the left RCC column to balance roof loads and integrate with the midbay steel structure. The foundation consists of combined RCC footings, while the superstructure integrates RCC beams, ISMB steel beams, and a composite slab of 150 mm thickness with 0.8 mm decking sheets and 13 mm shear studs as specified by design drawing and as-built drawings at site. A lift pit was also integrated within the footing level to accommodate vertical transportation systems observing need of residential building and owner's need for future provision as a part of urban amenities.

The case study draws attention to how construction technology adaptations were performed to overcome site limitations. Typical crane mobilization was less feasible, leading to the acceptance of pulley based erection methods with anchor support to RCC columns. This method confirmed safe and efficient lifting of PEB beams overcome the site limitation. Service integration was addressed through the lift pit provision, while detailing technologies such as decking sheets and shear studs ensured effective composite action between RCC and steel PEB structural members.

While focusing on this academic study, the paper rec-ords practical breakthroughs in Nepal's construction industries, demonstrating how local methods pulley systems, lift pit integration, and slab detailing con-tribute to the successful project execution of structure composition of RCC–PEB. Pre-engineered buildings are structure designed and fabricated using standard and verified material be-cause of its advantages like reduced construction time, cost efficient, lighter weight and flexibility in design than that to typical concrete structure with followed by improved sustainability compared to traditional construction approach practiced in general construction industries.

2. LITERATURE REVIEW

The structure composition of RCC–Pre Engineered Building (PEB) reflects a hybrid construction technique that combines the stability of reinforced cement concrete (RCC) with the modern and efficient design of pre engineered buildings. Concrete structure has traditionally dominated Nepal's construction industries due to material availability and familiarity but struggles in such a way as heavy and self weight followed by slower construction speed, and formwork difficulty limit its efficiency [1]. In context, PEB systems are fabricated off site and on-site and assembled quickly, offering modularity, reduced construction duration, and cost-effective options [2].

Varieties of comparative studies have spotlighted the merits of PEB structure systems. Ingole and Changhode [2] showcased faster construction cycles and reduced costs, while Parveen and Hegde [3] underlined superior strength to weight ratios using software like STAAD Pro and SAP2000. Patidar and Maru [4] reasoned that these kinds of composite structure are more reliable and sustainable compared to typical RCC structure. International works (Kalesha et al. [5]; Sharma et al. [6]; Saleem et al. [7, 8, 9]; Roopesh et al. [10]) add more force to these findings, focusing optimization of steel sections, sustainability, and proficient practices. The studies highlighting comparision (Meera [11]; Jinsha & Mathew [12]; Vishnu Sai et al. [13]; Zoad [14]; Wakchaure & Dubey [15]; Zende et al. [16]; Charkha & Sanklecha [17]) continuously focuses to reduced construction time and cost, although most are best suited for industrial contexts.

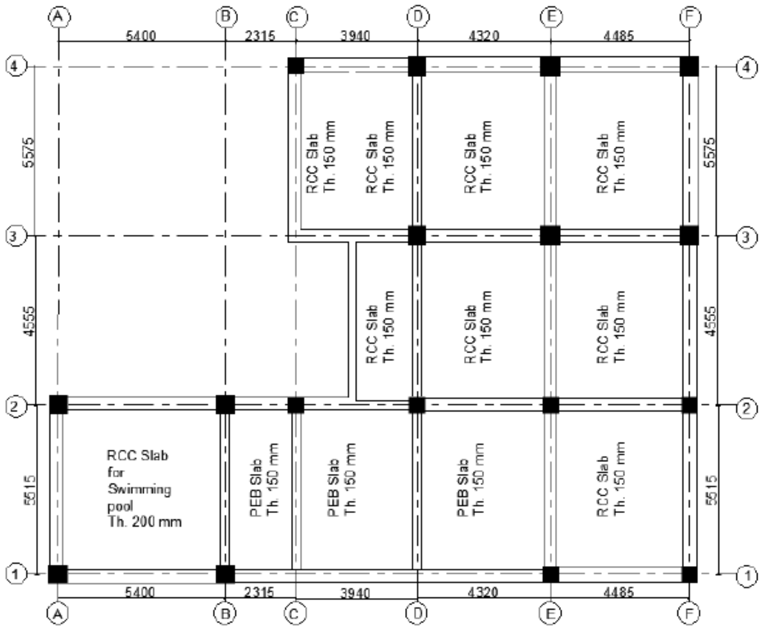

FIGURE 1. Schematic representation of the slab plan at the G+2 floor level above Columns A1, A2, and B1 where 2 ISMC sections installed as columns

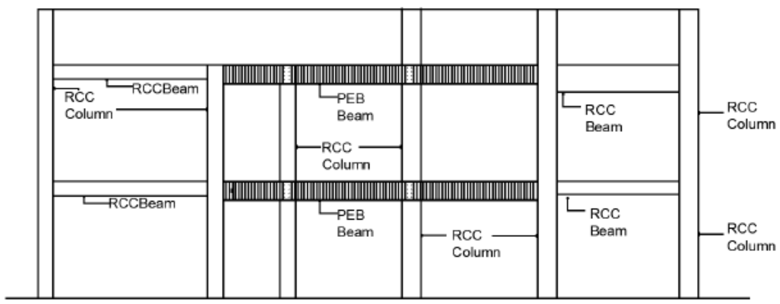

FIGURE 2. Schematic representation of structural elevation

Despite these points, most studies focus on design and analysis rather than construction technology adaptations in real world. International practice and codes emphasize mechanized erection approach such as cranes and hydraulic lifts, but these are often difficult in execution in Nepal's dense urban metropolitan cities. Local techniques, such as pulley systems, scaffolding based lifting, and modular assembly, remain under documented academically yet being impactful. Codes such as IS 456 [1], IS 800 [18, 19], IS 2062 [20], and the updated version IS 11384:2022 [21] defines the need for concrete, steel, and composite construction, while IS 14665 [22] and OSHA guidelines [23] provide safety touchstone. Thus, practical components such as decking sheet thickness or shear stud diameter are rarely accentuated in published papers and studies.

The National Building Code (NBC) of Nepal has provisions for the regulatory framework for both seismic and composite construction through NBC 105:2025 (Seismic Design of Buildings in Nepal), NBC 111:1994 (Steel) , NBC 201 (Mandatory Rules of Thumb for Reinforced Concrete Buildings with Masonry Infill), NBC 205 : 2024 (Ready-to-Use Detailing Guideline for Low-Rise Reinforced

Figure 3. Erection of PEB 600 beam section in G+1 and G+2 floor level

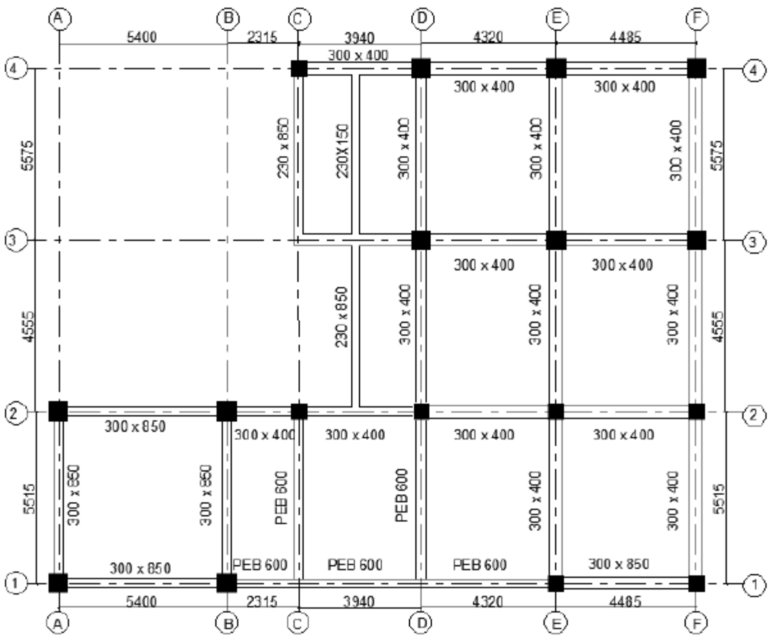

Figure 4. Schematic representation of structural beam layout plan

Concrete Buildings without Masonry Infill), and NBC 206: 2024 (Architectural Design Requirements). This code related regulatory protocol are essential for the frames for site practices, which often depends upon Indian Standards such asthe IS 875 series [24, 25, 26] and IS 1893:2016 [27]. In general, revising references from IS 11384:1985 to IS 11384:2022 is highly relevant for composite slab design in both structural engineering and construction engineering and management. Also, international references books, including MBMA (2006) [28] and Zamil Steel (1999) [29], provide insightful knowledge for the design and execution plan of pre-engineered building structures.

Current Nepalese studies cater essential context for the structures which are composed of RCC–PEB construction buildings in Kathmandu Valley. Shrestha et al. (2019) [30] and Khadka, Motra, G.B., et al. (2022) [31], examined seismic performance and hybrid RCC–steel building systems, underlining NBC 105 and NBC 201 observance. Shrestha & Shrestha (2024) [32], also with Motra, focused studies in construction technology in constrained urban sites which is more related to current Kathmandu valley, directly applicable to pulley based erection methods. K.C., Motra, G.B., et al. (2019) [33] and Shrestha, Motra, G.B., et al. (2024) [34], recorded behavior of composite slab and reconstruction practices executed post earthquake, reflecting hybrid structure like RCC–PEB adopted in residential contexts to equilibrium speed and resilience. International case studies also encourage the role of bracing in steel frame structures. Adithya et al. (2015) [35] explains that single diagonal bracing systems are more efficient than other setups in reducing bending moments and shear forces in columns of high rise steel frame buildings. Similarly, Suwal et al. (2022) [36] showed that bracing positions significantly affect story drift and base shear in Nepalese steel buildings, reinforcing the importance of arrangements for bracing strategies within regulatory framework design for seismic activities.

Prevailing literature confirms the superiority of composite RCC–PEB structures in regards of efficiency, sustainability, and seismic performance. However, there is a research gap in construction technology documentation — specifically in context of developing countries like Nepal in specific — where pulley systems, lift pit provisions, slab detailing, and bracing strategies are judgmental adjustment. By situating site observations and difficulties within the framework of updated codes (NBC 105, NBC 111, NBC 201, NBC 205, NBC 206, IS 11384:2022) and fresh Nepalese research studies (Suwal et al. [36]; Shrestha et al. [30]; Khadka et al. [31]; Shrestha & Shrestha [32]; K.C. et al. [33]; Shrestha et al. [34]), this research addresses that gap through a case study from urban sites located within Kathmandu Valley, thereby contributing both for academic oration and practical assistance for construction and design industries of Nepal.
Institutional contribution led by the National Society for Earthquake Technology–Nepal (NSET) have recorded code compliance and retrofitting practices executed in various location of Nepal. NSET publications, including the Building Permit Process Resource Book and Building Code Implementation Success Stories [37], underlies the municipal enforcement of NBC provisions and practical execution of retrofitting strategies for concrete and pre engineered buildings. These works go with academic studies by situating hybrid structure composed of concrete and steel within broader resilience agenda of Nepal particularly focusing in post earthquake reconstruction practices. The rational work by Bhatt et al. [38] estimated concrete, steel, and structure composited of both using ETABS under NBC 105:2020. Their study found that hybrid frames achieved 17% lower base shear than RCC, intermediate drift and displacement values, and superior pushover performance with no hinges formed at performance point. The hybrid system balanced rigidity at the base with ductility at upper levels, making it a practical, efficient, and resilient key for staged mid rise construction in context of seismic zone of Nepal.

3. SCOPE

There are several published research articles but limited are published on construction technology for composite structure of RCC and PEB. This paper hold opportunity to document the construction technology adaptation in structure composed of RCC and steel PEB in mid-rise and post-earthquake reconstruction activities, it also ensures standard code compliance ensuring safety and integrating Nepal specific literature review.

4. LIMITATION

This document is limited to simple arithmetic calculation and does not constitute any kind of structural modeling or analysis. Although, all construction activities were performed as per design

FIGURE 5. Erection of 2 ISMC column (toe to toe connection)

structural drawing. Therefore, the paper is composed as qualitative field documentation which enable to represent construction technology with clearly stated scope limitations.

5. METHODOLOGY

This research was conducted on a composite RCC–Pre Engineered Building (PEB) located in Kathmandu Valley. The structure has a total height of 12 m and consists of three and a half stories. The site was selected due to its constrained urban setting, where typical crane deployment was prohibited. This provided an opportunity to document construction technology adaptations, specifically pulley based erection, lift pit provision, and composite slab detailing.

Connection details were prepared with all dimensions expressed in millimeters (mm) unless otherwise specified. The building is located on plain terrain with an overall slope of less than 3°, though a local terrain height difference of approximately 3600 mm was observed across the site. The total ground coverage of the building is 383 m^2. Two types of flooring systems were adopted:

- Steel deck composite slab supported by steel PEB girders.
- RCC slab supported by RCC beams.

These deviations reflect the integration of RCC and PEB systems to optimize construction under site constraints.

5.1. **Structural Description.** The composite structure of RCC–PEB building was designed with RCC columns on either side and PEB sections in the midbay, with further adaptation at the top floor:

- **Left Side:** RCC columns of sizes 500 × 500 mm cross section.
- **Right Side:** RCC columns of sizes 600 × 600 mm cross section.
- **Midbay:** PEB steel sections fabricated from IS 2062 E250 grade steel of sizes 400 and 600 mm along with ISMB beam 150, 200 and 250 as per design requirement.
- **Top Floor components:** 2 ISMC 300 built-up columns above the left RCC column installed to support roof loads and provide scalable consistency.

FIGURE 6. Case study methodology flowchart for pulley-assisted PEB erection in constrained sites

This setup showcases a composite structural system where RCC provides stability and anchorage at the edges, while PEB sections confirms modularity and reduced erection time in the midbay section.

5.2. **Construction Technology Observed.**

- **Pulley System:** Manual chain pulley was harnessed for beam erection. Each pulley had a rated breaking load of 3000 kg, with observed field capacity of 2300 kg at site during erection phase.
- **Anchorage system:** RCC columns provided stable fastening points for pulley installation.
- **Sequence:** Beams were lifted floor by floor, with pulleys fixed at beam ends and midbay.
- **Adaptation setup:** The pulley system was selected due to site constraints that prohibited crane mobilization.

Observed Parameters:

- Beam length: 6.0 m
- Beam weight: 850 kg
- Number of pulleys used: 3
- Load per pulley: 283 kg
- Breaking load per pulley: 3000 kg
- Safety Factor: 10.6
- Efficiency: 76.7%

5.3. **Analytical and Regulatory Framework.** The analytical and regulatory framework adopted in this study was intentionally limited to field based calculations, documented from direct site observation. The primary parameters considered were load distribution across pulleys, safety factor, and efficiency ratio. These were calculated using simple arithmetic relationships based on observed beam weights, pulley capacities, and erection sequences:

$$\text{Efficiency}(\%) = \frac{\text{Observed Field Capacity}}{\text{Rated Capacity}} \times 100$$

This setup showcases the execution of construction drawings by site engineers as per structural drawings. While structural modeling under NBC 105:2025 and IS 1893:2016 would provide deeper analysis, such modeling was not feasible due to confidentiality of design data and resource limitations. The study therefore does not claim to provide full design verification; instead, it records construction technology adaptations in urban sites where mechanized erection was inaccessible or limited for mobilization during execution phase.

The physical cross-sections of the existing RCC column heads were measured and documented to examine their capacity to anchor the lightweight extension, aligning with the structural ideology of National building code (NBC) issued by Nepal for construction practices.

FIGURE 7. PEB Beam connection to RCC column in G+1 and G+2 floor

Steel-to-RCC Column Connection Detailing: The dimensions, spacing, edge distances, and anchor bolt setup securing the 2 ISMC 300 vertical elements to the concrete column heads were recorded. These physical adaptations were analyzed using the limit state design principles of IS 800:2007 in regards of safety concerns.

Composite Floor Geometry: The thickness of the composite slab (150 mm), the profile of the 0.8 mm steel deck sheets, and the layout of the 13 mm diameter shear studs were executed as per as-built drawings.

The observational findings are interpreted within the benchmark of updated codes— NBC 105:2025 (Seismic Design of Buildings in Nepal), NBC 201 (Mandatory Rules of Thumb for Reinforced Concrete Buildings with Masonry Infill), NBC 205 : 2024 (Ready-to-Use Detailing Guideline for Low-Rise Reinforced Concrete Buildings without Masonry Infill), NBC 206: 2024 (Architectural Design Requirements ,IS 11384:2022 (Composite Construction in Structural Steel and Concrete – Code of Practice, First Revision), and S 1893 (Part 1):2016 (Criteria for Earthquake Resistant Design of Structures – Part 1: General Provisions, Sixth Revision) .This alignment demonstrates

awareness of requirements defined by building construction code while specifying the limits between documentation and design for execution.
During the lifting procedure, structural liability relating to localized web buckling and web crippling at concentrated load zones were recorded. To mitigate this risk without altering the primary member configurations, transverse plate stiffeners (10 mm thickness, spaced at 300 mm c/c) were introduced at critical hoisting hooks and bearing connections. This field-driven adaptation was verified post-execution using the detailing criteria of IS 800:2007.
Ethical compliance was maintained throughout the study. The confidentiality of project drawings, technical documents, and ownership information was strictly preserved. No conflicts of interest were identified or declared by the author. Furthermore, the field notes, site observations, and supporting diagrams used in the study are available upon reasonable request, subject to confidentiality requirements and project authorization.

Table 1. General Architectural Description

Attributes	**Specification**
Type of Building	Residential
Number of floors	3.5
Building Height	12 m
Terrain	Plain terrain (slope $< 3°$)
Ground Coverage	383 sq. m
Floor System Types	1. Steel deck composite slab supported by steel PEB girders 2. RCC slab supported by RCC beams
Service Provision	RCC lift pit for vertical transportation
Foundation Type	Combined footing supported by RCC piles as a deep foundation system

Table 2. General Structural Description

Attributes	**Specification**
Structural System	Composite RCC–PEB hybrid frame
Column Sizes	500 × 500 mm, 600 × 600 mm (with 2 ISMC 300 Built-up columns above at top floor)
RCC Beam Sizes	350 × 400 mm and 300 × 400 mm
Steel Beam	ISMB 150, ISMB 200 and ISMB 250
PEB Beam Sizes	400 mm and 600 mm
Stiffener Sizes	10 mm TH. Stiffening sizes 300 c/c
Base Plate Size	500 × 500 × 20 mm PLATE

5.4. **Data Collection.**

- **Direct Observation:** Measurements of structural components, pulley loads, and lifting heights were recorded during the site execution phase.
- **Permits and Safety Records:** Lifting permits and safety checklists were examined to verify compliance with safety protocols.
- **Documentation Approach:** Due to confidentiality restrictions, original design drawings were not produced. Instead, tabular summaries and schematic drawings have been used to illustrate the construction technology.

The study evaluated the safety margins, losses recorded during efficiency evaluation, and the possibility of pulley-based erection methods as a sustainable application in the construction industry.

TABLE 3. Data of Structural Elements

Element	Material Properties	Rebar Properties
RCC Columns & Beams	M25 grade concrete	Fe 500 D reinforcement steel
PEB Steel Sections	IS 2062 E250 grade steel	–
Composite Slab	150 mm slab with 0.8 mm decking sheet	13 mm shear studs (for composite action)
RCC Slab	150 mm RCC slab supported by RCC beams	Fe 500 D reinforcement steel
Foundation	Combined footing supported by concrete piles as a deep foundation system	Fe 500 D reinforcement steel

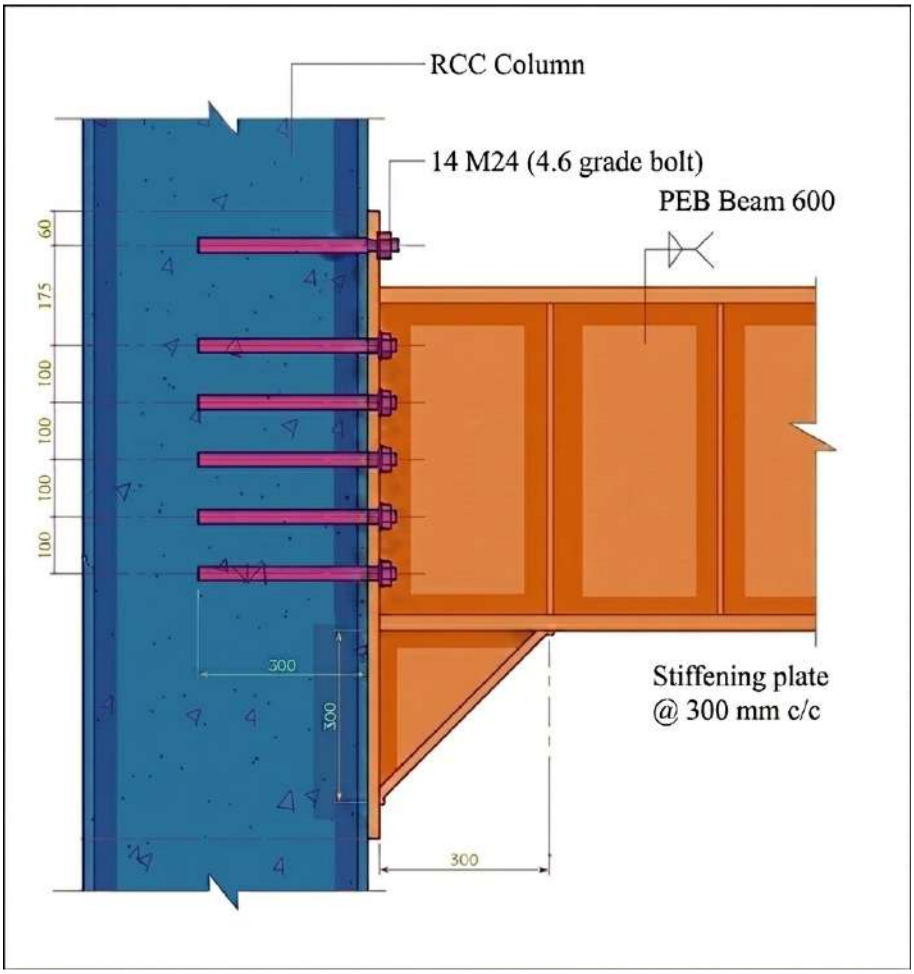

FIGURE 8. Schematic representation of RCC column–PEB beam connection

A stiffener is a secondary plate or member welded or bolted to the main structural element (such as a beam web or flange) to prevent local buckling, distribute stresses, and enhance rigidity at concentrated load points.

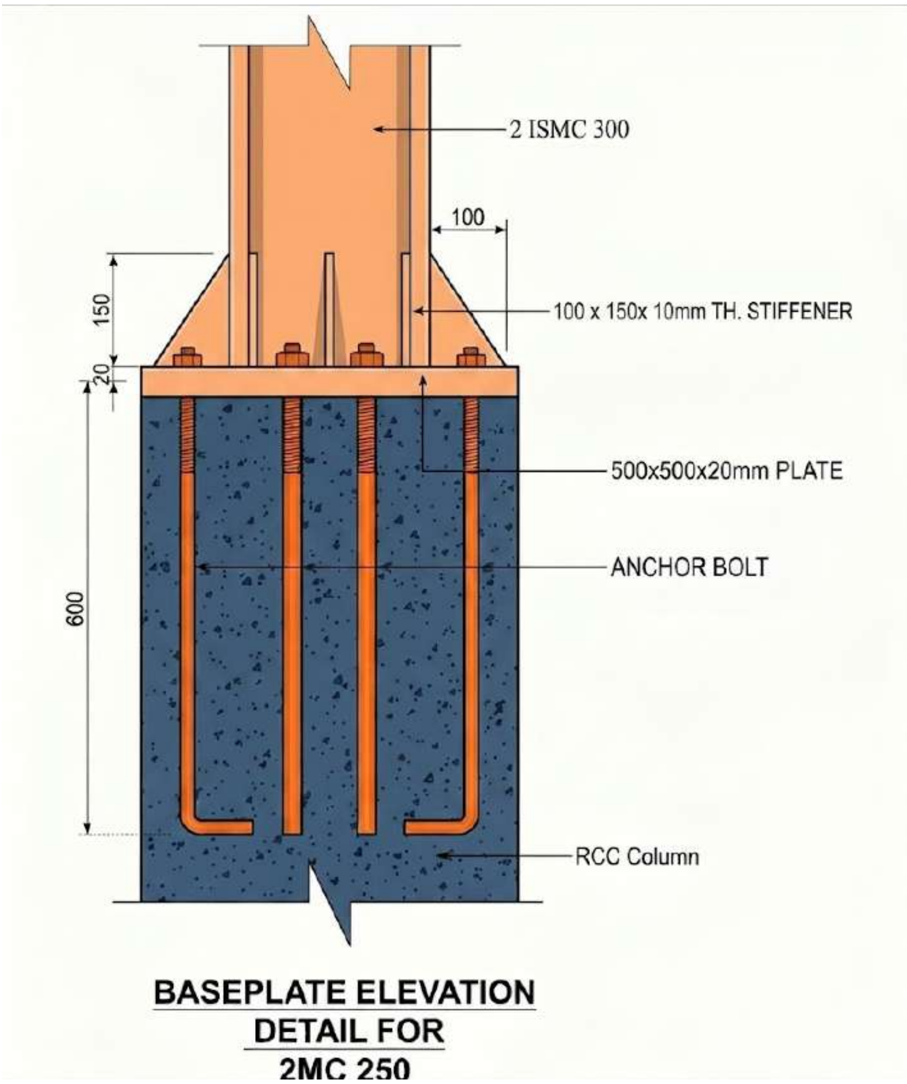

FIGURE 9. Schematic representation of RCC–2 ISMC built-up column connection detail

Web buckling is a structural failure mode in which the thin vertical portion (web) of a beam deforms or collapses under concentrated loads or reactions. It occurs when the web thickness is insufficient to resist compressive stresses and is commonly mitigated using stiffeners.

6. FINDINGS

This paper concentrates on the construction technology of structural systems composed of RCC–PEB structures where pulley-based erection applications are implemented in the Kathmandu Valley, where typical crane deployment is limited.

The following findings were derived from site observations, activity logs, and analytical calculations:

6.1. **Load Distribution.** A PEB beam weighing 850 kg was lifted using three pulleys. The load distribution per pulley was evaluated as:

$$\text{Load Per Pulley} = \frac{\text{Total Member Weight}}{\text{Number of Pulleys}}$$

For a PEB 600 beam of length 6 m, with a calculated weight of 850 kg and three pulleys:

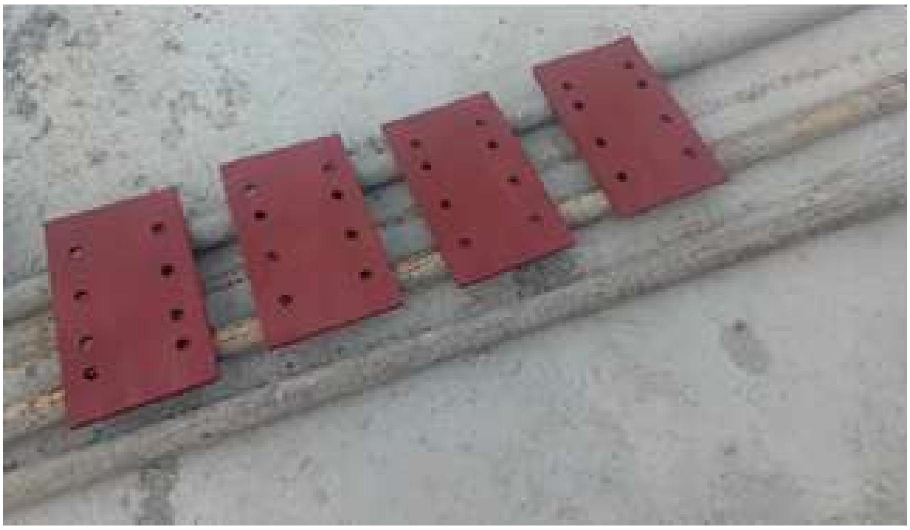

FIGURE 10. Base plate prepared for installation as per structural design and as-built drawings

$$\text{Load Per Pulley} = \frac{850}{3} = 283 \text{ kg}$$

This distribution ensured that considerable loads were transferred across each pulley system installed for erection.

6.2. **Safety Factor.** Each pulley had a rated breaking load capacity of 3000 kg. The safety factor was determined by comparing the breaking load capacity of the pulley with the applied load:

$$\text{Safety Factor} = \frac{\text{Manufacturer's Rated Breaking Load}}{\text{Applied Load per Pulley}}$$

Given:

$$\text{Manufacturer's Rated Breaking Load} = 3000 \text{ kg}$$

$$\text{Applied Load per Pulley} = 283 \text{ kg}$$

$$\text{Safety Factor} = \frac{3000}{283} = 10.6$$

This value exceeds the recommended safety margin of 4–6, demonstrating that the pulley system provided a high level of reliability under site conditions for rigging equipment used in the erection of fabricated PEB beams.

6.3. **Efficiency Ratio.** The observed field capacity of the pulley system was 2300 kg compared with the rated capacity of 3000 kg.
The efficiency ratio was calculated as:

$$\text{Efficiency}(\%) = \frac{\text{Observed Field Capacity}}{\text{Rated Capacity}} \times 100$$

Substituting the values:

$$\text{Efficiency}(\%) = \frac{2300}{3000} \times 100$$

$$\text{Efficiency} = 76.7\%$$

FIGURE 11. Installation of base plate prior to PEB beam installation

The reduction in efficiency was attributed to worker fatigue, project coordination challenges, and site limitations related to resources and time scheduling.
The actual field capacity refers to the load-carrying capacity of a structural component observed under real site conditions. It accounts for installation practices, material tolerances, and environmental influences, and is often lower than the rated design capacity.
The rated field capacity is the theoretical maximum load-carrying ability of a structural component as specified by design standards and manufacturer data. It is calculated under ideal conditions and serves as the benchmark for performance comparison.

7. DISCUSSION

This study highlights how construction technology adaptations enable composite structures to be executed effectively in urban sites with limited resources for crane deployment. Conventional crane deployment, though efficient, was impractical in most parts of the Kathmandu Valley due to narrow access, site restrictions, and insufficient road bearing capacity for the mobility of heavy vehicles.
The adoption of pulley-based erection facilities provides a safe, low-cost, and adaptable alternative, demonstrating how construction technology can be adjusted to local site conditions.
The pulley system achieved a safety factor of 10.6, far exceeding the recommended margins in construction and structural engineering practice, confirming its reliability for beam erection. Although efficiency was reduced to 76.7% of rated capacity, this was primarily attributed to worker fatigue and coordination challenges rather than inherent limitations of the technology.
With standardized procedures and improved training, pulley systems can deliver both safety and efficiency, making them a reliable construction technology for project execution in urban sites similar to the Kathmandu Valley where crane deployment is limited during the construction phase.
Beyond erection methods, construction technology adaptations also extend to service integration.
The provision of a lift pit within the foundation demonstrates foresight in accommodating vertical transportation systems and modern building facilities. This provision ensures functional compatibility with contemporary building requirements, reflecting how construction technology must balance structural and service requirements in composite structures.

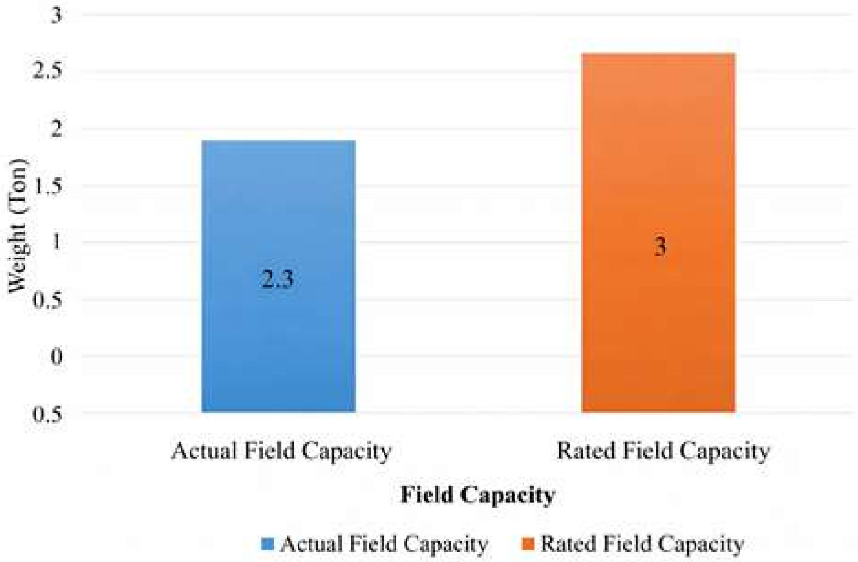

FIGURE 12. Comparison of rated versus actual pulley capacity showing efficiency gap

The integration of structural components such as shear studs and steel decking sheets with concrete slabs contributes to the overall structural integrity of composite steel structures.

8. RECOMMENDATIONS

This paper recommends that future studies expand beyond arithmetic calculations by incorporating structural modelling and analysis to evaluate bending moment, shear force, deflection, and other relevant structural parameters. Further research should examine code compliance of composite structural connections and apply finite element modelling techniques for hybrid structural systems. The study also proposes the development of standardized procedures for pulley-based erection methods through regulatory bodies and industrial partnerships. Conventional crane systems should be deployed wherever feasible to improve construction efficiency.

9. CONCLUSION

This study presents a unique construction technology executed through a structural system composed of concrete and steel PEB elements, demonstrating distinctive design approaches in residential buildings while highlighting advantages in terms of cost, time, and construction execution. The integration of concrete structures with steel components such as PEB beams, ISMB beams, and 2ISMC built-up columns demonstrates the potential of hybrid structural systems. This study documents field execution and design implementation, showing that resilient and efficient construction practices can emerge from site-specific adaptations. The study provides academic researchers with evidence of evolving construction technologies and offers guidance to practitioners seeking to balance structural integrity, resource limitations, and construction feasibility. Therefore, this case study highlights the importance of recording and analysing real-world construction practices to strengthen academic research and professional practices in construction activities.

Acknowledgement. The author gratefully acknowledges the cooperation of the site construction team and contractor, who provided access to lifting registers and observational data during the erection of Pre-Engineered Building beams and steel structures. Their assistance in documenting field data and observations enabled the preparation of this case study on construction technology applications for urban sites with limited access for crane deployment.

References

[1] Bureau of Indian Standards, "IS 456: Code of Practice for Plain and Reinforced Concrete," Bureau of Indian Standards, New Delhi, Tech. Rep., 2000.

[2] P. Ingole and S. Changhode, "Comparative structural analysis of pre engineered buildings and conventional steel structures," *International Journal of Engineering Research and Technology*, vol. 11, no. 5, pp. 45–52, 2022.

[3] S. Parveen and R. Hegde, "Numerical evaluation of pre engineered building systems using staad pro and sap2000," *Journal of Structural Engineering Technology*, vol. 8, no. 3, pp. 112–120, 2021.

[4] R. Patidar and S. Maru, "Sustainability and performance of composite rcc–steel structures: A comparative review," *International Journal of Civil Engineering Research*, vol. 12, no. 2, pp. 89–97, 2023.

[5] S. Kalesha, B. Ratnamala Reddy, and D. C. K. Jagarapu, "An analytical study on pre engineered buildings using staad pro," in *Materials Today: Proceedings*. Elsevier, 2020.

[6] L. Sharma, N. Taak, and P. K. Mishra, "A comparative study between pre engineered structures and conventional structures using staadpro," *Materials Today: Proceedings*, vol. 45, pp. 3469–3475, 2021.

[7] M. Saleem, N. Khurram, H. Qureshi, Z. Kazmi, and Z. Siddiqui, "Optimization of flange and web slenderness for pre engineered built up steel sections," 2018.

[8] M. Saleem and H. Qureshi, "Design solutions for sustainable construction of pre engineered steel buildings," *Sustainability*, vol. 10, no. 1761, 2018.

[9] M. Saleem, Z. Siddiqi, and H. Qureshi, "Minimum weight design of pre engineered steel structures using built up sections and cold formed sections," in *Advanced Materials Research*, vol. 684, 2013, pp. 125–129.

[10] N. Roopesh, K. Swamy, and B. Das, "Pre engineered building design of gas insulated substation housed under pressurized ventilation," in *Lecture Notes in Civil Engineering*. Springer, 2021, vol. 105.

[11] C. Meera, "Pre engineered building design of an industrial warehouse," *International Journal of Engineering Science and Emerging Technologies*, vol. 5, no. 2, pp. 75–82, 2013.

[12] M. Jinsha and L. Mathew, "Analysis of pre engineered buildings," *International Journal of Science and Research*, vol. 5, no. 7, 2016.

[13] V. Vishnu Sai, P. Poluraju, and B. Venkat Rao, "Structural performance of pre engineered building: A comparative study," in *IOP Conference Series: Materials Science and Engineering*, vol. 1197, 2021.

[14] D. Zoad, "Evaluation of pre engineering structure design by is 800 as against aisc," *International Journal of Engineering Research and Technology*, vol. 1, no. 5, 2012.

[15] S. Wakchaure and N. Dubey, "Design and comparative study of pre engineered building," *International Journal of Engineering Development and Research*, vol. 4, no. 2, 2016.

[16] A. Zende, A. Kulkarni, and A. Hutagi, "Comparative study of analysis and design of pre engineered buildings and conventional frames," *IOSR Journal of Mechanical and Civil Engineering*, vol. 5, no. 1, 2013.

[17] S. Charkha and L. Sanklecha, "Economizing steel building using pre engineered steel sections," *International Journal of Research in Civil Engineering, Architecture and Design*, vol. 2, no. 2, 2014.

[18] Bureau of Indian Standards, "IS 800: General Construction in Steel – Code of Practice," Bureau of Indian Standards, New Delhi, Tech. Rep., 2007.

[19] ——, "IS 800: General Construction in Steel – Code of Practice," Bureau of Indian Standards, New Delhi, Tech. Rep., 2007.

[20] ——, "IS 2062: Specification for Structural Steel," Bureau of Indian Standards, New Delhi, Tech. Rep., 2011.

[21] ——, "IS 11384: Code of Practice for Composite Construction in Structural Steel and Concrete," Bureau of Indian Standards, New Delhi, Tech. Rep., 2022, first Revision.

[22] ——, "IS 14665: Safety Code for Lift Installation," Bureau of Indian Standards, New Delhi, Tech. Rep., 2000.

[23] Occupational Safety and Health Administration, "Guidelines for Safe Use of Lifting Equipment," U.S. Department of Labor, Washington, DC, Tech. Rep., 2019.

[24] Bureau of Indian Standards, "IS 875 (Part 1): Code of Practice for Design Loads (Other than Earthquake) – Dead Loads," Bureau of Indian Standards, New Delhi, Tech. Rep., 2015.

[25] ——, "IS 875 (Part 2): Code of Practice for Design Loads (Other than Earthquake) – Live Loads," Bureau of Indian Standards, New Delhi, Tech. Rep., 2015.

[26] ——, "IS 875 (Part 3): Code of Practice for Design Loads (Other than Earthquake) – Wind Loads," Bureau of Indian Standards, New Delhi, Tech. Rep., 2015.

[27] ——, "IS 1893 (Part 1): Criteria for Earthquake Resistant Design of Structures," Bureau of Indian Standards, New Delhi, Tech. Rep., 2016.

[28] Metal Building Manufacturers Association, *Metal Building Systems Manual*, Metal Building Manufacturers Association, Cleveland, Ohio, USA, 2006.

[29] Zamil Steel, *ZST Manual: Pre Engineered Buildings Division*, Zamil Steel, Saudi Arabia, 1999.

[30] N. Shrestha, G. Motra *et al.*, "Seismic performance of composite frames in kathmandu valley," in *Proceedings of IOE Graduate Conference*, 2019.

[31] R. Khadka, G. Motra *et al.*, "Hybrid rcc–steel systems for mid rise buildings in nepal," in *Proceedings of IOE Graduate Conference*, 2022.

[32] S. Shrestha, N. Shrestha, and G. Motra, "Construction technology adaptations in constrained urban sites," in *Proceedings of IOE Graduate Conference*, 2024.

[33] B. K.C., G. Motra *et al.*, “Composite slab behavior under seismic loads,” in *Proceedings of IOE Graduate Conference*, 2019.

[34] N. Shrestha, G. Motra *et al.*, “Post earthquake reconstruction practices in rcc–peb hybrids,” in *Proceedings of IOE Graduate Conference*, 2024.

[35] M. Adithya, K. Swathi Rani, H. Shruthi, and B. Ramesh, “Study on effective bracing systems for high rise steel structures,” *International Journal of Engineering Research and Applications (IJERA)*, vol. 5, no. 3, pp. 05–09, 2015.

[36] R. Suwal, P. Dahal, and P. Shrestha, “Comparative analysis of steel buildings with and without bracings in nepal,” *Journal of Structural Technology*, vol. 7, no. 3, pp. 33–43, 2022.

[37] National Society for Earthquake Technology–Nepal (NSET), “Building code implementation success stories and building permit process resource book,” National Society for Earthquake Technology–Nepal (NSET), Kathmandu, Tech. Rep., 2022.

[38] L. Bhatt, G. Kunwar, M. Ojha, M. Chaulagain, N. Koirala, O. Rijal, and P. Poudel, “Performance assessment of rcc–steel hybrid structure,” *Journal of Engineering Issues and Solutions*, vol. 4, no. 1, pp. 56–66, 2025.

Everest Advances in Science and Technology (EAST) Vol. 2, No. 1, 2026
ISSN: 3102-0410 (Print), 3102-0429 (Online)
DOI: 10.3126/east.v2i1.98628

Estimation of Suspended Sediment Load and Spatial Distribution of Sediment Yield in the Marsyangdi River Basin, Nepal

SADIKSHYA GHIMIRE[1]*, RAM KRISHNA REGMI[2]

Abstract. Himalayan river basins are characterized by exceptionally high sediment loads driven by active tectonics, glacial influence, steep terrain, and intense monsoon precipitation, yet quantitative estimates of spatially distributed sediment generation remain scarce in Nepal. This gap constrains the sustainable planning and operation of run-of-river hydropower projects, where excessive sediment loads increase turbine abrasion, maintenance costs, and production losses. This study applied the Soil and Water Assessment Tool (SWAT) to estimate sediment yield and sediment concentration in the Marsyangdi River Basin, Nepal, a 2,944 km^2 glaciated tributary of the Gandaki River system hosting three operational run-of-river hydropower stations with a combined installed capacity of 189 MW. The model was calibrated for 2012–2014 and validated for 2015, reproducing streamflow with very good performance (NSE = 0.864, R^2 = 0.874 in calibration; NSE = 0.830, R^2 = 0.867 in validation) and sediment load with satisfactory performance (NSE = 0.556, R^2 = 0.608 in calibration; NSE = 0.516, R^2 = 0.617 in validation). Simulation for 2012–2024 indicated that about 89% of total basin sediment generation originates from five southern sub-basins characterized by higher orographic precipitation, whereas northern rain-shadow sub-basins contribute only marginally. Average annual sediment export at the basin outlet was estimated at 9.42 Mt/yr, with mean sediment concentration of 1,385 mg/L. About 73% of the annual sediment load occurred during the monsoon months, with concentrations exceeding the 1,500 ppm operational threshold on 95 days a year, highlighting a distinct period of elevated hydropower operational risk and the need for targeted monitoring and watershed management.

Keywords: Hydropower, Marsyangdi River Basin, Monsoon, Nepal, Sediment Concentration, Sediment Yield, Soil and Water Assessment Tool, Watershed Management

[1], [2] Institute of Engineering, Pulchowk Campus, Lalitpur, Nepal
E-mail: 080mshpe015.sadikshya@pcampus.edu.np
* Corresponding author

Manuscript received: 16 March 2026; Revised: 10 June 2026; Accepted: 15 July 2026.

1. INTRODUCTION

Sediment transport is a distinguishing hydrologic and geomorphic feature of the Himalayan rivers. In Nepal, high sediment yield occurs due to the effect of active tectonics, steep topography, strong seasonality of monsoonal precipitation, and frequent slope failures. Moreover, orographic gradients enhance rainfall and erosion processes within short spatial extents. These factors make sediment load generation very variable in space and time. As a consequence, basins in Nepal possess among the highest sediment contents in fluvial channels all over the world [1, 2].

This sedimentation process is not only an important geomorphologic factor but also a serious problem for infrastructure development. Sediment affects river geomorphology, storage capacity, and ecological balance, hydropower stations are affected by abrasion of turbines, clogging of waterways, increased need for maintenance, and decreased efficiency. These problems become especially acute for the run-of-river hydropower plants, because in this type of plants sediment-rich water passes through diversion structures and turbine during the monsoon period [3]. Therefore, reliable estimation of sedimentation becomes crucial for hydropower development in mountainous regions, like central Nepal.

However, quantification of sediment load in Himalayan catchments is difficult task due to a lack of continuous measurements and seasonal hysteresis in sediment concentration relative to streamflow. It means that sediments cannot be evaluated based on streamflow due to the modulation of the runoff partitioning, hillslope contributions, and seasonal storage-release processes [4]. It results in deficiency of basin scale assessments of sediment generation and sediment sources in Nepal despite the urgency of these problems [5].

Hydrologic process-based modeling can become a good solution to these problems. Several modeling tools are available; however, Soil and Water Assessment Tool (SWAT) becomes widely used for modeling watersheds hydrology, sediment dynamics, and the effect of land management practices. This physically based semi-distributed model incorporates the heterogeneity of the basin through sub-basins and hydrologic response units, and becomes very suitable for basin-scale modeling [6, 7]. Some previous researches showed that SWAT gives good estimations of hydrological variables in Himalayan and Nepalese catchments. Also, it was proved that the model is applicable for the sediment source identification without extensive field data [8].

Marsyangdi River Basin becomes a good object for such a study because this catchment includes 2,944 km^2 glaciated basin and is a part of the Gandaki River system. The upper Marsyangdi River supports three operational run-of-river hydropower stations: Upper Marsyangdi A, Middle Marsyangdi, and Marsyangdi with total installed capacity of 189 MW. The sediment affects not only downstream hydropower performance but also the upstream landscape processes. Thus, a spatially explicit estimate of sediment generation is important in this basin.

The present study applies SWAT to the Marsyangdi River Basin: (1) To estimate sediment load and sediment concentration, (2) To identify the dominant sediment-contributing sub-basins and (3) To provide a basin-scale sediment framework relevant to watershed management and hydropower sustainability.

2. STUDY AREA

Marsyangdi River Basin, shown in Fig. 1, is a major tributary of the Gandaki River system. It is located in central Nepal and it forms an important hydropower potential catchment of Nepal. For the study, the basin was delineated with outlet point at the Bhakundebesi gauging station (Station 439.35), giving a catchment area of 2,943.36 km^2. The basin shows a strong topographic and climatic variability as the elevation extends from 718 m to 7,925 m above sea level. The Marsyangdi

River originates from the confluence of the Jharsang Khola and Khangsar Khola above 3,600 m northwest of the Annapurna range and flows for about 150 km before joining the Trishuli River at Mugling. Therefore, the basin provides a suitable setting for investigating hydrological and sediment dynamics in a monsoon-influenced Himalayan catchment.

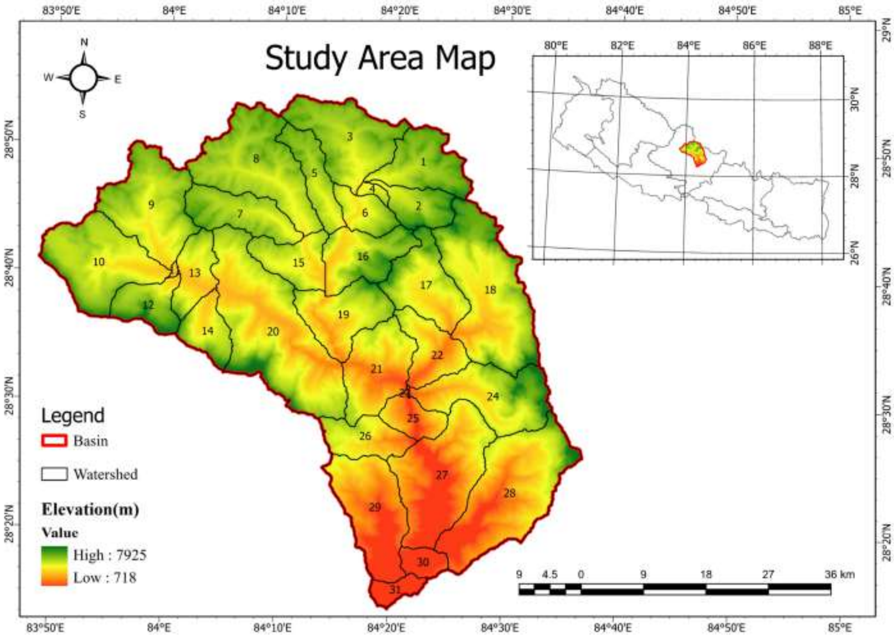

FIGURE 1. Study area map of Marsyangdi River Basin.

3. MATERIALS AND METHODS

3.1. DATA SOURCES AND PREPARATION.

3.1.1. *TOPOGRAPHIC DATA.* The Digital Elevation Model (DEM) data used in this study was obtained from the Shuttle Radar Topography Mission (SRTM) with resolution of 30 m. It provides a detailed representation of the terrain and allows for thorough hydrological modeling.

3.1.2. *LAND USE AND LAND COVER DATA.* Land use and land cover (LULC) data were obtained from the ICIMOD 2010 land cover map of Nepal. Fig. 2 represents the major land cover types of the Marsyangdi catchment and provides the spatial basis for representing vegetation cover, agricultural land, barren surfaces, snow/glacier areas, and water bodies in the model. Table I summarizes the corresponding distribution of land use classes in terms of area and percentage. LULC was used to define SWAT land cover classes for Hydrological Response Unit (HRU) generation.

3.1.3. *SOIL DATA.* Soil information was obtained from the Soil and Terrain Database (SOTER) for Nepal (Fig. 3), available through the ISRIC data hub. It was used to assign the soil physical properties required for SWAT simulation. The Marsyangdi catchment contains seven major soil groups. Gelic Leptosols occupies the largest share of the basin, indicating widespread shallow and weakly developed mountain soils typical of steep high-altitude terrain. Table II summarizes the distribution of the major soil categories in terms of area and percentage.

TABLE 1. Land use distribution in the Marsyangdi River Basin

Land use	Code	Area (km^2)	% of Area
Forest	FRST	438.343	14.892
Shrubland	SHRB	133.4868	4.535
Grassland	GRAS	683.4466	23.219
Agricultural Land	AGRL	42.0917	1.43
Barren Land	BARR	487.9701	16.578
Waterbodies	WATB	13.8637	0.471
Snow / Glacier	ICES	1142.5117	38.815
Urban Area	URBN	1.76608	0.06

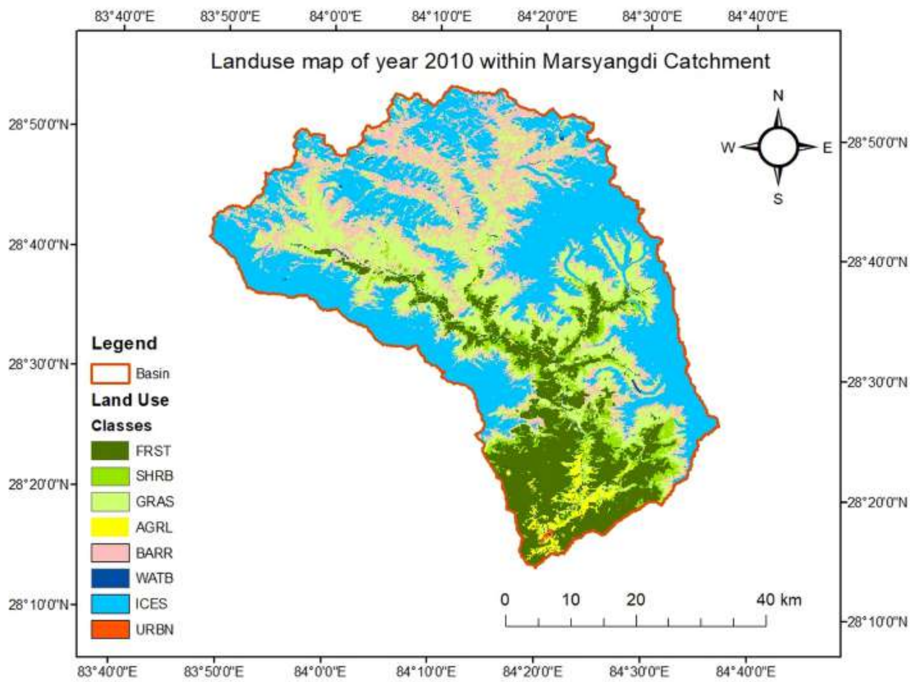

FIGURE 2. Land Use and Land Cover map of Marsyangdi Basin.

TABLE 2. Distribution of soil type in the Marsyangdi Catchment

Soil Type	Area (km^2)	Area (%)
Eutric REGOSOLS	340.97	11.584
Gelic LEPTOSOLS	2093.84	71.135
GLACIER	29.99	1.019
Humic CAMBISOLS	407.34	13.839
Eutric CAMBISOLS	49.36	1.677
Chromic CAMBISOLS	19.16	0.651
Gleyic CAMBISOLS	2.796	0.095

3.1.4. *METEOROLOGICAL DATA.* The daily precipitation data for stations around the vicinity of the study area are obtained from Department of Hydrology and Meteorology (DHM) (Table III) for year 2010 to 2019. Six meteorological stations were selected to provide comprehensive coverage (Fig. 4). The selection of these stations was supported by Thiessen polygon analysis.

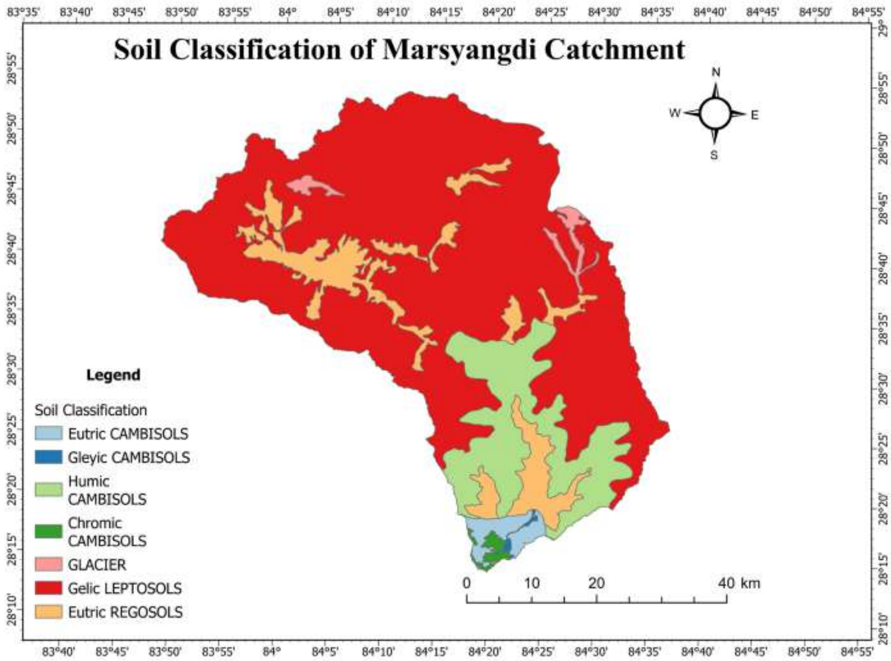

FIGURE 3. Soil classification map of the Marsyangdi River Basin.

3.1.5. *HYDROLOGICAL DATA.* Daily discharge data is obtained from DHM. The location of the gauging station is shown in Fig. 4. The analysis used daily discharge record from year 2010 to 2015 for the station 439.35 (Bhakundebesi station).

3.1.6. *SEDIMENT DATA.* Observed suspended sediment concentration (SSC) data was obtained from DHM at the Bhakundebesi station. The data was intermittent and for the year 2012–2015. SSC observations were available for only 694 of 1,461 days (47.5% coverage). Monsoon-season availability (371 of 488 June–September days, 76%) was relatively better, but high-flow event representation above 300 m^3/s was limited. To obtain a continuous daily SSC series for analysis, the missing sediment data were estimated using an optimization-based suspended sediment rating approach following [9]. This approach was adopted to reduce bias in sediment estimation and to better represent long term sediment variability under intermittent observations.

TABLE 3. Data Collection

Type of data	**Source**	**Spatial/Temporal Resoluti**
DEM	SRTM, USGS `https://earthexplorer.usgs.gov`	30 m × 30 m
Land Cover	ICIMOD Land Cover map 2010	30 m × 30 m
Soil Map	ISRIC, SOTER (Dijkshroon and Huting, 2009)	1:1 million
Climatic (Daily Precipitation)	DHM, Nepal	Station number: 802, 806, 820
Daily Discharge Data	DHM, Nepal	Station number: 439.35
Sediment Concentration	DHM, Nepal	Station number: 439.35

3.2. **SWAT MODEL DESCRIPTION.** SWAT is a semi distributed, process based and continuous time watershed model that simulates hydrology and sediment transport at the level of sub-basins and HRUs. In SWAT, basin hydrology is governed by the water balance equation (1),

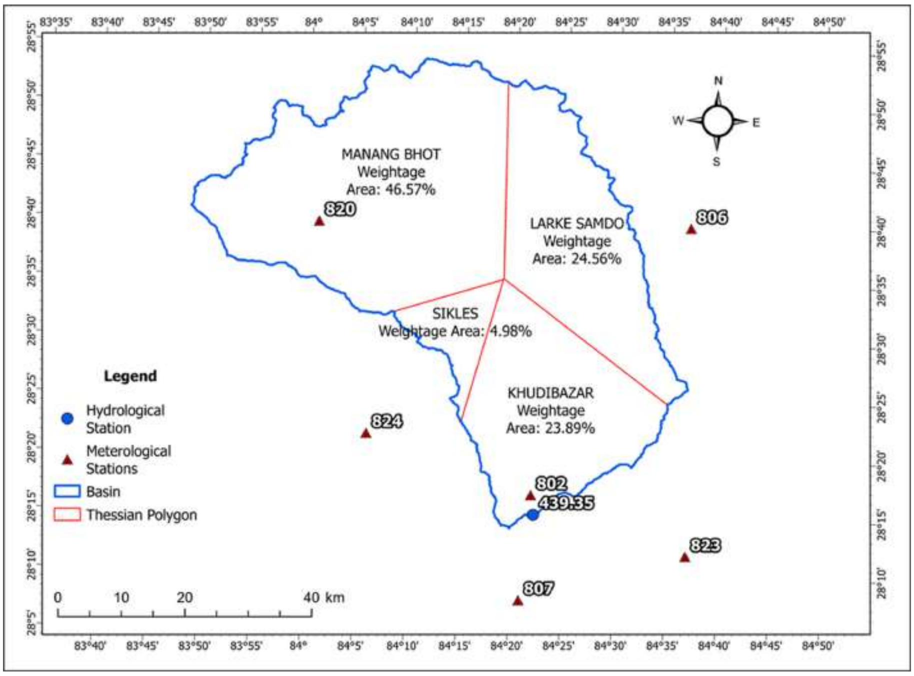

FIGURE 4. Basin boundary at Station 439.35 with meteorological and hydrological stations near the basin, that represent its hydrology.

which forms the basis for runoff generation and subsequent sediment transport:

$$SW_t = SW_0 + \sum_{i=1}^{t} (R_{day} - Q_{surf} - E_a - W_{seep} - Q_{gw}) \tag{1}$$

where SW_t is the final soil water content, SW_0 is the initial soil water content, R_{day} is precipitation, Q_{surf} is surface runoff, E_a is evapotranspiration, W_{seep} is percolation from the soil profile and Q_{gw} is return flow.

In SWAT, sediment yield from each HRU is estimated using the Modified Universal Soil Loss Equation (MUSLE), in which runoff energy replaces rainfall erosivity [10].

The MUSLE formulation used in SWAT is:

$$Sed = 11.8\,(Q_{surf} * q_{peak} * A_{hru})^{0.56} * K_{USLE} * C_{USLE} * P_{USLE} * LS_{USLE} * CFRG \tag{2}$$

where, Sed is sediment yield from the HRU, Q_{surf} is surface runoff volume, q_{peak} is peak runoff rate, A_{hru} is HRU area, K_{USLE} is the soil erodibility factor, C_{USLE} is the cover-management factor, P_{USLE} is the support-practice factor, LS_{USLE} is the topographic factor and $CFRG$ is the coarse fragment factor. Thus, sediment generation in SWAT is controlled by runoff magnitude, peak flow, land cover, soil properties and slope conditions.

Previous applications have also shown that SWAT can perform satisfactorily in Nepalese mountain basins, including the Karnali and West Rapti basins, supporting its use for basin-scale hydrological and sediment-related assessment in data-scarce Himalayan catchments (Dhami, Himanshu, Pandey, and Gautam, 2018; Shrestha and Thakuri, 2025).

[10] further states that erosion and sediment yield are estimated for each HRU using MUSLE and sediment generated on hillslopes is then released to and routed through the channel network. MUSLE uses runoff as the erosive driver rather than rainfall. Therefore, it has improved sediment-yield prediction, removes the need for sediment delivery ratios and allows estimation at the event scale. This makes the approach suitable for monsoon dominated basins where runoff is the main driver of suspended sediment mobilization. Sediment focused SWAT applications in the Himalayan region further support the use of SWAT for estimating sediment yield and identifying dominant source areas under data-limited conditions [5].

3.3. **SWAT MODEL SETUP.**

3.3.1. *WATERSHED DELINEATION.* The Marsyangdi watershed was delineated in ArcSWAT using the 30 m DEM, with the basin outlet fixed at the Bhakundebesi gauging station. Stream network extraction and sub-basin definition were performed after standard DEM preprocessing. A threshold drainage area of 500 ha was adopted for stream initiation, which discretized the basin into 31 sub-basins. This sub-basin framework was used to represent the spatial variability of hydrological and sediment processes across the catchment.

3.3.2. *HRU DEFINITION.* Hydrologic Response Units (HRUs) were generated by overlaying land use, soil, and slope layers within each sub-basin. Slope was classified into five classes: 0–5%, 5–15%, 15–30%, 30–45%, and >45%. All unique combinations of land use, soil, and slope resulted in 108 HRUs. This discretization allowed runoff generation and sediment yield to be simulated at a spatially distributed level.

3.3.3. *SIMULATION PERIOD AND TIME STEP.* The model was run at a daily time step using the prepared spatial layers and hydro-meteorological inputs. The simulation period covered 2012–2024, with an initial warmup period used to stabilize soil moisture, groundwater storage, and related state variables before model evaluation. Observed discharge and suspended sediment data at the basin outlet were later used for calibration during 2012–2014 and validation in 2015.

3.4. **CALIBRATION AND VALIDATION.**

3.4.1. *CALIBRATION APPROACH.* Model calibration and validation were carried out using the SWAT Calibration and Uncertainty Program (SWAT-CUP) with the Sequential Uncertainty Fitting algorithm (SUFI-2), which is applied for SWAT parameter optimization and uncertainty analysis in Himalayan basins. Calibration was performed at a daily time step using observed discharge and SSC data at the Bhakundebesi outlet station. Following standard SWAT practice, streamflow was calibrated first to establish a reliable hydrological response, after which sediment-related parameters were adjusted using the calibrated hydrological simulation as the basis for sediment generation and routing.

The model was run for the period 2012–2015, with an initial warm-up period to stabilize model state variables. Calibration was conducted for 2012–2014 and validation was performed for 2015 using an independent dataset.

3.4.2. *SELECTION OF CALIBRATION PARAMETERS.* Calibration parameters were selected based on their physical relevance to runoff generation, groundwater response, snowmelt processes, channel routing and sediment generation in steep Himalayan catchments, together with guidance from previous SWAT applications and published literature [5, 8, 11, 12]. For streamflow calibration, parameters influencing surface runoff, baseflow, groundwater delay, soil water processes, snowmelt, elevation-related climatic variation and channel flow routing were considered, consistent with SWAT-based hydrological studies in mountainous and Nepalese river basins [8, 12]. For sediment calibration, parameters related to soil erodibility, support practice, cover-management, channel re-entrainment and sediment routing were emphasized following sediment-focused SWAT applications in Himalayan catchments [5]. Parameter ranges were initially assigned from literature and SWAT documentation and were progressively refined through successive SUFI-2 iterations, following the calibration and uncertainty framework of SWAT-CUP/SUFI-2 [11]. The final set of calibration parameters and their fitted ranges are presented in Table IV and Table V.

3.4.3. *PARAMETERS EVALUATION METRICS.* Model performance was evaluated by comparing observed and simulated data, discharge and suspended sediment concentration, using the Nash–Sutcliffe Efficiency (NSE), coefficient of determination (R^2) and percent bias (PBIAS) given by (3), (4) and (5) respectively. NSE was used to assess the agreement between observed and simulated time series. R^2 was used to evaluate the strength of association between observed and simulated values. PBIAS was used to quantify the average tendency of the model to overestimate or underestimate observations.

The majority of sediment transport in the basin occurs during high flow monsoon conditions and these periods are most relevant to sediment management and hydropower operations. Thus, the model performance for suspended sediment was also interpreted with particular emphasis on monsoon-period observations.

$$NSE = 1 - \frac{\sum_{i=1}^{n} \left(Q_{sim} - Q_{obs}\right)^2}{\sum_{i=1}^{n} \left(Q_{sim} - \bar{Q}_{obs}\right)^2} \tag{3}$$

$$PBIAS = \frac{\sum_{i=1}^{n} \left(Q_{obs} - Q_{sim}\right)}{\sum_{i=1}^{n} Q_{obs}} \times 100\% \tag{4}$$

$$R^2 = \left[\frac{n\sum Q_{obs}Q_{sim} - \sum Q_{obs}\sum Q_{sim}}{\sqrt{\left(n\sum Q_{obs}^2 - \left(\sum Q_{obs}\right)^2\right)\left(n\sum Q_{sim}^2 - \left(\sum Q_{sim}\right)^2\right)}}\right]^2 \tag{5}$$

Table 4. Streamflow Calibration Parameters and Ranges Used in SWAT-CUP

Parameters	**Min**	**Max**
R__CN2.mgt	-0.2	0.2
V__ALPHA_BF.gw	0	1
V__GW_DELAY.gw	0	100
R__SOL_Z.sol	-0.25	0.25
R__SOL_K.sol	-0.8	0.8
R__SOL_AWC.sol	-0.2	0.4
V__GW_REVAP.gw	0	0.2
V__OV_N.hru	0	30
V__CH_N2.rte	0	0.3
V__CH_K2.rte	-0.01	500
V__SFTMP.bsn	-5	5
V__SMFMN.bsn	0	10
V__SMFMX.bsn	0	10
V__SNOCOVMX.bsn	0	500
V__PLAPS.sub	0	200
V__TLAPS.sub	-10	10
V__EPCO.bsn	0	1

Table 5. Sediment Calibration Parameters and Ranges Used in SWAT-CUP

Parameters	**Min**	**Max**
V__PRF_BSN.bsn	0.03	0.7
V__ADJ_PKR.bsn	0.5	2
R__USLE_K.sol	-0.15	0.3
R__USLE_P.mgt	-0.3	0.25
V__LAT_SED.hru	500	30000
V__SPCON.bsn	0.0025	0.02
V__SPEXP.bsn	1	2
V__CH_COV1.rte	0	1
V__CH_COV2.rte	0	1

4. RESULTS

4.1. SWAT MODEL PERFORMANCE.

4.1.1. *STREAMFLOW PERFORMANCE.* Daily streamflow at the Marsyangdi basin outlet simulation in SWAT produced very good performance in both calibration and validation. As shown in Table 6, during calibration (2012–2014), the model achieved NSE = 0.8641, R^2 = 0.8739, and PBIAS = +4.37%, and in validation for 2015 produced NSE = 0.8301, R^2 = 0.8678, and PBIAS = -9.42%. According to the evaluation criteria of Moriasi et al., 2007, these results indicate that SWAT captured the basin hydrology reliably. The model reproduced the overall seasonal hydrograph pattern, the monsoon changes, peak-flow period and recession behavior well (Fig. 5).

4.1.2. *SEDIMENT LOAD PERFORMANCE.* Sediment simulation was more moderate, within the satisfactory range for basin-scale application. As shown in Table 6, SWAT achieved NSE = 0.5560, R^2 = 0.6080, and PBIAS = +14.4% in calibration and produced NSE = 0.5160, R^2 = 0.6170, and PBIAS = +24.2% in validation. Thus the model reproduced the broad seasonal pattern of sediment transport, especially the concentration of sediment delivery during the monsoon months, but with greater uncertainty than streamflow simulation. SWAT tends to smooth the sharp monsoon sediment peaks (Fig. 5b) and was less effective in reproducing high-magnitude sediment events. However, the performance is adequate for annual, seasonal and spatial sediment assessment within the basin.

Table 6. SWAT Model Calibration and Validation Performance Summary (Moriasi et al. 2007 Criteria)

Parameter	**Flow Calibration**	**Flow Validation**	**Sed Calibration**	**Sed Validation**
NSE	0.864	0.830	0.556	0.516
R^2	0.874	0.867	0.608	0.617
PBIAS (%)	+4.37	-9.42	+14.4	+24.2
Rating	Very Good	Very Good	Satisfactory	Satisfactory

4.2. **SEDIMENT YIELD AND SPATIAL DISTRIBUTION.** The SWAT model estimated an average annual sediment export of 9.42 Mt/yr at the Marsyangdi basin outlet over the simulation period 2012–2024. The spatial distribution of model-produced sediment yield was highly uneven across the basin. Sediment generation was concentrated in a limited number of southern and southeastern sub-basins rather than being uniformly distributed throughout the catchment (Fig. 8). Sub-basins 28, 27, 21, 29 and 26 together contributed about 89% and the remaining 26 sub-basins contributed only about 11% of the total basin sediment generation (Table VII). This indicates that sediment yield in the Marsyangdi basin is strongly concentrated in a small number

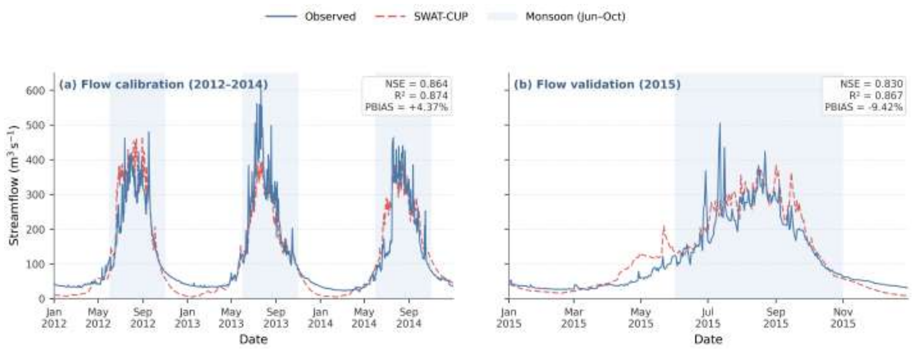

FIGURE 5. Observed and SWAT-simulated daily streamflow during calibration and validation at the basin outlet.

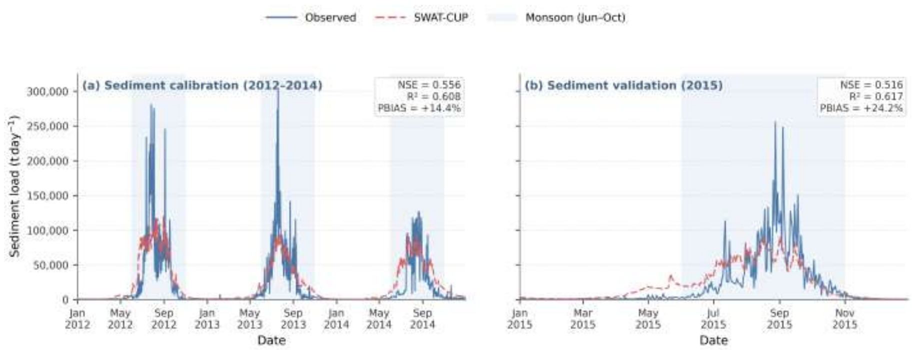

FIGURE 6. Observed and SWAT-simulated daily streamflow and sediment load during calibration and validation at the basin outlet.

of hotspot areas.

The distribution of average annual precipitation and sediment yield is shown in Fig. 6a and Fig. 6b respectively. The wetter part of the basin is concentrated mainly in the southern and southeastern sub-basins, while the northern and northwestern parts of the basin receive comparatively lower precipitation. The major sediment-contributing sub-basins, particularly 28, 27, 21, 29, and 26, lie within the wetter southern sector. Whereas many of the lower-yield northern and northwestern sub-basins correspond to the lower-precipitation zone. This indicates that the dominant sediment generating areas are concentrated within the monsoon-exposed southern part of the basin.

TABLE 7. Major Sediment-Contributing Sub-Basins and Cumulative Contribution to Total Basin Sediment Generation

Rank	Sub-basin	Individual Contribution %	Cumulative %
1	28	23%	23%
2	27	22%	45%
3	21	17%	62%
4	29	16%	78%
5	26	11%	89%

Although the precipitation pattern provides an important basis for understanding the broad distribution of sediment yield, some eastern sub-basins with relatively high precipitation do not show the similar spatial correspondence with high sediment yield. Thus, precipitation alone cannot completely explain the observed spatial variability. Therefore, additional catchment controls are likely involved in determining the intensity of sediment generation across individual sub-basins.

The model consistently identifies a limited number of dominant sediment-source sub-basins within the watershed. This spatial concentration is one of the main quantitative findings of the study.

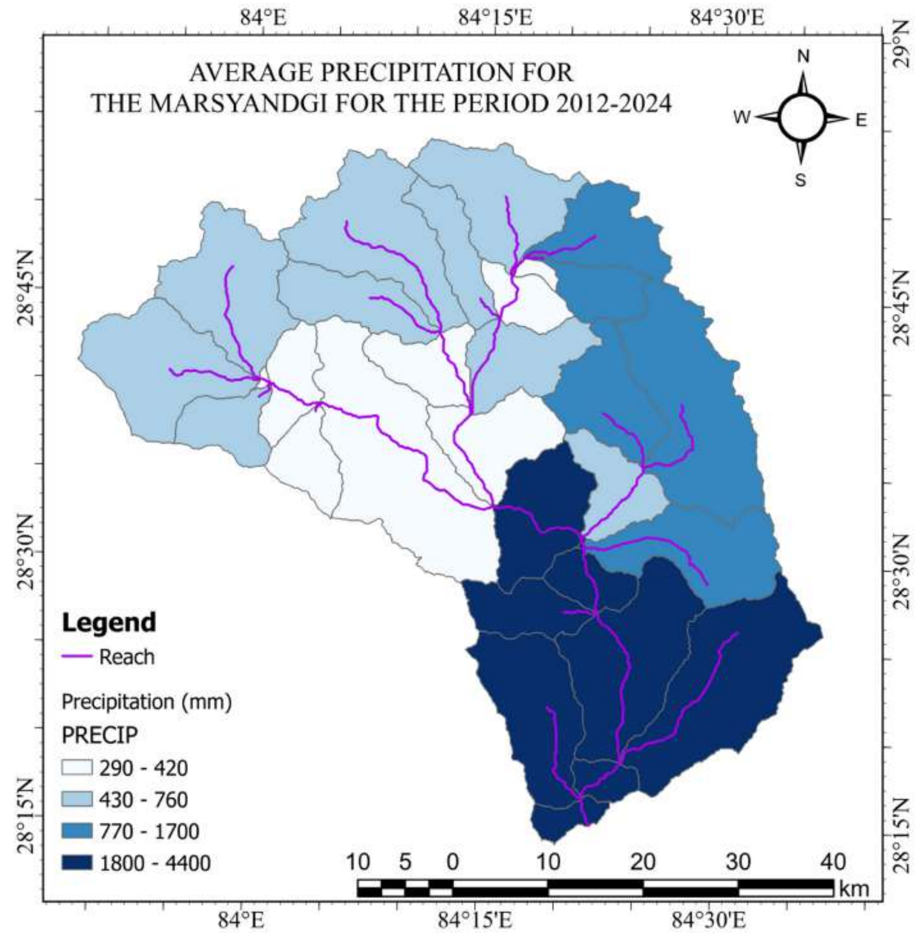

FIGURE 7. Average annual precipitation in the Marsyangdi Basin for the period 2012–2024.

4.3. **SUSPENDED SEDIMENT CONCENTRATION AND HYDROPOWER OPERATIONAL RISKS.** The mean annual sediment concentration over 2012–2024 was 1,385 mg/L at the basin outlet, indicating high-sediment conditions in the basin. As shown in Fig. 7 and Table 8, sediment concentration follows a strong seasonal pattern, remaining low during the dry months but rising sharply with the onset of the monsoon. The sediment transport is heavily concentrated within the monsoon season. Monthly average concentration increased to 4,500 mg/L in June, peaked at 5,200 mg/L in July, remained high at 4,800 mg/L in August, and declined to 2,800 mg/L in September. In contrast, monthly average concentrations during the dry months remained minimum with the lowest values occurring between December and March.

Fig. 8 shows that average sediment concentration is spatially heterogeneous across the basin. The highest reach-scale concentrations concentrated in the southern and southeastern parts of the

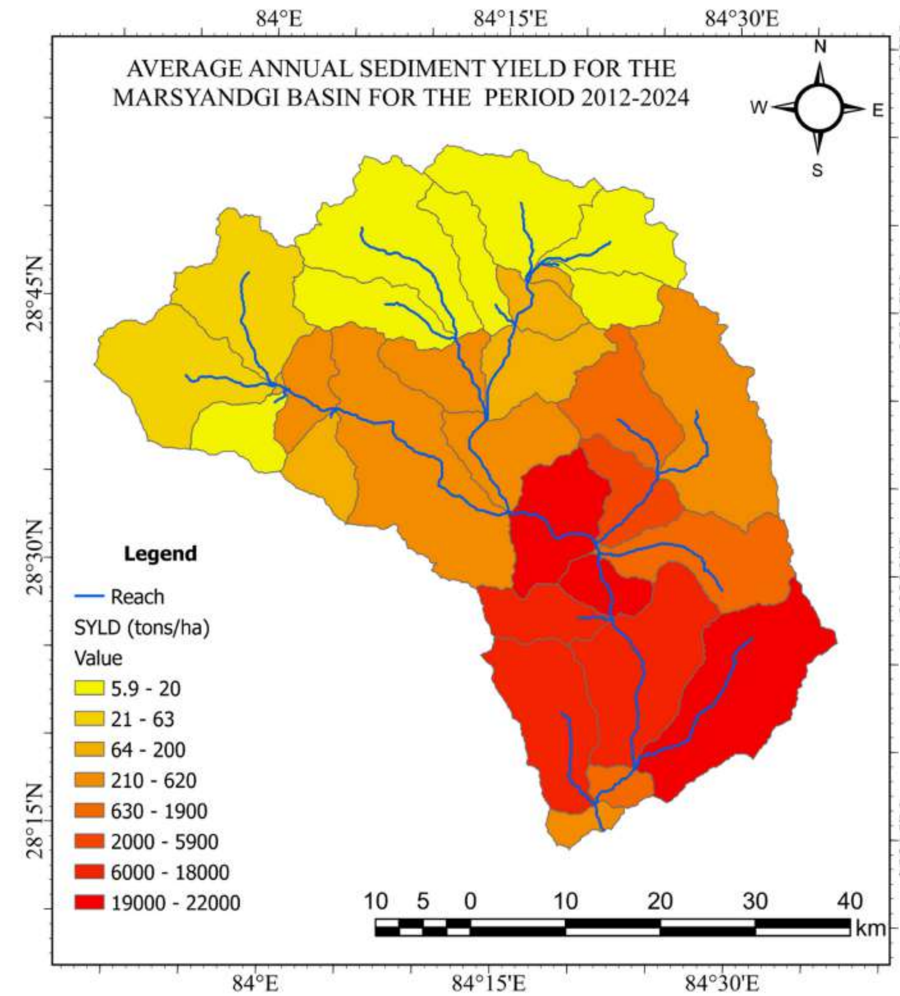

Figure 8. Average annual sediment yield in the Marsyangdi Basin for the period 2012–2024.

catchment.

Table 8. Monthly Average Discharge, Sediment Concentration, Annual Sediment Share, and Operational Risk Level at the Marsyangdi Basin Outlet (2012–2024)

Month	**Avg Q (m^3/s)**	**Avg SSC (mg/L)**	**% Annual Sediment**	**Days >1500 ppm**	**Risk Level**
January	70	250	2%	0	Low
February	65	200	2%	0	Low
March	75	280	2%	0	Low
April	95	450	3%	0	Low
May	180	800	5%	1	Medium
June	350	4500	18%	25	High
July	400	5200	22%	28	High
August	380	4800	21%	27	High
September	280	2800	12%	15	Medium-High
October	150	800	4%	1	Low
November	100	400	2%	0	Low
December	70	250	2%	0	Low

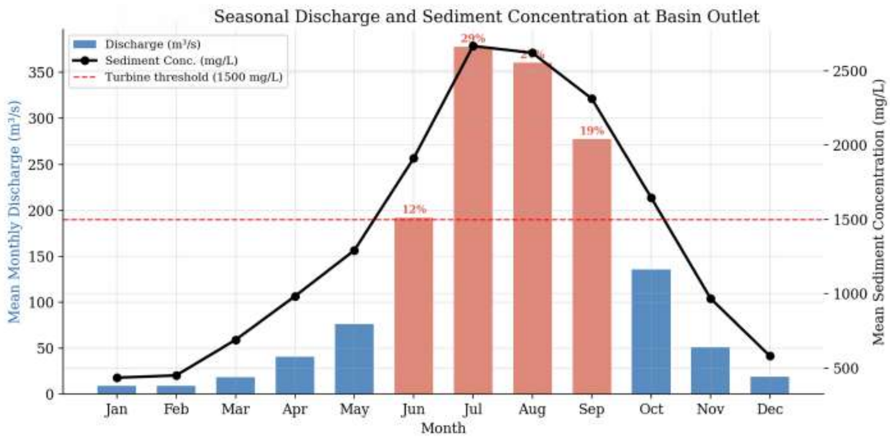

FIGURE 9. Mean monthly discharge and sediment concentration at the Marsyangdi basin outlet showing the sharp monsoon rise in sediment concentration.

With regard to hydropower operation, it becomes important to discuss the increasing SSC throughout the seasons because the sediment concentration, together with its particle size, shape, hardness, flow velocity and impingement angle determines hydro-abrasive wear of the turbine elements in sediment-rich Himalayan rivers. According to [13], despite sediment settling and flushing facilities, Nepalese run-of-river HPPs, such as Marsyangdi, Khimti, and Jhimruk operate with a high rate of turbine erosion caused by sediments. Additionally, an IHA case study of the Jhimruk HPP mentions an example of an operating rule based on the level of sediment concentration when the plant operates at full capacity below 1,500 ppm, starts to turn off the units from 1,500 to 3,000 ppm, and operates at full shut down above 3,000 ppm. Thus, according to this study, the level of exceedance of 1,500 mg/L in the outlet of Marsyangdi basin can be considered as a relevant operational criterion for periods of increased erosion risk for turbines.

Based on Table 8, this criterion is exceeded for 95 days a year, mostly in the period of June–September, accounting for 73% of the annual sediment amount. The SSC in the dry seasons does not exceed this criterion much, indicating that this is the low-risk period for turbine inspection and maintenance operations. Fig. 7 and Fig. 8 and Table 8 show that the sediment hazard in Marsyangdi basin is highly seasonal in the outlet and heterogeneous in the whole basin, and the major risk for run-of-river hydropower operation is concentrated during monsoon months [13, 14].

5. DISCUSSION

5.1. CONTROLS ON SPATIAL SEDIMENT YIELD. The spatial pattern implies that precipitation is the main factor controlling sediment production in the Marsyangdi Basin. Hotspot sub-basins occur in the wetter south of the drainage area, while northern and northwestern sub-basins exist in the dry rain shadow zone. The pattern fits the findings related to the role of monsoon forcing on hydrology and sediment delivery at the basin scale in the Himalayas [4]. Moreover, the pattern conforms to the conclusions drawn from SWAT modeling in Nepal and the Kaligandaki Basin, which states that sediment yield in this case involves complex interplay between multiple factors i.e., rainfall, topography, and channel network [5, 8].

At the same time, precipitation is not sufficient to explain the pattern. Eastern sub-basins have a significant amount of rainfall but lower sediment yield, meaning that other factors, slopes, relief and connectivity, play an important role. Therefore, one can conclude that while precipitation

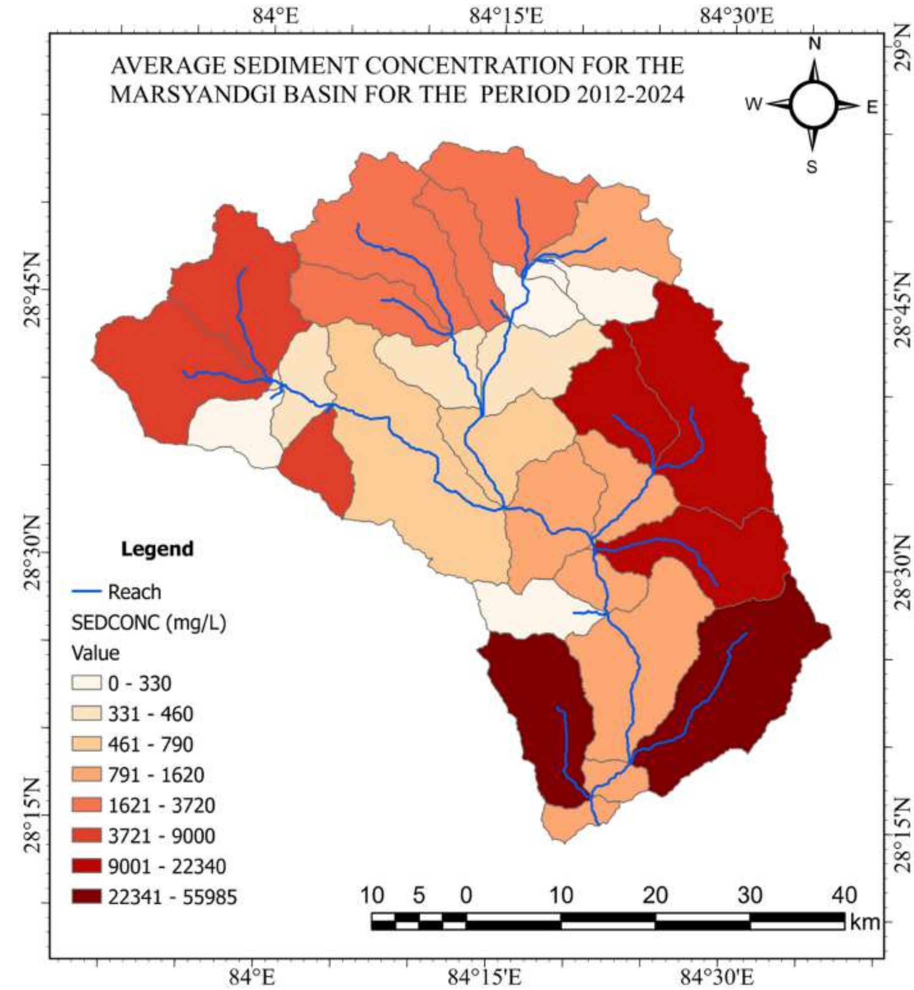

FIGURE 10. Spatial distribution of average sediment concentration by reach, showing pronounced spatial heterogeneity and concentration hotspots in the southern and southeastern reaches.

controls the general north-south pattern, the local intensity of sediment processes is controlled by topographic factors.

5.2. **MODEL PERFORMANCE AND UNCERTAINTY.** Performance in terms of streamflow was better than sediment, which was expected in the steep Himalayan basins considered in this research. While streamflow is representative of the entire basin's hydrology, sediment is sensitive to monsoonal rain events and to the local sediment supply. The process-based model SWAT estimates sediment yield by means of MUSLE, which simulates runoff erosion more accurately than modeling landslides, debris flow, and mass wasting events [7, 10, 15]. Hence, this could explain why the model captured the seasonal sediment cycle but smoothed out the maximum monsoon peaks.

The uncertainty in the results could stem from the limitations of the observational data used in this study. The sediment data utilized in calibration were not continuous, and the model was calibrated and validated based on one location only. Thus, while the outlet response was correctly simulated, the spatial pattern within the watershed remains an outcome of the model, without validation. Other similar studies conducted in the Himalayan area using SWAT have also reported difficulties related to uncertainty of spatial pattern resulting from one-site calibration [8]. Thus, the hot-spot sub-watersheds must be interpreted relatively rather than quantitatively.

5.3. **HYDROPOWER RELEVANCE.** In relation to hydropower plants, the key finding pertains to the temporal clustering of the sediment-related risk, which is pronounced during the monsoon period. While abrasive wear in hydropower turbines depends both on sediment concentrations and sediment grain hardness, shape, sizes and flow regime [3], the threshold used in this study can be considered only indicative.

Therefore, the current research is most useful as a basin-wide planning technique that helps to define the areas where sediment sources are clustered and the periods of the maximum sediment stress. A comparison between the sediment predictions of the model and more traditional discharge-SSC curves is needed for clarifying the added benefit of the model in this basin.

6. CONCLUSION

This study applied SWAT to estimate suspended sediment yield, sediment concentration and their spatial pattern in the Marsyangdi River Basin. SWAT can provide a useful basin-scale framework for sediment assessment in the basin as it reproduced streamflow very well and sediment with satisfactory performance. The results show that sediment yield is strongly concentrated in a small number of southern sub-basins, while the remaining sub-basins contribute relatively little. Sediment transport is also strongly seasonal with the monsoon period dominating the annual sediment regime. These findings indicate that sediment pressure in the Marsyangdi Basin is both spatially concentrated and seasonally focused.

The comparison between precipitation and sediment yield suggests that the major sediment-source areas are linked to the wetter southern part of the basin, although precipitation alone does not explain the full spatial pattern. From a practical point of view, the study helps identify where sediment-source areas are concentrated and when sediment exposure is highest. Therefore, it is useful for targeted sediment monitoring and basin-scale planning.

Part of the SSC series used in the analysis was completed using a rating-based approach because the observed sediment record was intermittent. In addition, the SWAT sediment module mainly represents runoff-driven erosion and does not explicitly simulate landslides, debris flows and other mass-wasting processes that are important in steep Himalayan catchments. The calibration and validation were also carried out at the basin outlet only, therefore the spatial sediment pattern should be read as a relative modeled pattern rather than an exact sub-basin estimate. Future work should therefore focus on improved monsoon-period sediment observations, multi-site validation, and comparison with discharge-SSC rating methods.

Acknowledgment. The authors gratefully acknowledge the Department of Hydrology and Meteorology (DHM), Nepal, for providing the hydrological and precipitation data used in this study. The authors also acknowledge the Institute of Engineering, Pulchowk Campus, for academic and institutional support. Special thanks are extended to all individuals and organizations whose data resources and technical support contributed to the completion of this work.

References

[1] B. Bookhagen, R. C. Thiede, and M. R. Strecker, “Late quaternary intensified monsoon phases control landscape evolution in the northwest himalaya,” *Geology*, vol. 33, no. 2, pp. 149–152, Feb. 2005.

[2] R. K. Dahal and S. Hasegawa, “Representative rainfall thresholds for landslides in the nepal himalaya,” *Geomorphology*, vol. 100, no. 3–4, pp. 429–443, Aug. 2008.

[3] L. Poudel, B. Thapa, B. P. Shrestha, B. S. Thapa, K. P. Shrestha, and N. K. Shrestha, "Computational and experimental study of effects of sediment shape on erosion of hydraulic turbines," in *IOP Conference Series: Earth and Environmental Science*, 2012.

[4] C. Andermann, S. Bonnet, A. Crave, P. Davy, L. Longuevergne, and R. Gloaguen, "Sediment transfer and the hydrological cycle of himalayan rivers in nepal," *Comptes Rendus - Geoscience*, vol. 344, no. 11–12, pp. 627–635, Nov. 2012.

[5] P. Chinnasamy and A. Sood, "Estimation of sediment load of kaligandaki basin," *Journal of Earth System Science*, May 2020.

[6] J. G. Arnold *et al.*, "Swat: Model use, calibration, and validation," *Transactions of the ASABE*, vol. 55, no. 4, pp. 1491–1508, 2012. [Online]. Available: http://swatmodel.tamu.edu

[7] P. W. Gassman, M. R. Reyes, C. H. Green, and J. G. Arnold, "The soil and water assessment tool: Historical development, applications, and future research directions," *Transactions of the ASABE*, vol. 50, no. 4, pp. 1211–1250, 2007.

[8] B. Dhami, S. K. Himanshu, A. Pandey, and A. K. Gautam, "Evaluation of the swat model for water balance study of a mountainous snowfed river basin of nepal," *Environmental Earth Sciences*, vol. 77, no. 1, Jan. 2018.

[9] S. Ghimire, U. Singh, and P. K. Bhattarai, "Generation of a suspended sediment rating curve of a himalayan river based on a long-term data: A case study of kabeli river," in *IOE Graduate Conference*, no. 10, Aug. 2021, pp. 2350–8906.

[10] S. L. Neitsch, J. G. Arnold, J. R. Kiniry, and J. R. Williams, "Soil and water assessment tool theoretical documentation: Version 2009," Texas Water Resources Institute, Texas A&M University, Tech. Rep., 2011. [Online]. Available: https://www.researchgate.net/publication/306205252_Soil_and_water_asessment_tool_theoritical_documentation_version_2009_Texas_Water_Resources_Institute_technical_report_No_406_Texas_Water_Resources_Institute_Texas_AM_University_Texas

[11] K. C. Abbaspour, E. Rouholahnejad, S. Vaghefi, R. Srinivasan, H. Yang, and B. Kløve, "A continental-scale hydrology and water quality model for europe: Calibration and uncertainty of a high-resolution large-scale swat model," *Journal of Hydrology*, vol. 524, pp. 733–752, May 2015.

[12] T. P. Joshi and B. K. Mishra, "Assessment of run-of-river hydropower potential using swat modeling and gis in the marsyangdi river basin, nepal," *Journal of Hydrology and Meteorology*, vol. 12, no. 1, pp. 11–22, Dec. 2024.

[13] B. Thapa, R. Shrestha, P. Dhakal, and B. S. Thapa, "Problems of nepalese hydropower projects due to suspended sediments," *Aquatic Ecosystem Health and Management*, vol. 8, no. 3, pp. 251–257, Jul. 2005.

[14] International Hydropower Association, "Sediment management case studies, nepal - jhimruk," Jul. 2026, accessed: 2026-07-06. [Online]. Available: https://www.hydropower.org/sediment-management-case-studies/nepal-jhimruk

[15] J. G. Arnold *et al.*, "Swat: Model use, calibration, and validation," *Transactions of the ASABE*, vol. 55, no. 4, pp. 1491–1508, 2012. [Online]. Available: http://swatmodel.tamu.edu

Everest Advances in Science and Technology (EAST) Vol. 2, No. 1, 2026
ISSN: 3102-0410 (Print), 3102-0429 (Online)
DOI: 10.3126/east.v2i1.98614

Homogeneity Testing and Quantile Regression for Regional Flood Estimation in the Narayani Basin, Nepal

TEJENDRA BIST[1*], MUKESH RAJ KAFLE[2]

ABSTRACT. Regional flood estimation in Nepal is challenged by short, uneven, and spatially sparse hydrometric records, particularly in Himalayan basins where strong physiographic and hydroclimatic contrasts make regional pooling difficult. This study examines the combined use of homogeneity testing and quantile regression for regional flood estimation in the Narayani Basin, Nepal. Annual maximum discharge records from gauged stations, together with selected catchment descriptors, were analyzed within an L-moment framework to evaluate regional homogeneity and identify a pooling group suitable for regional analysis. Quantile regression models were then developed to estimate flood quantiles directly from catchment descriptors and limited annual maximum series. The results show that achieving strict homogeneity in the Narayani Basin is difficult without substantially reducing the available station-year data, reflecting the marked variability of the basin. However, homogeneity screening allowed the identification of a defensible pooling group for regional flood estimation. The quantile regression results indicate that the method makes effective use of limited regional information and provides reasonable flood estimates for low to moderate return periods, with stable performance up to about the 50-year return period. Uncertainty increases for rarer events, and the reliability of regional estimates declines. The study shows that Hosking-Wallis homogeneity assessment combined with quantile regression provides a practical basis for estimating design floods in data-scarce Himalayan basins.

Keywords: Data-scarce Basin, Design Flood, Homogeneity Testing, Narayani Basin, Quantile Regression, QRT, Regional Flood Estimation

[1],[2] Institute of Engineering, Pulchowk Campus, Lalitpur, Nepal
E-mail: 080mshpe024.tejendra@pcampus.edu.np
* Corresponding author

Manuscript received: 04 March 2026; Revised: 16 June 2026; Accepted: 12 July 2026.

1. INTRODUCTION

Design flood estimation still remains a challenge in Nepal because many river basins are ungauged or poorly gauged. The available hydrometric records are short, uneven and insufficient for reliable at-site design flood estimation [1]. This limitation is more serious in Himalayan basins that produce substantial spatial variability in flood response over short distances due to their characteristic steep topographic gradients, strong monsoon influence and distinct hydroclimatic contrasts. Thus, direct extrapolation of short annual maximum series (AMS) to return periods for design flood has uncertainty, for the design of bridges, culverts, spillways, embankments, and hydropower infrastructure [2, 3, 4].

Regional flood frequency analysis (RFFA) offers a practical alternative where local records are inadequate. Regional methods can improve the stability of flood estimates for ungauged or poorly gauged sites, by pooling information from hydrologically similar catchments [5]. The success of regional methods depends on whether a hydrologically defensible catchment group can be identified. This is especially difficult in Himalayan basins of Nepal, where physiographic diversity is extreme and national scale homogeneity cannot reasonably be assumed. Nepalese basins cannot be treated as a single homogeneous flood region [1, 6]. Regional estimation must be based on careful screening of hydrological similarity and appropriate regional distribution selection [1, 6]. In practice, stricter homogeneity improves regional coherence at the cost of reducing the number of stations and total station-years available for analysis.

Among regional flood estimation methods, regression-based approaches are particularly attractive for data-scarce environments because they relate design floods directly to measurable catchment characteristics [7, 8]. Quantile Regression Technique (QRT) estimates conditional flood quantiles directly and can make efficient use of observed flood information without relying on intermediate at-site quantile estimation only [9]. This framework can exploit available information more effectively than conventional regression approaches in RFFA, even where the record lengths are limited [9]. Subsequent studies have also shown that quantile-regression-based regional models can provide useful predictive relationships in settings where strict regional homogeneity is difficult to achieve, although their performance still depends on descriptor quality, sample support, and model stability [10, 11, 12].

Nepal has remained focused on regionalization using index-flood relationships, simulation-supported analyses and majorly on empirical methods for ungauged basins [1, 13]. QRT for regional flood estimation has not been adequately explored in Nepalese basins. QRT supported within an L-moment-based regional framework that first establishes an acceptable homogeneous pooling group and regional parent distribution.

The present study investigates homogeneity testing and quantile regression for regional flood estimation in the Narayani Basin, Nepal. AMS from gauged stations were analyzed using an L-moment framework to identify an acceptable homogeneous pooling group and to select an appropriate regional parent distribution. QRT models were then developed for selected return periods using catchment descriptors derived from physiographic and climatic data. The regional estimates were finally examined through comparison with at-site flood estimates at a representative station, with the longest available discharge record among the pooled stations. By focusing on a data-scarce Himalayan basin, the study aims: (1) To assess whether a regional framework can be established. (2) To evaluate QRT can provide credible flood estimates for practical design applications.

2. STUDY AREA AND DATA

The study was carried out in the Narayani River system of central Nepal (Fig. 1). The basin extends from the high Himalaya to the middle-mountain valleys and therefore exhibits strong contrasts in elevation, relief and hydroclimatic characteristics. These contrasts are important for regional flood analysis because they influence runoff generation, channel response and the spatial variability of annual flood peaks.

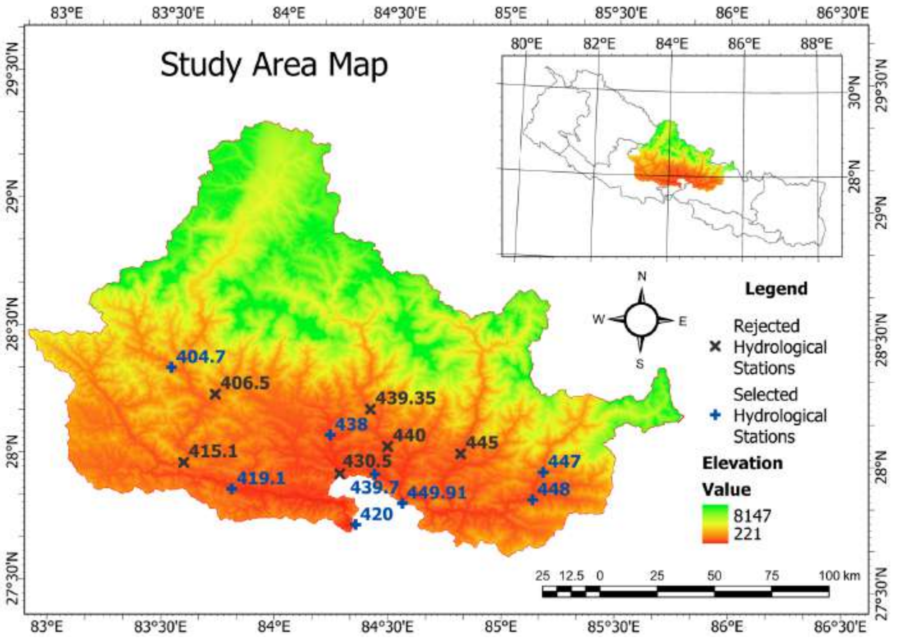

FIGURE 1. Study area map

2.1. **HYDROLOGICAL DATA.** Hydrological data were obtained from the Department of Hydrology and Meteorology (DHM), Government of Nepal. DHM is the national authority responsible for taking hydrological observations and distribution of quality controlled hydrometric records. The dataset comprised maximum monthly and yearly discharge records for the selected gauging stations.

2.2. **CATCHMENT DESCRIPTORS.** The selection of catchment descriptors was based on their hydrological relevance to flood generation and their applicability in regional flood frequency analysis (RFFA). Catchment descriptors should directly influence flood generation processes and be physically meaningful and readily obtainable and provide independent explanatory information.

Seven descriptors were considered in this study: drainage area (AREA), mean basin elevation (ELEV), mean annual rainfall (MAR), basin shape factor (SF), drainage density (SD), main channel slope (S1080) and forest cover (FOREST). Drainage area governs the volume of runoff contributing to flood events, while elevation and mean annual rainfall characterize the topographic and climatic controls on runoff generation respectively. Basin shape, drainage density and channel slope influence flow concentration time and drainage efficiency. Forest cover affects interception, infiltration, and surface runoff generation. These descriptors have been adopted in regional flood frequency studies [11, 12] because they represent the dominant physiographic and climatic controls on catchment flood response.

Catchment descriptors used in the regional analysis were derived from a 30 m digital elevation model (USGS), land-use and land-cover data (ICIMOD) and daily precipitation records from DHM.

3. METHODOLOGY

3.1. **DATA PREPROCESSING.** AMS was constructed using the annual maximum discharge values reported by DHM for each station.

The discharge records were subjected to data screening through visual inspection to identify missing records, inconsistencies and irregular observations. These procedures are consistent with previous regional flood studies conducted in Nepal [1, 6]. Years with incomplete annual records were filled by taking average flood of adjacent months of same year and same month of adjacent year. AMS were extracted from the monthly discharge records for each gauging station.

Hydrological analysis began with 14 gauged stations for which AMS was prepared from the available discharge records. Record lengths ranged from 20 to 60 years providing an initial total of 526 station-years.

The selected catchment descriptors, including drainage area, mean basin elevation, mean annual rainfall, basin shape factor, drainage density, main channel slope and forest cover, were compiled from GIS-based analyses and verified for consistency in units and spatial reference.

Predictor variables were subsequently standardized using log conversion. The standardized catchment descriptors were then used for QRT model and the original hydrological observations were used for L-moment estimation and at-site flood frequency analysis.

3.2. **L-MOMENT FRAMEWORK.** The analysis was based on AMS extracted. AMS was adopted because it provides a consistent representation of annual flood behavior and remains the standard basis for flood frequency analysis [3]. Station wise L-moment ratios were then estimated from the AMS in HEC-SSP v2.3. The regional screening used the dimensionless ratios L-CV (t), L-skewness (t_3), and L-kurtosis (t_4), as they are more stable than conventional product moments for skewed hydrological data [5, 14].

Regional weighted averages of the L-moment ratios were computed using station record length as the weighting factor.

3.3. **HOMOGENEITY ASSESSMENT AND POOL REFINEMENT.** Regional homogeneity was evaluated within the Hosking-Wallis L-moment framework [5, 14]. The procedure began with discordancy screening, in which each station was represented by the vector of its sample L-moment ratios:

$$u_i = [t_i, t_{3,i}, t_{4,i}]^T \tag{1}$$

The discordancy measure D_i was computed as [14]:

$$D_i = \frac{1}{3}(u_i - \bar{u})^T A^{-1}(u_i - \bar{u}) \tag{2}$$

where $\bar{u}$ is the regional mean of the station vectors and A is the pooled sums-of-squares and cross-products matrix. Stations with $D_i > 3$ were treated as discordant [5, 14].

After discordancy screening, heterogeneity was assessed using the Hosking-Wallis H_1 statistic, based on the dispersion of at-site L-CV values about the regional mean:

$$V = \left[\frac{\sum_{i=1}^{k} n_i (t^{(i)} - t^R)^2}{\sum_{i=1}^{k} n_i}\right]^{1/2} \tag{3}$$

$$H_1 = \frac{V - \mu_V}{\sigma_V} \tag{4}$$

where μ_V and σ_V are the mean and standard deviation of V respectively obtained from Monte Carlo simulations of homogeneous regions having the same number of sites and record lengths as the observed candidate pool [5, 14] using R-script libraries. The study used the H_1 measure because the retained pool lies within the low-skewness range [15]. The interpretation followed the standard criteria: $H_1 < 1$, homogeneous; $1 \leq H_1 < 2$, possibly heterogeneous; and $H_1 \geq 2$, definitely heterogeneous [5, 14].

Stations were removed iteratively on the basis of their discordancy and their contribution to regional inconsistency, when the station pool failed the homogeneity test. After each removal, the L-moment ratios, discordancy values and H_1 statistic were recalculated until an acceptably homogeneous pool was obtained. After multiple iterations a defensible homogeneous pool was obtained. The process revealed the trade-off between improved statistical similarity and reduced station-year support.

3.4. **REGIONAL PARENT-DISTRIBUTION SELECTION.** Using the accepted pool stations, candidate three-parameter regional distributions were tested within the Hosking-Wallis goodness-of-fit framework [5]. Candidate models included Pearson Type III (PE3), Generalized Extreme Value (GEV), Generalized Normal (GNO), Generalized Logistic (GLO) and Generalized Pareto (GPA). A distribution was considered acceptable when its absolute goodness-of-fit statistic satisfied:

$$|Z_{DIST}| \leq 1.64 \tag{5}$$

When several candidates were acceptable, the regional parent distribution was taken as the one with the lowest absolute $|Z_{DIST}|$ value [5].

3.5. **DESCRIPTOR SCREENING AND QUANTILE-REGRESSION FORMULATION.** Regional flood quantiles were modeled by quantile regression using the catchment descriptors AREA, ELEV, MAR, SF, SD, S1080, and FOREST. All descriptors were examined in logarithmic form to represent multiplicative scaling behavior and to maintain a linear structure in transformed space. Candidate predictors were screened using pairwise correlation analysis together with hydrologic interpretability. Final predictor combinations for each return period were selected independently using LOOV and MPLF, allowing different descriptor combinations to be retained where they improved predictive performance.

For a selected non-exceedance quantile τ, the general model form was:

$$\log Q_{i,\tau} = \beta_0 + \sum_{j=1}^{p} \beta_j \log X_{ij} \tag{6}$$

where $Q_{i,\tau}$ is the flood quantile τ at station i and the X_{ij} is the jth catchment descriptor for station i and β_0, β_j are regression coefficients. The coefficients were estimated by minimizing the quantile loss function [8]:

$$\min_{\beta} \sum_{i=1}^{n} \rho_\tau(y_i - \widehat{y_i}) \tag{7}$$

with,

$$\rho_\tau(u) = \begin{cases} u(\tau - 1), & u < 0 \\ u\tau, & u \geq 0 \end{cases} \tag{8}$$

where $\rho_\tau(u)$ is the pinball loss function, $y_i = \log(AMS_i)$ and $\widehat{y_i}$ is the fitted value [8]. Separate equations were searched for the return periods $T = 2, 5, 10, 25, 50, 100, 200, 500$ and 1000 years. In the final interpretation, emphasis was placed on the 2-year to 50-year range.

Higher-return period equations were reported only briefly and treated cautiously because they are supported by sparse upper-tail information.

3.6. **LEAVE-ONE-STATION-OUT VALIDATION (LOOV) AND MEAN PIECEWISE LOSS FUNCTION (MPLF) BASED MODEL RANKING.** Candidate equations for each return period were screened by LOOV. In each fold, all observations from one station were withheld, the model was calibrated using the remaining stations and predictive performance was evaluated on the omitted station. LOOV is appropriate for regional modeling because it tests whether a fitted equation can be transferred to an ungauged or withheld basin rather than merely reproducing stations already used for calibration.

Model ranking was based primarily on the MPLF, derived directly from quantile regression loss [9]:

$$MPLF = 1000 \times \frac{1}{N} \sum_{i=1}^{N} \rho_\tau(y_i - \widehat{y_i}) \tag{9}$$

where N is the total number of validation observations across all LOOV folds. Station wise prediction error was also examined as:

$$PE_s = \frac{1}{n_s} \sum_{i=1}^{n_s} \rho_\tau(y_i - \widehat{y_i}) \tag{10}$$

where n_s is the number of AMS observations at station s. Lower MPLF and lower mean station prediction error were interpreted as indicating better transfer performance. Final equations were selected on the basis of both predictive performance and hydrologic defensibility.

4. RESULTS AND DISCUSSION

4.1. **ACCEPTED HOMOGENEOUS POOL.** The initial 14 station candidate pool was clearly heterogeneous, with a starting H_1 value of 6.439 as shown in Figure. 2. Iterative removal of discordant or regionally inconsistent stations was required before pool could be treated as an acceptable regional group. After successive refinement the final pool reached $H_1 = -1.362$, satisfying the criterion for an acceptably homogeneous region. The retained stations were 404.7, 419.1, 420, 438, 439.7, 447, 448 and 449.91, with discordancy values ranging from 0.096 to 1.488, all below the threshold of 3 as observed in Table. 1. The weighted regional L-moment ratios of the accepted pool were $t = 0.197$, $t_3 = 0.140$ and $t_4 = 0.116$, indicating a compact low-skewness regional group.

A key result is that homogeneity was achieved only after a substantial reduction in data support. The original 526 station-years were reduced to 326 station-years, a loss of about 38%. This trade-off is important in the Nepalese context. [1, 6] showed that Nepal cannot be treated as one homogeneous flood region because of strong physiographic and climatic contrasts, and their regionalization study similarly required region revision after L-moment-based homogeneity testing. [1, 6] further showed that some Nepalese hydrologic regions contained too few gauged stations for reliable regional estimation and had to be supplemented with synthetic data. Relative to those studies, the Narayani result confirms the same fundamental difficulty at basin scale: statistical homogeneity is achievable, but only with notable sacrifice of station-year support.

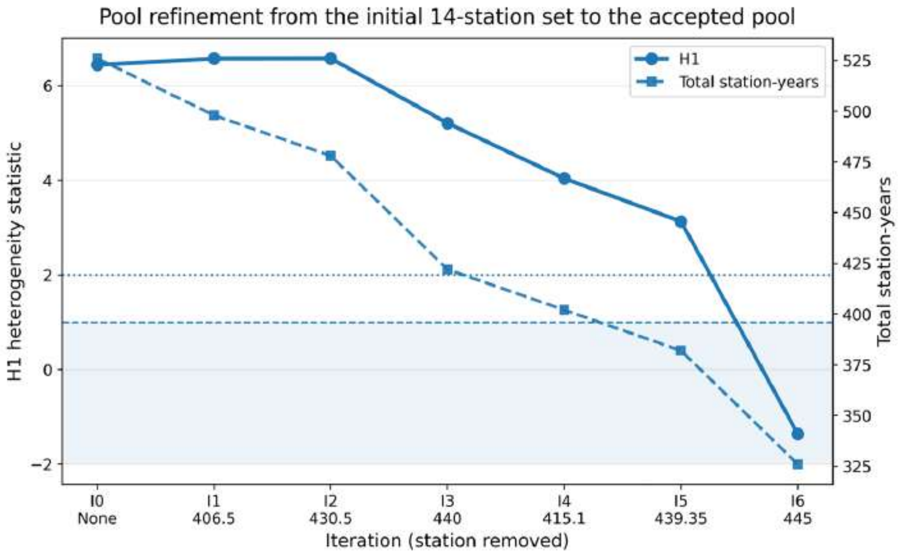

FIGURE 2. Refinement of the candidate pool from the initial 14-station set to the accepted eight-station homogeneous group. The figure combines the decline in H1 with the accompanying loss of station-year support.

TABLE 1. Final accepted homogeneous pool and discordancy values

Station ID	n (years)	Discordancy, D_i
404.7	44	1.328
419.1	24	0.310
420	60	0.686
438	45	0.741
439.7	33	1.026
447	43	1.488
448	51	0.096
449.91	26	1.326

4.2. **REGIONAL PARENT DISTRIBUTION.** After the final pool had been accepted, candidate regional distributions were evaluated using the Hosking-Wallis goodness-of-fit statistic. Three distributions satisfied the acceptability criterion $|Z_{DIST}| \leq 1.64$: PE3, GNO, and GEV as seen in 2. Among these, PE3 gave the lowest absolute goodness-of-fit value ($|Z_{DIST}| = 0.735$) and was therefore selected as the most suitable regional parent distribution. GNO and GEV were also acceptable, but with weaker fit. GLO and GPA were clearly unacceptable.

This result is consistent with the broader pattern that no single parent distribution is universally best. Skewed three-parameter models are often deemed appropriate for flood data in data-scarce basins. Nepal-wide regional scale study [1] also selected regional distributions using the $|Z_{DIST}|$ criterion. It also emphasized that reliable distribution selection depends strongly on the adequacy of regional pooling. In the present study, PE3 was selected only after the candidate pool had first been refined to an acceptable homogeneous group, which strengthens the interpretability of the result.

4.3. **QUANTILE-SPECIFIC QRT EQUATIONS.** No dominant predictor structure was identified for the entire flood return period scale according to the LOOV analysis. Optimal predictor structures for the 2-year and 5-year return periods were equations that contained AREA and SD,

Table 2. Goodness-of-Fit of Candidate Regional Distributions for the Accepted Pool

Distribution	Fitted t_4	Z_{DIST}	Assessment
PE3	0.129	0.735	Selected
GNO	0.138	1.224	Acceptable
GEV	0.139	1.293	Acceptable
GLO	0.183	3.591	Rejected
GPA	0.046	-3.605	Rejected

which implies that floods corresponding to lower return periods are influenced both by basin-scale characteristics and drainage network features. The best performing equation in the case of 10-year return period contains AREA, S1080, and FOREST variables. At the 25-year and 50-year return periods, equations were reduced to AREA variable, while models with higher return periods adopted a completely different set of predictors (ELEV, MAR, and SD). Therefore, it can be said that different predictor structures are supported by the regional sample at different parts of the flood return period distribution.

The appearance of the FOREST variable in the equation for the 10-year return period is explained by return-period-specific variable selection based on the LOOV procedure, rather than being a universal predictor of flood magnitude. In other words, candidate equations for each return period were evaluated separately based on their ability to predict correctly using the MPLF criterion, and only those descriptors that improved the validation performance were selected. While the forest cover contributes to better performance of the 10-year flood model by explaining differences in the basin-scale processes of interception, infiltration, and runoff formation, for lower return periods (2–5 years) drainage characteristics represented by the AREA and SD variables have better explaining power. On the other hand, at larger return periods (starting with 25 years) the magnitude of the flood event depends mainly on basin-scale physiographic and climatic characteristics. Therefore, the FOREST variable adds little to the explanation of the flood magnitude and does not provide additional predictive power to justify its inclusion in the LOOV-selected equations.

From the point of application, the most reliable results of the QRT procedure are those up to 50-year return period. Within this range, the fitted equations remain fairly simple and hydrologically meaningful, and at the same time validation metrics are systematically increasing from $T = 2$ to 50 years. For higher return periods (above 50 years) fitted equations are more affected by upper tail sparsity and therefore should be treated cautiously. This explanation is consistent with the argumentation presented by [9], claiming that one of the main advantages of quantile regression in the regional context is the use of flood observations directly and allowance for sites with short records. However, it suggests, model evaluation should remain grounded in predictive performance rather than apparent fit alone. It also aligns with [10, 11, 12], who found that useful regional prediction equations can still be obtained in difficult settings, even where homogeneity is challenging. Although this study supports the broader view of previous studies, it also suggests that credible practical use should remain focused on low to moderate return periods under the available data support.

4.4. **COMPARISON AT STATION 420.** Station 420 was selected for direct comparison because it has the longest AMS record in the study dataset and therefore provides the strongest at-site reference available. QRT estimates were compared with at-site PE3 quantiles for return periods from 2 to 1000 years. The comparison shows that QRT follows the at-site PE3 estimates reasonably well at low to moderate return periods, but diverges strongly in the upper tail. At the 2-year return period, the QRT estimate (3767.21 m^3/s) was very close to the at-site PE3 value (3714.70 m^3/s), with a relative error of 1.41%. At the 5-year, 10-year, 25-year, and 50-year return periods, QRT overestimated the at-site PE3 quantiles by 12.77%, 1.51%, 15.28%, and 17.08%, respectively. These results suggest that the regional equations provide a mostly credible representation of flood magnitude up to the medium return-period range, with a clear tendency toward positive bias.

Table 3. Comparison of QRT and At-Site PE3 at Station 420

T	**QRT (m^3/s)**	**PE3 (m^3/s)**	**RE (%)**
2	3767.21	3714.70	1.4
5	5620.00	4983.50	12.8
10	5810.00	5723.70	1.5
25	7598.86	6591.50	15.3
50	8441.02	7209.80	17.1
100	8517.92	7816.00	9.0
200	17550.35	8421.70	108.4
500	17550.38	9234.80	90.1
1000	17550.38	9867.00	77.9

Beyond 50 years, however, the QRT estimates become much less reliable. At 100 years, the relative error remained moderate at 8.98%. From 200 years onward the QRT estimates increased abruptly to about 17,550 m^3/s and then remained almost unchanged. The at-site PE3 quantiles continued to rise more gradually from 8421.70 to 9867.00 m^3/s for 200 years to 1000 years. This produced very large positive errors of 108.39%, 90.05%, and 77.87% at the 200-year, 500-year and 1000-year return periods respectively.

Table 4. Best LOOV-Selected QRT Equations and Validation Metrics

T	**Best LOOV Model**	**MPLF**	**PEs**
2	$\log_{10}(Q_2) = 1.029 + 0.764\log_{10}(AREA) + 0.947\log_{10}(SD)$	76.81	8.0%
5	$\log_{10}(Q_5) = 1.131 + 0.791\log_{10}(AREA) + 1.011\log_{10}(SD)$	69.34	6.8%
10	$\log_{10}(Q_{10}) = -0.334 + 1.036\log_{10}(AREA) + 0.536\log_{10}(S1080) + 1.579\log_{10}(FOREST)$	38.25	3.7%
25	$\log_{10}(Q_{25}) = 0.553 + 0.817\log_{10}(AREA)$	19.80	2.0%
50	$\log_{10}(Q_{50}) = 0.599 + 0.817\log_{10}(AREA)$	11.13	1.1%
100	$\log_{10}(Q_{100}) = 0.758 + 0.779\log_{10}(AREA)$	5.63	0.6%
200	$\log_{10}(Q_{200}) = 11.248 - 1.788\log_{10}(ELEV) - 0.674\log_{10}(MAR) + 1.178\log_{10}(SD)$	2.36	0.2%
500	$\log_{10}(Q_{500}) = 11.248 - 1.788\log_{10}(ELEV) - 0.674\log_{10}(MAR) + 1.178\log_{10}(SD)$	1.08	0.1%
1000	$\log_{10}(Q_{1000}) = 11.248 - 1.788\log_{10}(ELEV) - 0.674\log_{10}(MAR) + 1.178\log_{10}(SD)$	0.66	0.1%

The comparison therefore indicates that the present QRT framework is defensible mainly for low to moderate return periods and should not be relied upon for higher-return-period design estimation under the available station-year support. This interpretation is consistent with the body of work in regional-flood estimation from the Nepalese region [1, 6, 13] and shows how regional estimation can be significantly constrained by the paucity of gauging information and difficulty in making strong inference given limited sample size. This is consistent with previous study claim that quantile regression-based regional models must be assessed on prediction performance [9].

5. CONCLUSIONS AND RECOMMENDATIONS

This study explores homogeneity testing and quantile regression methods for regional flood frequency analysis using AMS data obtained at 14 gauged stations of the Narayani Basin. The results show that the first group of stations did not exhibit regional homogeneity and needed to be trimmed down to an eight-station final pool, decreasing data support from 526 to 326 station-years. This means that a regionally homogeneous flood frequency analysis is only possible in this area under the condition of considerable data reduction. For the second pool, the most appropriate parent

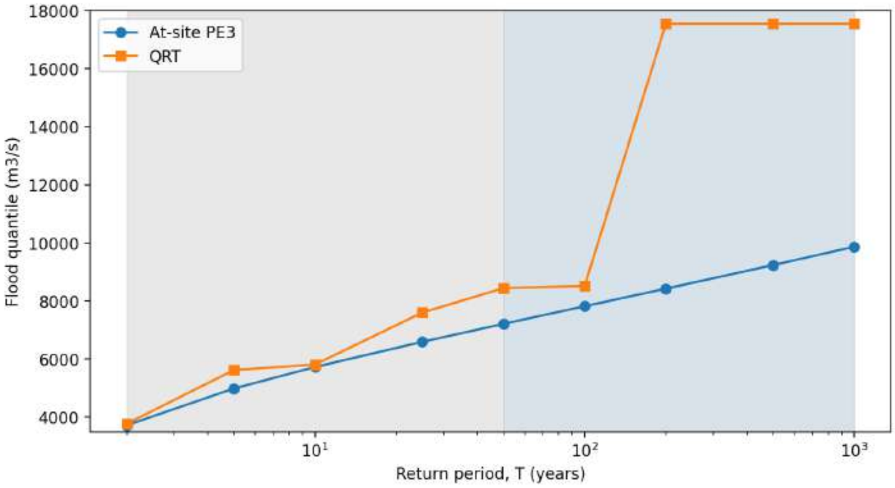

FIGURE 3. QRT versus at-site PE3 at Station with the shaded zone marks the range above 50 years.

distribution is the three-parameter Pareto (PE3).

The results of quantile regression technique (QRT) show that there is no unique predictor set for the entire flood range: equations for lower and moderate return periods can be rather simple and meaningful, while those for higher return periods become different and less defensible. Comparison of the QRT-based estimates and observed values at Station 420 shows that the estimates of QRT can be considered valid for lower return periods up to approximately 50 years, while estimates in the upper tail become increasingly inaccurate starting from this point.

From the practical perspective, this study provides evidence for the applicability of the Hosking-Wallis method and quantile regression technique as a combination for data-scarce Himalayan basin regions but limited to low to moderate return periods. Therefore, when using QRT-based regional estimates in engineering practice, caution is recommended starting from the 50-year return period due to insufficient station-year support. For the future research, extending of hydrometric time series, increasing the density and continuity of the gauging network, as well as testing of other predictors with the physical meaning such as rainfall intensity, snow and glacier impact, and storage effect in the basin can be recommended. This will allow determining if the range of accurate estimates can be extended beyond medium return periods.

Acknowledgment. The authors gratefully acknowledge the Department of Hydrology and Meteorology (DHM), Nepal, for providing the hydrological and precipitation data used in this study. The authors also acknowledge the Institute of Engineering, Pulchowk Campus, for academic and institutional support. Special thanks are extended to all individuals and organizations whose data resources and technical support contributed to the completion of this work.

References

[1] B. K. Mishra, K. Takara, Y. Yamashiki, and Y. Tachikawa, "Hydrologic simulation-aided regional flood frequency analysis of nepalese river basins," *Journal of Flood Risk Management*, vol. 2, no. 4, pp. 243–253, Dec. 2009.

[2] T. Dalrymple, "Flood-frequency analyses, manual of hydrology: Part 3," U.S. Geological Survey, Tech. Rep., 1960.

[3] J. F. England *et al.*, "Guidelines for determining flood flow frequency bulletin 17c book 4, hydrologic analysis and interpretation techniques and methods 4-b5," U.S. Geological Survey, Tech. Rep., 2019.

[4] Z. Khan, A. Rahman, and F. Karim, "An assessment of uncertainties in flood frequency estimation using bootstrapping and monte carlo simulation," *Hydrology*, vol. 10, no. 1, Jan. 2023.

[5] J. R. M. Hosking and J. R. Wallis, *Regional Frequency Analysis: An Approach Based on L-Moments.* Cambridge University Press, 1997.

[6] B. K. Mishra, K. Takara, and Y. Tachikawa, "Regionalization of nepalese river basins for flood frequency analysis," Tech. Rep., 2008.

[7] R. Koenker and K. F. Hallock, "Quantile regression," *Journal of Economic Perspectives*, vol. 15, no. 4, pp. 143–156, 2001.

[8] R. Koenker and G. Bassett, "Regression quantiles," *Econometrica*, 1978.

[9] D. Ouali, F. Chebana, and T. B. M. J. Ouarda, "Quantile regression in regional frequency analysis: A better exploitation of the available information," *Journal of Hydrometeorology*, vol. 17, no. 6, pp. 1869–1883, Jun. 2016.

[10] K. H. Ahn and R. Palmer, "Regional flood frequency analysis using spatial proximity and basin characteristics: Quantile regression vs. parameter regression technique," *Journal of Hydrology*, vol. 540, pp. 515–526, Sep. 2016.

[11] A. Ahmed, Z. Khan, and A. Rahman, "Searching for homogeneous regions in regional flood frequency analysis for southeast australia," *Journal of Hydrology: Regional Studies*, vol. 53, Jun. 2024.

[12] A. Zalnezhad, A. Rahman, F. Ahamed, M. Vafakhah, and B. Samali, "Design flood estimation at ungauged catchments using index flood method and quantile regression technique: A case study for south east australia," *Natural Hazards*, vol. 119, no. 3, pp. 1839–1862, Dec. 2023.

[13] B. Acharya and B. Joshi, "Flood frequency analysis for an ungauged himalayan river basin using different methods: A case study of modi khola, parbat, nepal," *Meteorology Hydrology and Water Management*, vol. 8, no. 2, pp. 46–51, Dec. 2020.

[14] J. R. M. Hosking and J. R. Wallis, "Some statistics useful in regional frequency analysis," 1993.

[15] A. Viglione, F. Laio, and P. Claps, "A comparison of homogeneity tests for regional frequency analysis," *Water Resources Research*, vol. 43, no. 3, Mar. 2007.

Everest Advances in Science and Technology (EAST), Vol. 2, No. 1, 2026
ISSN: 3102-0410 (Print), 3102-0429 (Online)
DOI: 10.3126/east.v2i1.98618

Lexicographic Static FlowLoc with/without Excess Storage

SACHIN WAGLE[1], DURGA PRASAD KHANAL[2*], TANKA NATH DHAMALA[3]

Abstract. Maximizing the flow value in a multi-terminal (multiple sources and multiple sinks) network using lexicographic supply from sources to sinks, reduce conflicts in the movement of flows toward the destinations. However, installing facilities on arcs reduce the arc capacities, which may hinder the maximum flow value. Nevertheless, such installations are necessary to supply facilities to the commodity. On the other hand, if intermediate nodes have storage capacity, the excess flow which cannot reach the sinks, can be stored at these nodes. As a result, the overall flow value can be improved.

In this paper, we integrate the concepts of facility allocation togather with intermediate storage and introduce lexicographic maximum static flow problems with and without intermediate storage. We investigate their corresponding flow models. The multi-facility problems are solved using heuristic approaches, whereas polynomial-time algorithms are presented for the single-facility problem.

Keywords: Lexicographic flow, FlowLoc, intermediate storage, $\mathcal{NP}-$completeness, heuristic

AMS Subject Classification: Primary 90C35; Secondary 05C21, 90B10, 90C27

[1] Institute of Engineering, Purwanchal Campus, Tribhuvan University, Dharan, Nepal
E-mail: sachinwagle100@gmail.com
[2] Saraswati Multiple Campus, Tribhuvan University, Kathmandu, Nepal
E-mail: durgapsdkhanal@gmail.com
[3] Central Department of Mathematics, Tribhuvan University, Kathmandu, Nepal
E-mail: tanka.nath.dhamala@gmail.com
[*] Corresponding author

Manuscript received: 10 February 2026; Revised: 10 June 2026; Accepted: 5 July 2026.

1. Introduction

Motivation. The lexicographic maximum static flow (LMSF) problem in a transportation network topology involves maximizing the simultaneous movement of a commodity flow, like people, goods, etc., from the fixed origin (sources) to the prescribed destination (sinks) without violating the capacity constraints. In the lexicographic maximum flow framework, flows are optimized according to the predefined priority patterns at the sources and sinks, such that the higher-priority terminals are satisfied first. Also, the flow location (FlowLoc) problem involves the installation of facilities at optimal locations. The main objective is to facilitate the commodity and minimizing the reduction in the network's maximum flow value. On the other hand, due to the minimum cut capacity, it is often not possible to fully utilize the outgoing arc capacities from the source. However, if intermediate nodes have storage capacity, the excess flow that cannot reach the sinks can be stored there. As a result the full arc capacity can be utilized. The integration of the models is very useful in the transportation network for optimizing the movement of the flow from the source to the sink by supplying the facility to the commodity.

Literature review. The maximum flow problem deals with the largest possible flow that can be transshipped from the source to the sink. The maximum static flow problems was first introduced and solved by Ford and Fulkerson [1]. They proved that the maximum amount of static flow in a network is equal to the bottleneck capacity. The maximum flow problem in abstract network was solved in [2]. The various maximum flow problems applied in evacuation planning are presented in [3, 4, 5].

The lexicographic maximum flow (LMF) problem concerns with the maximization of the flow value by a fixed leaving pattern at the sources and reaching pattern at the sinks. The lexicographic maximum static flow (LMSF) problem was solved by presenting a polynomial-time algorithm in [6, 7]. The lexicographic multi-objective network flow problems are found in Calvete and Mateo [8]. The application of lexicographic max flow in the context of evacuation planning can be found in [9, 10, 11]. The different network flow problem and models applicable in evacuation planning are found in survey paper of Dhamala [12].

In a network, if the out going arc capacity from the sources is greater than the minimum cut capacity, then the total capacity cannot be used. Pyakurel and Dempe [13] solved this problem by storing the excess flow at the intermediate nodes. The lexicographic contraflow problems with excess flow storage were solved by Pyakurel et al. [14]. The mathematical model about the fuzzy flow with the excess storage was investigated in [15, 16]. The different network flow problem with excess storage can be found in [2, 17, 18, 19, 20, 21, 22, 23, 24].

The flow location (FlowLoc) problem concerns with the determination of the exact locations for the facilities and optimization of the flow value. The first industrial facility location theory was introduced by Weber [25]. The different discrete facility location models were investigated by Daskin [26]. Hamacher et al. [27] combined the network flows theory with locational analysis and introduced the flow location (FlowLoc) problem. They developed the models and presented polynomial time algorithm and heuristic for single and multi-facility cases, respectively. Dhungana and Dhamala [28] solved maximum static and maximum dynamic ContraFlowLoc problems in polynomial time. The single and multi-quickest FLowLoc problems were solved by Nath et al. [29]. The maximum static and dynamic FlowLoc problems with the excess flow storage were introduced by Dhamala et al. [30]. They solved the single and multi-facility cases by polynomial time algorithms and heuristics, respectively. The lexicographic maximum flow location problem in a single source, multi-sink network was solved by Wagle et al. [31]. Using the temporally repeated approach, the maximum dynamic FlowLoc, earliest arrival FlowLoc and ContraFlowLoc problems were solved by Wagle et al. [32].

Research gap. In the existing literature, mathematical models for the lexicographic maximum static flow (LMSF) problem with and without excess-flow storage as well as the maximum FlowLoc problem have been studied in two terminal network. An integrated approach that deals with these problems with and without excess flow storage in a multi-terminal networks is a major research gap.

Our contribution. For the single as well as multi-facility, the lexicographic maximum static FlowLoc problems with and without excess flow storage are introduced in multi-terminal network for the first time. Polynomial time algorithms and heuristics are presented for the case of single and multi-facilities, respectively.

Organization of the paper. The basic notation used through out the paper are provided in Section 2. The mathematical models of the problems: lexicographic maximum static flow about multiple facility (LMSqFL) and single facility (LMS1FL) are provided in Section 3. This section provides the polynomial time heuristic and algorithm for multiple and single facility cases, respectively. Section 4 provides the results with excess flow storage in a single source and multi-sink network. Section 5 concludes the paper.

2. Preliminaries

Let, G be a static network having the set of vertices V with $|V| = n$, arcs A with $|A| = m$, sources $S = \{s_k, k = 1, 2, \ldots, h\}$ with priority order $s_1 \succ s_2 \succ \cdots \succ s_h$ (i.e. s_1 has the first priority and so on), intermediate nodes I and sinks $D = \{d_k, k = 1, 2, \ldots, l\}$ with order $d_1 \succ d_2 \succ \cdots \succ d_l$. Each arc $a = (u, v) \in A$ has an attribute, a nonnegative capacity $b_a : A \to \mathbb{Z}^+$ that bounds flow on the arc. Suppose that the set of incoming arc to and outgoing arc from $u \in V$ are denoted by $A^-(u)$ and $A^+(u)$, respectively. If $L \subseteq A$ be the set of possible locations for the given set of facilities $\mathbb{P}$, then the network is denoted by $G = (V, A, L, b_a, S, I, D)$. The functions $r : \mathbb{P} \to \mathbb{N}$ and $\mu : \mathbb{P} \to L$ are the size and allocation of the facilities on $a \in L$, respectively. Assume that the function $\eta : L \to \mathbb{N}$ bound the number of facilities on $a \in L$. The network is reduced to $G^R = (V, A, b_a^R, S, I, D)$ by installing facilities on L, where $b_a^R = b_a - \max\{r_p : \mu(p) = a\}$. Thus, if multiple facilities are installed on the same arc, its capacity is reduced by the largest facility size among them. We want to maximize the flow value in G^R.

3. Lexicographic FlowLoc without intermediate storage

In this section the LMSqFL problem, its integer programming formulation are introduced and solved by heuristic. Further more the single facility problem (i.e. $q = 1$) is solved by polynomial time algorithm.

Problem 1. *Let $G = (V, A, L, b_a, S, I, D)$ be a given network. The LMSqFL problem maximizes the prioritized $S - D$ flow value by locating the q facilities on $a \in L$ where each arc $a \in L$ can hold at most $\eta(a)$ facilities.*

Mathematical formulation. Let G be the given network with static flow function $x_a : A \to \mathbb{R}^+$. Let us define a decision variable

$$y_{ap} = \begin{cases} 1 & \text{if the facility } p \text{ is placed on } a \in L \\ 0 & \text{otherwise} \end{cases}$$

then the mathematical programming formulation of Problem 1 is to maximize Objective 1 subject to Constraints (2)–(7).

$$\max \sum_{a \in A^-(D)} x_a = \sum_{a \in A^+(S)} x_a \tag{1}$$

subject to

$$\sum_{a\in A^+(v)} x_a \quad - \quad \sum_{a\in A^-(v)} x_a = 0, \forall v \in V \setminus \{S, D\} \tag{2}$$

$$\sum_{p\in\mathbb{P}} y_{ap} \quad \leq \quad \eta(a), \forall a \in L \tag{3}$$

$$\sum_{a\in L} y_{ap} \quad = \quad 1, \forall p \in \mathbb{P} \tag{4}$$

$$0 \quad \leq \quad x_a + y_{ap} r_p \leq b_a, \forall p \in \mathbb{P}, a \in L \tag{5}$$

$$0 \quad \leq \quad x_a \leq b_a, \forall a \in A \tag{6}$$

$$y_{ap} \quad \in \quad \{0, 1\}, \forall a \in L, p \in \mathbb{P}. \tag{7}$$

Here, Constraints (2) show the flow conservation to each intermediate vertices. The number of facilities on any location are bounded by Constraints (3). According to Constraints (4), each facility has to be fixed on exactly one location. Constraints (5) and (6) bound the flow on each arc.

Hamacher et al. [27] reduced the q-FlowLoc problem in two terminal network to 3 SAT and proved that the problem is $\mathcal{NP}-$complete. Also the q-FlowLoc in multi-terminal is more complex so is $\mathcal{NP}-$complete (c.f. Theorem 1).

Theorem 1. *The LMSqFL problem is $\mathcal{NP}-$complete*

Note that taking $q = 1$ the problem is reduced to single facility (LMS1FL) problem which is to maximize Objective 1 subject to Constraints (2), (5)–(7).

3.1. **Solution procedure.** In this subsection, the LMSqFL and LMS1FL problems are solved.

3.1.1. *q-FlowLoc.*

. First of all, we compute the lexicographic maximum static flow with fixed priority ordering without placing any facility on the given locations as follows. Let $S_1 = \{s_1\}, S_2 = \{s_1, s_2\}, \ldots, S_h = \{s_k, k = 1, 2, \ldots, h\} = S$ and $D_1 = \{d_1\}, D_2 = \{d_1, d_2\}, \ldots, D_l = \{d_k, k = 1, 2, \ldots, l\} = D$ be the set of sources and sinks, respectively. Then we get the set inclusion, $S_1 \subset S_2 \subset \cdots \subset S_l = S$ and $D_1 \subset D_2 \subset \cdots \subset D_j = D$. According to [7], if $X(D)$ is the maximum flow value that enters the sinks in D, then $X(D_i), i = 1, 2, \ldots, l$ represents the maximum flow value to each D_i, which is a lexicographic maximum static flow on sinks. Similarly, $X(S_i)$ delivers the lexicographic maximum static flow value out from each source $S_i, i = 1, 2, \ldots, h$. We maximize out flow from S, which is pushed to D under a fixed priority ordering. The residual capacities of each location are then calculated and sorted them according to the capacities. Also, the facilities are sorted using their size. Now, the location $e_1 \in L$ with the largest residual capacity is selected and fixed $\eta(e_1)$ facilities there and continue until all the facilities are fixed on L. Note that for any location a_i, if the largest facility to be fixed is $p_k \in \mathbb{P}$ such that $r_{p_k} > b_{a_i}$, then $p_{k_1}, p_{k_2}, \ldots, p_{\eta(a_{i+1})}$ are fixed on the next location $a_{i+1} \in L$, and so on. After placing the given facilities, the network is then reduced to $G^R = (V, A, b_a^R, S, I, D)$. The LMSF is then computed on G^R. Now present a polynomial time heuristic, in Algorithm 1.

Example 1. *Let G be the given network with the set of locations $L = \{(s_2, y_1), (s_2, y_3), (s_1, y_2),$ $(s_1, y_3), (y_1, y_2), (y_2, d_3)\}$ (c.f. Fig. 1(a)). Suppose that $S = \{s_1,\ s_2\}$ and $D = \{d_1,\ d_2,\ d_3\}$ are the set of sources and sinks with order $s_1 \succ s_2$ and $d_1 \succ d_2 \succ d_3$, respectively. Also we have $S \succ D$. Let $\eta(a) = 3, \forall a \in L$ and $\mathbb{P} = \{p_1,\ p_2,\ p_3,\ p_4,\ p_5,\ p_6,\ p_7,\ p_8,\ p_9,\ p_{10}\}$ with size $r_{p_1} = 5$, $r_{p_2} = 4$, $r_{p_3} = 2$, $r_{p_4} = 6$, $r_{p_5} = 1$, $r_{p_6} = 3$, $r_{p_7} = 2$, $r_{p_8} = 1, r_{p_9} = 3, r_{p_{10}} = 4$.*

First of all using the solution procedure of [7], the LMSF is computed in G without placing any facility on L by introducing the super terminal nodes D_1 and D_2 (c.f Fig. 1(b)-1(f)). Using the paths: $D_2 - s_1 - y_1 - d_1 - D_1$, $D_2 - s_1 - y_3 - d_1 - D_1$, $D_2 - s_1 - y_1 - y_2 - d_2 - D_1$, $D_2 - s_1 - y_1 - d_2 - D_1$, $D_2 - s_1 - y_2 - d_2 - D_1$, $D_2 - s_1 - y_2 - d_3 - D_1$, $D_2 - s_2 - y_1 - d_2 - D_1$, $D_2 - s_2 - y_1 - d_3 - D_1$ and $D_2 - s_2 - y_3 - d_3 - D_1$, we can push 27 units of static flow. Of these, 21 and 6 units of flow

Algorithm 1: LMSqFL algorithm

Input : Network G , facilities $\mathbb{P}$, size $r : \mathbb{P} \to \mathbb{N}$.
Output: The LMSqFL, locations.

(1) Obtain the LMSF in G without fixing the facilities on any $a \in L$.
(2) Sort the facilities with their size: $r_{p_1} \succ r_{p_2} \succ \cdots \succ r_{p_q}$.
(3) Sort the locations according to their residual capacities: $a_1 \succ a_2 \succ \cdots \succ a_{|L|}$.
(4) Place the facilities $p_1, p_2, \ldots, p_{\alpha(a_1)}$ on $a_1 \in L$ and so on.
(5) When placing facilities at a location $a_i \in L$, if the largest facility that should be fixed on it is $p_k \in \mathbb{P}$. Also if $r_{p_k} > b_{a_i}$, then interchange a_i and a_{i+1} and so on. The network is reduced to $G^R = (V, A, b^R_a, b_a, S, I, D)$.
(6) Compute the maximum static flow with priority ordering in G^R.

are sent from s_1 and s_2, respectively. Consequently the sinks d_1, d_2 and d_3, receive 7,10 and 10 units of flow, respectively. The residual capacities $b^r_a = b_a - x_a$ for $a \in L$ are $b^r_{(s_2,y_1)} = 5$, $b^r_{(s_2,y_3)} = 3$, $b^r_{(s_1,y_2)} = 0$, $b^r_{(s_1,y_3)} = 0$, $b^r_{(y_1,y_2)} = 0$ and $b^r_{(y_2,d_3)} = 4$. Using the residual capacity the locations in L are sorted as: $(s_2, y_1) \succ (y_2, d_3) \succ (s_2, y_3) \succ (s_1, y_2) \succ (s_1, y_3) \succ (y_1, y_2)$. Also the facilities in $\mathbb{P}$ are sorted as there size: $p_4 \succ p_1 \succ p_2 \succ p_{10} \succ p_6 \succ p_9 \succ p_3 \succ p_7 \succ p_5 \succ p_8$.
Using Algorithm 1, (s_2, y_1) gets p_4, p_1, p_2, (y_2, d_3) gets p_{10}, p_6, p_9, (s_2, y_3) gets p_3, p_7, p_5 and (s_1, y_1) gets p_8. After fixing these facilities, the network is reduced to G^R (c.f. Fig. 2(a)). The LMSF is computed in G^R, (c.f.Fig. 2(b))

3.1.2. *1-FlowLoc.* To solve 1-FlowLoc problem, at first, LMSF is computed in G without placing the given facility p on any location $a \in L$ and the residual capacity of each $a \in L$ is calculated. We check, whether there is any $a \in L$ whose residual capacity is enough to host the facility. If such a location exists, p is fixed there. In this case LMSF is not reduced. If we cannot get such location, p is placed on one of the location $a_1 \in L$ and LMSF is computed in G^R. After this, p is removed from a_1, fix it on another $a_2 \in L$ and repeat the process. This process is continued to every remaining $a_i \in L$. Each time we get the lexicographic maximum flow value. Finally, we select the reduced network G^R in which overall the LMSF is maximized. Here, we present Algorithm 2 to obtain the LMS1FL.

Algorithm 2: LMS1FL algorithm

Input : Given network G, location L, facility p with size r_p
Output: The LMS1FL and location.

(1) Compute Steps (1)–(2) to obtain LMSF and residual capacity b^r_a of each $a \in L$.
(2) If there exists an $a \in L$ with $b^r_a \geq r_p$, place p on a. The LMSF obtained from Step 1 is the LMS1FL.
(3) If $b^r_a < r_p \forall a \in L$ proceed as follows.
   (a) Fix the facility p on an $a_1 \in L$, the network is reduced to $G^R = (V, A, b^R_a, S, I, D)$.
   (b) Obtain the LMSF in the network G^R.
   (c) Remove p from a_1, fix it on another $a_2 \in L$, repeat the Steps (3a)– (3b) and continue to each remaining $a \in L$.
   (d) Neglect $a \in L$ if $b_a < r_p$.
   (e) Pick up the location $a \in L$ overall maximum flow value.

Theorem 2. *The LMS1FL problem can be solved optimally in a polynomial time.*

Proof. First of all, we prove the the solution obtained from Algorithm 2 is feasible. Here, locating the facility, constructing reduced network and obtaining the LMSF in the reduced network are feasible.

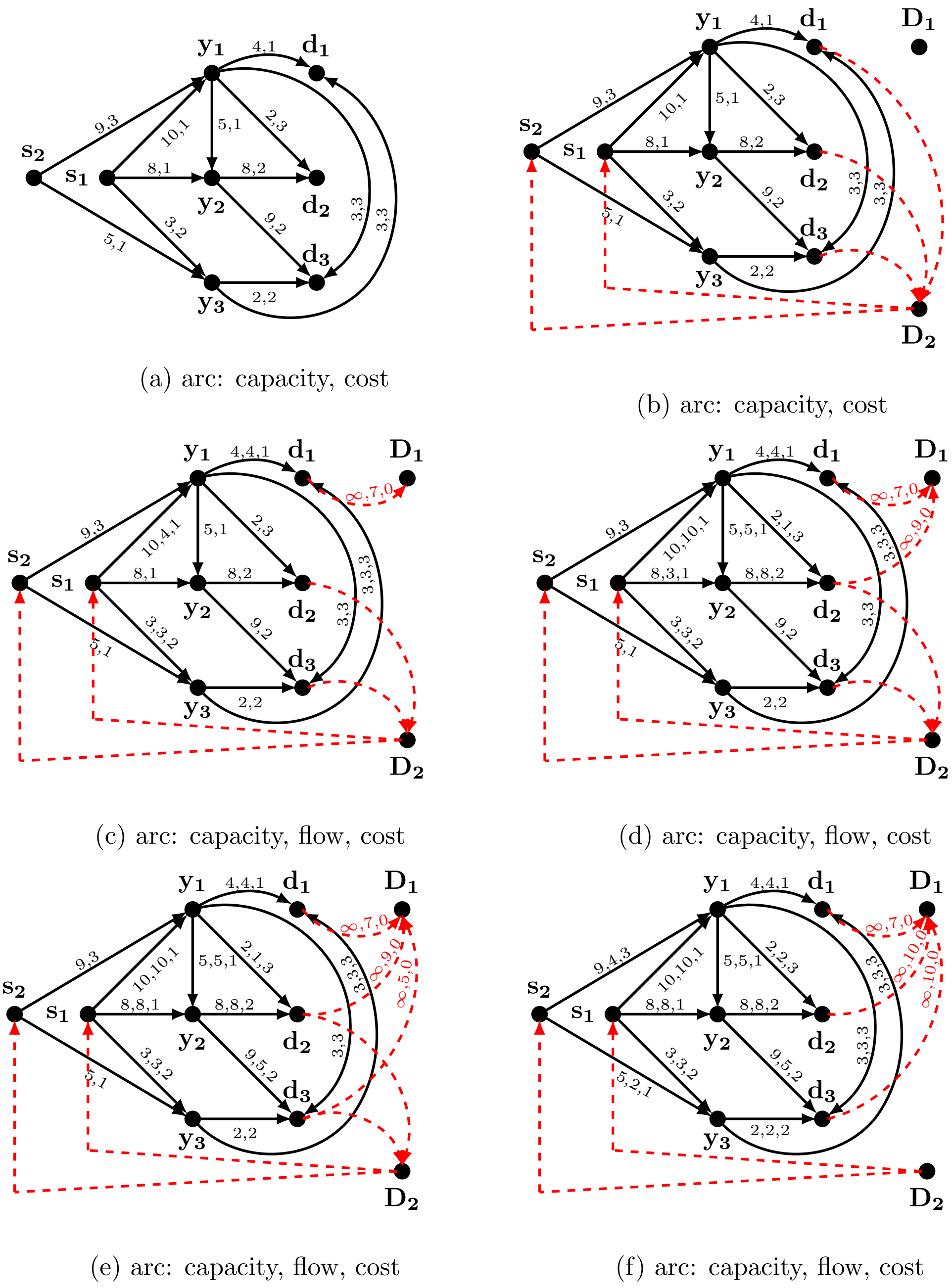

(a) arc: capacity, cost

(b) arc: capacity, cost

(c) arc: capacity, flow, cost

(d) arc: capacity, flow, cost

(e) arc: capacity, flow, cost

(f) arc: capacity, flow, cost

FIGURE 1. (a) Given network G, (b)–(f) process of obtaining LMSF in G

Now, we prove optimality. Using Algorithm 2, LMSF is computed in G without fixing the facility p, residual capacity b^r_a of each $a \in L$ is calculated and checked whether there exists an $a \in L$ with $b^r_a > r_p$. If such location finds, p is fixed there. The LMSF is LMS1FL. If $b^r_a < r_p$ is found for each $a \in L$, then p is fixed on a randomly selected location $a_1 \in L$, LMSF is computed in G^R as proceeding above and continue to all remaining $a_i \in L$. Each time we get an optimal solution. Finally, we select maximum flow value among these solutions which is the MS1FL solution.
Here, the Lex-maximum flow problem in G can be solved in $O(\delta mn)$ time, where δ is the number of terminals. Since the reduced network can be obtained in linear time, Algorithm 2 solves LMS1FL problem in $O(|L|\delta mn)$ time. $\square$

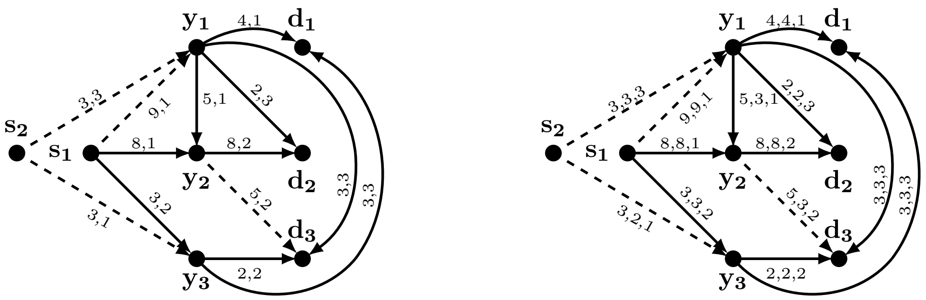

(a) arc: capacity, cost (b) arc: capacity, flow, cost

FIGURE 2. (a) Reduced network, (b) LMSqFL solution

Example 2. *Let G be a given network having set of the sources $S = \{s_1, s_2\}$ with order $s_1 \succ s_2$, set of sinks $D = \{d_1, d_2, d_3\}$ with order $d_1 \succ d_2 \succ d_3$ as in Fig. 1(a). Suppose that a facility p with size $r_p = 5$ has to be fixed on the exact location so that the maximum flow can be computed in G. For this, as in Example 1, LMSF is computed in G (which is 27 units) and the residual capacity b_a^r of each $a \in L$ is calculated. Since $b^r_{(s_2,y_1)=5}$, so p is fixed on (s_2, y_1). So there is no loss in the maximum flow value. Hence, the LMS1FL is 27 with the optimal location (s_2, y_1)*

Example 3. *If we consider $r_p = 6$ in Example 2, then $b_a^r < r_p$ for each $a \in L$. So we compute LMSF by fixing the facility p one at a time for each $a \in L$. Also arcs $(s_2, y_3), (s_1, y_3)$ and (y_1, y_2) have capacity less than r_p so are neglected form L. The LMSF values obtained by fixing p on the remaining locations are presented in Table 1.It is observed that the LMS1FL value equals 26, with the optimal location at (s_2, y_1).*

TABLE 1. LMS1FL solution

S.N.	*Location*	*Lex maximum flow vlue*					
		from s_1	*from s_2*	*at d_1*	*at d_2*	*at d_3*	*Total flow*
1	(s_2, y_1)	*21*	*5*	*7*	*10*	*9*	*26*
2	(s_1, y_2)	*15*	*6*	*7*	*9*	*5*	*21*
3	(y_2, d_3)	*21*	*4*	*7*	*10*	*8*	*25*

4. Lexicographic FlowLoc with Storage

In this section, we focus on storing the excess flow at the intermediate nodes. For this, the nodes are prioritized according to their longest distance from the source. In a multi-source and multi-sink network, the farthest node from a source may not be farthest from other sources, the intermediate node may not always be prioritized. So we restrict the network to a single source s while retaining multiple sinks D and extend the results of Sections 3 to the case where excess flow may be stored at intermediate nodes. For this, it is assumed that each intermediate node u has a storing capacity b_u such that $b_u \geq \sum_{a \in B(u)} b_a$. If $x_u : I \to \mathbb{R}^+$ be the static storage flow functions at $u \in I$, then the LMSqFL problem with excess flow storage is defined as follows.

Problem 2. *For the given $s - D$ network G, the LMSqFL problem with excess flow storage maximizes the amount of feasible flow leaving from s that is to be sent towards D plus the excess flow at I, by locating at most $\eta(a)$ facilities on the appropriate location $a \in L$.*

Mathematical formulation. Let G be a given network with fixed priority ordering on the sinks D. The LMSqFL problem with intermediate storage maximizes Objective (8) with respect to the constraints (3)-(7), (9)-(10).

$$\max \sum_{a\in A^+(s)} x_a = \sum_{a\in A^-(D)} x_a + \sum_{u\in I, b_u>0} x_u \tag{8}$$

$$x_u = \sum_{a\in A^-(u)} x_e - \sum_{a\in A^+(u)} x_a \geq 0, \forall u \in I \tag{9}$$

$$0 \leq x_u \leq b_u, \forall u \in I \tag{10}$$

$$\text{together with Constraints} \quad (3) - (7)$$

where Constraints (9) represent the excess flow and Constraints (10) bound the flow at each $u \in I$.

Theorem 3. *The LMSqFL problem with excess flow storage is $\mathcal{NP}$-complete.*

Note that, by taking $q = 1$, the problem is reduced to single facility (LMS1FL) problem with excess flow storage which is to maximize Objective 8 subject to Constraints (5)–(7), (9)–(10).

4.1. **Solution procedure.** In this subsection, we solve LMSqFL and LMS1FL problems with intermediate storage.

4.1.1. *q-FlowLoc.* To solve Problem 2, first we obtain the reduced network G^R as described in Subsection 3.1.1. To obtain the LMSqFL with intermediate storage, the solution procedure of [13] is used. We prioritize I according to the distance dist(s, u) of $u \in I$, create the virtual sink u' of $u \in I$ having dist$(u, u') = 0$ and $b_u = b_{u'}$. With this, the modified network $G^R_M = (V_M, A_M, b^R_a, b_u, s, I_M, D_M)$ is constructed, where I_M is the set of virtual sinks, $V_M = V \cup I_M$, $A_M = A \cup \{(u, u')\}$ and $D_M = D \cup I_M$. Here, G^R_M is a single source and multi-sink network without excess flow storage, where the sinks have priority order: $d_1 \succ d_2 \succ \cdots \succ d_l \succ u'_1 \succ u'_2 > \cdots \succ u'_i$. Note that $u_1 \in I$ farthest from s. Now, we compute the LMSF in G^R_M. Finally, the solution of G^R_M is transformed to G^R by eliminating I_M. Here, Algorithm 3 is presented to solve the problem.

Algorithm 3: LMSqFL with excess flow storage

Input : Given network G, facilities $\mathbb{P}$, size $r : \mathbb{P} \to \mathbb{N}$
Output: The LMSqFL solution with excess flow storage, and the locations.

(1) Compute Steps (1)- (5) of Algorithm 1 to obtain the reduced network $G^R = (V, A, b^R_a, b_u, s, I, D)$.
(2) Apply the shortest path algorithm to calculate the shortest distance dist$(s, u), \forall u \in I$.
(3) Give the first priority to the prioritized sinks D and next to the prioritized nodes I.
(4) Construct the modified network $G^R_M = (V_M, A_M, b^R_a, b_u, s, I_M, D_M)$ by creating the virtual sinks.
(5) Compute the LMSF in G^R_M, where max flow values at D are already obtained from Step (1).
(6) The solution of G^R_M is transformed to G^R by eliminating the virtual sinks.

Example 4. *Let G be a given network with source s, set of sinks $D = \{d_1, d_2, d_3\}$ with priority order $d_1 \succ d_2 \succ d_3$ and $L = \{(s, y_1), (s, y_2), (s, y_3), (y_1, y_2), (y_2, d_3)\ (y_3, d_3)\}$ as in Fig. 3(a). Suppose each $a \in L$ can hold 3 facilities. Let the intermediate nodes y_1, y_2 and y_3 have capacities: 10,8 and 9 respectively. Assume that, a set of facilities $\mathbb{P} = \{p_1, p_2, p_3, p_4, p_5, p_6, p_7, p_8, p_9, p_{10}\}$ with size $r_{p_1} = 5$, $r_{p_2} = 4$, $r_{p_3} = 2$, $r_{p_4} = 6$, $r_{p_5} = 1$, $r_{p_6} = 3$, $r_{p_7} = 2$, $r_{p_8} = 1, r_{p_9} = 3, r_{p_{10}} = 4$ has to fix on L. As in Example 1, LMSF is computed in G and residual capacity b^r_a, $a \in L$ is calculated. It is found that 1,0,2,0,4 and 0 are the residual capacity of (s, y_1), (s, y_2), (s, y_3), (y_1, y_2) and (y_2, d_3), respectively. Hence the priority order of the facilities and locations are: $p_4 \succ p_1 \succ p_2 \succ p_{10} \succ p_6 \succ p_9 \succ p_3 \succ p_7 \succ p_5 \succ p_8$ and $(y_2, d_3) \succ (s, y_3) \succ (s, y_1) \succ (s, y_2) \succ (y_1, y_2) \succ (y_3, d_3)$, respectively. Using Algorithm 3, the facilities: $\{p_4, p_1, p_2\}, \{p_{10}, p_6, p_9\}, \{p_3, p_7, p_5\}$ and p_8 are placed on $(y_2, d_3), (s, y_3), (s, y_1)$ and (s, y_2), respectively. The reduced network G^R is given in Fig. 3(b). The network is then modified to G^R_M (c.f. Fig. 3(c)). Finally the LMSF is computed in G^R_M. The LMSqFL with excess flow storage is 19 (c.f. Fig 3(d)).*

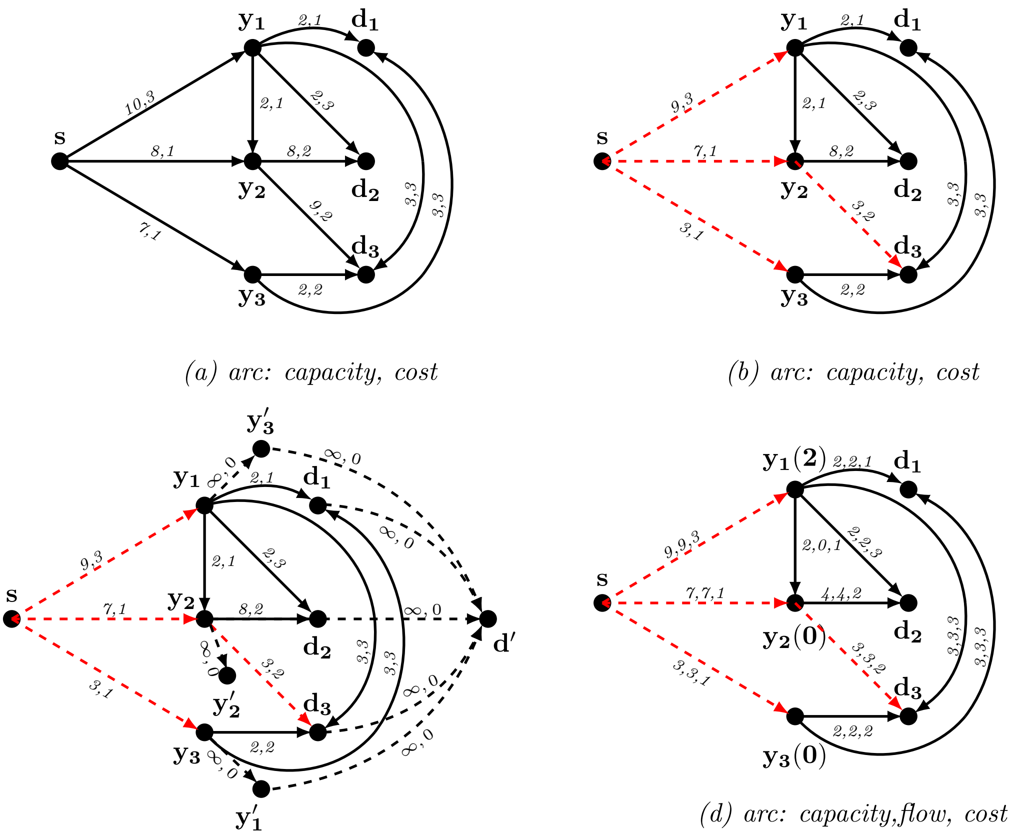

(a) *arc: capacity, cost* (b) *arc: capacity, cost*

(c) *arc: capacity, cost* (d) *arc: capacity,flow, cost*

FIGURE 3. (a) Given network, (b) reduced network, (c) modified network, (d) LMSqFL solution

4.1.2. *1-FlowLoc.* To solve the LMS1FL problem with excess flow storage, as in Subsection 3.1.2, the optimal reduced network G^R is constructed and modified to G^R_M (see Subsection 4.1.1). As in Subsection 4.1.1, LMSF computed in G^R_M. Here, we present Algorithm 4 to solve the problem.

Algorithm 4: LMS1FL with excess flow storage

Input : Given network G, facilities p, size r_p
Output: The LMS1FL with excess flow storage, and location.

(1) Compute Steps (1)- (3) of Algorithm 2 to obtain the reduced network $G^R = (V, A, b^R_a, b_u, s, I, D)$.
(2) Compute Steps (2)-(6) of Algorithm 3 to obtain the solution.

Theorem 4. *The LMS1FL problem with excess flow storage can be solved optimally in a polynomial time.*

Proof. To obtain the LMS1FL with excess flow storage, the reduced network G^R and modified network G^R_M are constructed in polynomial time. Here, G^R_M is a single source multi-sink network without storage at intermediate nodes. Using Theorem 2, the LMSF can be computed in G^R_M in polynomial time. □

5. Conclusions

Maximizing the flow value under a prescribed leaving pattern at the sources and/or a reaching pattern at the sinks (i.e. using lexicographic configuration) reduces conflicts in arc usage and helps ensure smoother flow in the network. The arc capacity is reduced by the size of the facility if we fix it at that arc. This may affect the maximum flow value in the network. However, it is very important to supply facilities to the commodity in the network. Also due to the bottleneck capacity the full arc capacity out from the source may not be used. If the intermediate nodes have storage capacity, then the excess flow can be stored there. This may improve the maximum flow value.

In this paper, integrating these concept, we have introduced the LMSqFL and LMS1FL problems with and without excess flow storage. We have investigated FlowLoc models of these problems. The multi-facility cases are solved by heuristics where as the single facility problem have solved in polynomial time. To the best of our knowledge, we have introduced and solved these problems for the first time. We aim to solve the problem using the installation charge of the facility on the location.

Limitations. The limitations of this study are:

- Priorities of sources and sinks are pre-determined.
- Facility establishment costs are not considered.
- All intermediate nodes are assumed to have sufficient storage capacity.

Acknowledgment. The first author (Sachin Wagle) thanks to the University Grants Commission, Nepal, for the Ph.D. research fellowship award 2023 with award no. PhD -79/80-S&T-10. Also, the first and second authors gratefully remember and cherish the late Prof. Dr. Urmila Pyakurel for her invaluable guidance, wisdom, and kindness throughout their research journey.

Author Declarations

- Funding - None available.
- Conflict of interest/Competing interests - None
- Ethics approval/declarations - Not applicable.
- Consent to participate - Not applicable.
- Consent for publication - Classical subscription mode without any payment.
- Availability of data and materials - Not used any additional data.
- Code availability - Not applicable.
- Authors' contributions - Tanka Nath Dhamala (conceptualization, methodology, revision, supervision); Sachin Wagle (conceptualization, documentation, methodology, editing); Durga Prasad Khanal (conceptualization, documentation, methodology, editing)

References

[1] L. R. Ford Jr and D. R. Fulkerson, "Maximal flow through a network," *Canadian journal of Mathematics*, vol. 8, pp. 399–404, 1956.

[2] D. P. Khanal, U. Pyakurel, and S. Dempe, "Temporally repeated maximum dynamic flow with intermediate storage," in *Operations Research Forum*, vol. 6, no. 3. Springer, 2025, p. 101.

[3] I. M. Adhikari, U. Pyakurel, and T. N. Dhamala, "An integrated solution approach for the time minimization evacuation planning problem." *International Journal of Operations Research*, vol. 17, no. 1, 2020.

[4] T. N. Dhamala, U. Pyakurel, and R. C. Dhungana, "Abstract contraflow models and solution procedures for evacuation planning," *Journal of Mathematics Research*, vol. 10, no. 4, pp. 89–100, 2018.

[5] U. Pyakurel, M. Goerigk, T. N. Dhamala, and H. W. Hamacher, *Transit dependent evacuation planning for Kathmandu valley: A case study*. Technische Universität Kaiserslautern, Fachbereich Mathematik, 2014.

[6] N. Megiddo, "Optimal flows in networks with multiple sources and sinks," *Mathematical Programming*, vol. 7, no. 1, pp. 97–107, 1974.

[7] E. Minieka, "Maximal, lexicographic, and dynamic network flows," *Operations Research*, vol. 21, no. 2, pp. 517–527, 1973.

[8] H. I. Calvete and P. M. Mateo, "Lexicographic optimisation in generalised network flow problems," *Journal of the Operational Research Society*, vol. 49, no. 5, pp. 519–529, 1998.

[9] I. M. Adhikari, "Lexicography in the context of evacuation planning issues," *Kaumodaki: Journal of Multidisciplinary Studies*, vol. 5, no. 1, pp. 84–92, 2025.

[10] U. Pyakurel and T. N. Dhamala, "Lexicographically contraflow problem for evacuation planning," in *Proceedings of the Second International Conference, Operations Research Society Nepal*, 2014, pp. 287–294.

[11] S. Wagle, "Network reconfiguration for prioritized flow improvement," Ph.D. dissertation, M. Phil Thesis, IOST, Tribhuvan University, Nepal, 2021.

[12] T. N. Dhamala, "A survey on models and algorithms for discrete evacuation planning network problems." *Journal of Industrial & Management Optimization*, vol. 11, no. 1, 2015.

[13] U. Pyakurel and S. Dempe, "Network flow with intermediate storage: models and algorithms," in *SN Operations Research Forum*, vol. 1, no. 4. Springer, 2020, p. 37.

[14] U. Pyakurel, S. Wagle, and M. Adhikari, "Efficient lane reversals for prioritized maximum flow," *International Journal of Innovative Science, Engineering & Technology*, vol. 7, pp. 354–363, 2020.

[15] E. Gerasimenko, "Dynamic flow algorithm with intermediate storage for emergency evacuation allowing lane reversal based on incomplete intuitionistic fuzzy preference relation," *The open transportation journal*, vol. 18, no. 1, 2024.

[16] E. Gerasimenko and V. Kureichik, "Hesitant fuzzy emergency decision-making for the maximum flow finding with intermediate storage at nodes," in *International Conference on Intelligent and Fuzzy Systems*. Springer, 2021, pp. 705–713.

[17] T. N. Dhamala, D. P. Khanal, and S. Nickel, "Optimizing evacuation via budget constrained maximum dynamic flow with speed variation and intermediate storage," *European Journal of Operational Research*, 2025.

[18] D. P. Khanal, "Multi-commodity dynamic flow problems with intermediate storage and varying transit times," Ph.D. dissertation, Institute of Science & Technology, 2023.

[19] D. P. Khanal, U. Pyakurel, and T. N. Dhamala, "Maximum multicommodity flow with intermediate storage," *Mathematical Problems in Engineering*, vol. 2021, no. 1, p. 5063207, 2021.

[20] B. P. Pangeni and T. N. Dhamala, "Maximum flow in hybrid network with intermediate storage," *OPSEARCH*, vol. 62, no. 2, pp. 833–849, 2025.

[21] U. Pyakurel, D. P. Khanal, and T. N. Dhamala, "Abstract network flow with intermediate storage for evacuation planning," *European Journal of Operational Research*, vol. 305, no. 3, pp. 1178–1193, 2023.

[22] T. N. Dhamala, M. C. Adhikari, D. P. Khanal, and U. Pyakurel, "Generalized maximum flow over time with intermediate storage," *Annals of Operations Research*, vol. 335, no. 1, pp. 111–134, 2024.

[23] D. P. Khanal and T. N. Dhamala, "Optimal dynamic contraflow with intermediate storage by anti-parallel path decomposition," in *Design Optimization Using Artificial Intelligence*. CRC Press, 2025, pp. 243–256.

[24] D. B. Amgain, D. P. Khanal, and T. Nath, "Temporally repeated fuzzy maximum dynamic flow with intermediate storage."

[25] A. Weber, "Uber den standort der industrien, tubingen," *Traduction anglaise: Theory of the location of industries. University Press, Chicago*, 1909.

[26] M. Daskin, "Network and discrete location: models, algorithms and applications," *Journal of the Operational Research Society*, vol. 48, no. 7, pp. 763–764, 1997.

[27] H. W. Hamacher, S. Heller, and B. Rupp, "Flow location (flowloc) problems: dynamic network flows and location models for evacuation planning," *Annals of Operations Research*, vol. 207, no. 1, pp. 161–180, 2013.

[28] R. C. Dhungana and T. N. Dhamala, "Maximum flowloc problems with network reconfiguration." *International Journal of Operations Research*, vol. 16, no. 1, 2019.

[29] H. N. Nath, U. Pyakurel, T. N. Dhamala, and S. Dempe, "Dynamic network flow location models and algorithms for quickest evacuation planning," *Journal of Industrial and Management Optimization*, vol. 17, no. 5, pp. 2943–2970, 2021.

[30] T. N. Dhamala, S. Wagle, and U. Pyakurel, "Flowloc problems with maximum excess flow," *Journal of Industrial and Management Optimization*, vol. 19, no. 12, pp. 8851–8870, 2023.

[31] S. Wagle, U. Pyakurel, and T. N. Dhamala, "Prioritized max-flowloc for evacuation planning," *The Nepali Mathematical Sciences Report*, vol. 40, no. 1-2, pp. 106–119, 2023.

[32] S. Wagle, D. P. Khanal, U. Pyakurel, S. Dempe, and T. N. Dhamala, "Maximum dynamic flowloc with intermediate storage: A temporally repeated approach," in *Operations Research Forum*, vol. 6, no. 1. Springer, 2024, p. 6.

Everest Advances in Science and Technology (EAST), Vol. 2, No. 1, 2026
ISSN: 3102-0410 (Print), 3102-0429 (Online)
DOI: 10.3126/east.v2i1.98619

A Nepali-Accented English Evaluation Dataset for Automatic Speech Recognition

SANTOSH DAHAL[1]*, KIRAN CHANDRA DAHAL[2]

Abstract. Automatic speech recognition (ASR) systems perform strongly on native-English benchmarks, yet their accuracy degrades sharply when the input speech comes from under-represented non-native accents. Nepali-accented English is particularly under-served: existing resources either focus on native Nepali speech, cover broader multi-accent settings without dedicated Nepali evaluation, or provide only limited Nepali-accent coverage. This paper presents a Nepali-accented English evaluation dataset designed to support robust ASR benchmarking under accent mismatch. The corpus was collected through a web-based platform that did not collect directly identifying metadata and contains recordings from 57 speakers. Each session follows a fixed 22-prompt protocol consisting of 11 phonetic prompts, 10 domain prompts, and 1 spontaneous prompt, providing complementary coverage of pronunciation, topical vocabulary, and natural speaking style. In addition to transcribed speech, the dataset includes participant metadata for coarse exploratory subgroup analysis and speaker-level manual recording-quality labels. Manual quality assessment shows that 50.9% of sessions are clean and 42.1% contain only mild noise. As a descriptive reference, open-source ASR baselines are substantially worse on this corpus than the corresponding LibriSpeech test-clean values reported in official model cards, reaching 38.15–55.00% WER on the collected set versus reported 2–4% WER on LibriSpeech test-clean. These baseline results position the corpus as a practical held-out resource for evaluating accent robustness and out-of-distribution generalization on Nepali-accented English.

Keywords: automatic speech recognition, Nepali-accented English, accented speech, evaluation dataset, word error rate

[1],[2] Department of Electronics and Computer Engineering, Institute of Engineering, Thapathali Campus, Tribhuvan University
E-mail: santosh.080msise16@tcioe.edu.np;
dahalkc@tcioe.edu.np
* Corresponding author

Manuscript received: 19 February 2026; Revised: 13 June 2026; Accepted: 15 July 2026.

1. Introduction

Recent ASR systems achieve very low error rates on standard native-English benchmarks, but these gains do not transfer reliably to accented speech. The gap is especially important for under-represented accents, where both training and evaluation resources remain scarce. Nepali-accented English belongs to this category: it appears only sparsely in existing corpora even though English is widely used in education, technology, public services, and professional communication in Nepal. The lack of a focused benchmark makes it difficult to answer a basic question: how well do current ASR models handle English spoken by Nepali L1 speakers? Multi-accent resources such as L2-ARCTIC provide valuable non-native English data, but they do not include Nepali speakers [1]. Other accented-English corpora cover a broader set of foreign accents yet still omit Nepali as a target evaluation accent [2]. Meanwhile, Svarah demonstrates the importance of evaluating ASR on Indian accents and includes a Nepali-accented English category, but the speakers in that subset are from India rather than Nepal. Its scope is also broader than a Nepali-specific benchmark and is not centered on controlled phonetic coverage for this accent [3]. Existing Nepali ASR work, in contrast, focuses on speech recognition for the Nepali language itself rather than English spoken with a Nepali accent [4, 5].

This paper presents a dataset created to fill that gap. The corpus is designed as an *evaluation-focused* benchmark rather than a large-scale pretraining resource. The collection protocol aims to keep per-speaker coverage comparable while still capturing three complementary dimensions of variation: phonetic coverage, domain vocabulary, and spontaneous speech. The resulting dataset is then used as a held-out benchmark for ASR evaluation.

The main contributions of this paper are as follows:

- A Nepali-accented English evaluation corpus with 57 speakers collected through a consistent prompt-based protocol.
- A prompt design that combines phonetic prompts, domain prompts, and spontaneous speech within every participant session.
- Metadata and speaker-level recording-quality annotations that support coarse exploratory subgroup analysis and data-quality filtering.
- Baseline evidence that modern open-source ASR systems degrade substantially on the corpus compared with their reported LibriSpeech performance.

2. Related Work

Several existing datasets motivate the need for a Nepali-specific accented-English benchmark. L2-ARCTIC is a widely used non-native English corpus containing six L1 accent groups and carefully read speech, making it valuable for accent adaptation research; however, it does not include Nepali-accented English [1]. The CSLU Foreign Accented English corpus broadens accent coverage, but it is likewise not targeted toward Nepali speakers [2]. Svarah extends the evaluation landscape by covering Indian-accented English and explicitly includes a Nepali-accented speech subset, showing that ASR systems experience pronounced degradation when moving away from native-English benchmarks. However, the speakers in that subset are from India rather than Nepal [3]. Still, Svarah is a multilingual-accent benchmark spanning many language backgrounds and speaking conditions; it does not offer a Nepali-only evaluation design with fixed per-speaker phonetic and topical coverage.

On the Nepali side, prior work has concentrated on ASR for native Nepali speech using convolutional, recurrent, and Conformer-style architectures [**?**, 4, 5]. These studies are important for low-resource speech technology in Nepal, but they address a different problem from recognizing English produced with Nepali phonetic transfer. The present corpus therefore complements both lines of work: it is not a replacement for broad multi-accent English datasets, and it is not a native Nepali ASR corpus; instead, it specifically targets evaluation of Nepali-accented English.

Table 1. Overview of the Nepali-accented English evaluation dataset.

Aspect	**Description**
Primary goal	Held-out evaluation benchmark for Nepali-accented English ASR
Participants	57 speakers
Collection mode	Remote recording through a web-based platform without directly identifying metadata
Speech styles	Controlled read speech and one spontaneous response per session
Session structure	22 prompts per participant
Prompt mix	11 phonetic prompts, 10 domain prompts, 1 spontaneous prompt
Metadata	Age range, gender, highest qualification, occupation, ethnicity, district of origin, and topic of interest
Quality annotation	Manual speaker-level recording-quality label on a five-point ordinal scale
Intended use	Accent-robust ASR evaluation, coarse subgroup analysis, and error analysis

Table 2. Prompt design used in each recording session.

Prompt type	**Count**	**Purpose**
Phonetic	11	Cover English phonemes and common phonotactic contexts using CMU Arctic-style prompts
Domain	10	Introduce topic-specific vocabulary from domains such as technology, science, history, environment, culture, health, education, geography, and society
Spontaneous	1	Elicit natural speech from a participant-selected interest topic such as sports, reading, music, or cooking

3. Dataset Design and Collection Protocol

The dataset was built around a simple design principle: each participant should contribute a comparable but diverse set of utterances so that the final corpus supports controlled evaluation rather than ad hoc sampling. Table 1 summarizes the overall design.

3.1. **Collection Platform and Workflow.** Data were collected through a dedicated single-page web application designed for guided remote participation. The participant workflow contains four stages: session initialization without directly identifying metadata, consent acknowledgement with metadata entry, prompt-wise recording with re-record or retry options, and final review with submission. This structure was chosen to keep the data collection experience lightweight while still improving consistency across speakers and sessions.

The platform records only analysis-oriented metadata needed for curation and descriptive analysis. Session information is stored together with timestamps and completion status, allowing the final evaluation set to be curated without collecting direct personal identifiers. Because speech recordings can still be identifying, any dataset distribution or reuse should remain within participant-consent boundaries and appropriate access control.

3.2. **Prompt Design.** Each participant session contains 22 prompts drawn from three prompt types, shown in Table 2. The phonetic prompts target pronunciation coverage, the domain prompts broaden lexical and topical variation, and the spontaneous prompt captures less constrained speech with more natural discourse structure.

The phonetic prompts were designed in the style of the CMU Arctic prompt inventory [6] and organized to keep phonetic coverage balanced across participants. Domain prompts were curated

Table 3. ASR back end used for spontaneous transcription.

Item	Value
Model	`gemini-3.1-pro-preview`
No-speech token	`[NO_SPEECH]` (exact)

from public text sources, then normalized for readability and collection consistency. The spontaneous prompt is tied to the participant's self-reported topic of interest so that the dataset includes at least one segment with less scripted speaking behavior per session.

3.3. **Transcription of Spontaneous Speech.** Spontaneous responses were derived from elicited recordings whose metadata designated the spontaneous condition, as distinct from read phonetic or domain-matched material. For each item, the corresponding waveform was assigned a short speaker identifier and a unique session–utterance ID, and stored under the `spontaneous` partition of the corpus.

Segmentation. Recordings longer than 20 s were split prior to automatic transcription. Silence boundaries were approximated with FFMPEG `silencedetect` using a noise threshold of −35 dB and a minimum silence duration of 1.0 s. Resulting speech intervals were further constrained so that no segment exceeded 20 s, with a minimum segment length of 0.25 s. Recordings of 20 s or less were left as a single segment.

Automatic speech recognition. Each segment was transcribed with the Google Generative Language API using the Python `google-genai` client. The generative model was `gemini-3.1-pro-preview`. For each call, the model received the audio in WAV form (`audio/wav`) together with a fixed text instruction. Whitespace in the model output was normalized; an empty hypothesis was treated as a no-speech case. Table 3 summarizes the ASR back end used for spontaneous transcription.

Instruction prompt (exact text). The following prompt was used for transcription:

```
Listen to this audio and transcribe the speech.
Rules:
- Output only the spoken words, in English (including any Nepali-accented
English as heard).
- No timestamps, no speaker labels, no ‘‘Transcript:’’ prefix, no
markdown.
- If there is no intelligible speech, output exactly: [NO_SPEECH]
```

Transcript assembly. For multi-segment recordings, per-segment transcriptions were concatenated in temporal order with inter-word spaces to form one line per session–utterance, stored in `trans.txt` in the form *utterance-id* followed by the full transcript, consistent with the read side of the corpus. Segments for which the model returned the token `[NO_SPEECH]` (exactly) were treated as non-contributing at the segment level when assembling the line.

3.4. **Metadata and Privacy.** The collection form supports age range (18–30, 30–45, 45–60, 60+), gender, highest qualification, occupation domain, ethnicity category, district of origin, and topic of interest. In the present paper, we report six summary attributes for analysis: gender, ethnicity, age group, highest qualification, occupation domain, and topic of interest. District of origin was collected during data acquisition but is not broken down in the aggregate tables below.

4. Corpus Statistics and Recording Quality

The final evaluation set contains 57 participants. Figure 1 shows the geographic distribution of participants by reported district of origin across Nepal, while Tables 4 and 5 summarize the collected metadata distributions.

The collected subset is not demographically balanced, but it does capture meaningful variation in age, education, ethnicity, occupation, and self-selected topics. The distribution is dominated by younger adults (78.9% in the 18–30 range), participants with bachelor's-level education (66.7%), and contributors from engineering or technology backgrounds (54.4%). Topic-of-interest responses

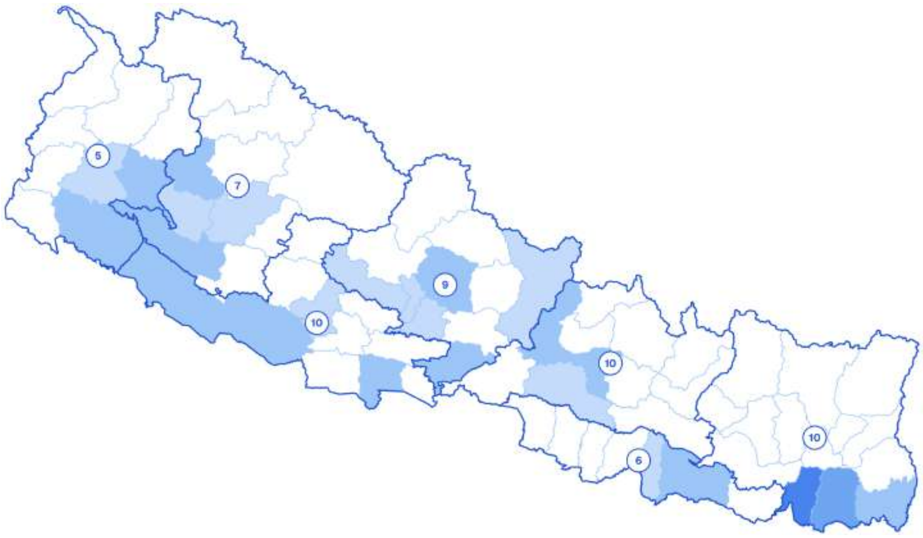

Figure 1. Geographic distribution of participants by reported district of origin across Nepal.

Table 4. Participant profile summary ($n = 57$).

Attribute	Category	Count	%
Gender	Male	37	64.9
Gender	Female	20	35.1
Age group	18–30	45	78.9
Age group	30–45	10	17.5
Age group	45–60	2	3.5
Qualification	Bachelors	38	66.7
Qualification	Masters	12	21.1
Qualification	+2 (higher secondary)	7	12.3

are led by travelling, sports, and reading, which helps diversify the spontaneous-speech portion of the corpus.

4.1. **Speaker-Level Recording Quality.** Because all utterances from a participant were recorded within a single session, ambient noise, microphone placement, and room acoustics are largely session-constant. For that reason, recording quality was summarized at the speaker level rather than the utterance level. The annotation procedure sampled three utterances uniformly at random for each speaker, played them under fixed listening conditions, and assigned one of five ordinal labels: clean, mild noise, noisy, very noisy, or bad recording.

Table 6 shows the resulting distribution. The large majority of sessions (93.0%) fall in the clean or mild-noise categories, suggesting that the dataset is generally suitable for ASR benchmarking while still preserving realistic variability from remote volunteer recordings. These labels should be interpreted as coarse speaker-level tags for exploratory filtering and error analysis rather than as a formally validated acoustic annotation layer.

5. Benchmark Evaluation with Open-Source ASR Models

To assess the difficulty of the corpus, the dataset was used as a held-out benchmark for several open-source ASR models. Table 7 contrasts the combined WER on the collected set with each model's reported LibriSpeech test-clean WER from the corresponding official model card [7, 8, 9, 10].

TABLE 5. Participant context attributes ($n = 57$).

Attribute	**Category**	**Count**	**%**
Ethnicity	Brahmin/Chhetri	43	75.4
Ethnicity	Madhesi	6	10.5
Ethnicity	Janajati	4	7.0
Ethnicity	Other	2	3.5
Ethnicity	Newar	1	1.8
Ethnicity	Dalit	1	1.8
Occupation	Engineering/Technology	31	54.4
Occupation	Student	13	22.8
Occupation	Health/Medicine	3	5.3
Occupation	Business/Management	3	5.3
Occupation	Education/Teaching	2	3.5
Occupation	Science	2	3.5
Occupation	Law/Government	2	3.5
Occupation	Other	1	1.8
Interest	Travelling	17	29.8
Interest	Sports	14	24.6
Interest	Reading	9	15.8
Interest	Movies/Entertainment	5	8.8
Interest	Painting/Drawing	4	7.0
Interest	Music	4	7.0
Interest	Cooking	3	5.3
Interest	Stitching/Sewing	1	1.8

TABLE 6. Manual speaker-level recording-quality labels.

Label	**Count**	**%**
Clean	29	50.9
Mild noise	24	42.1
Noisy	3	5.3
Very noisy	0	0.0
Bad recording	1	1.8

TABLE 7. Reported LibriSpeech test-clean WER from official model cards and observed WER on the collected Nepali-accented English set.

Model	**LibriSpeech test-clean**	**Collected set**
Conformer Small	3.70	46.00
Conformer Large	2.20	38.30
Whisper Small	3.43	55.00
Whisper Large	3.00	38.15

Because the LibriSpeech values are taken from official model cards rather than a single re-run pipeline, the comparison should be interpreted as a descriptive cross-dataset reference rather than a controlled estimate of accent-only degradation. For fully reproducible reuse, the benchmark release should package the corresponding reference transcripts, normalization rules, and scoring scripts alongside the audio and metadata.

All tested models degrade substantially on the collected benchmark. Even the strongest large-model baselines, Conformer Large and Whisper Large, rise from approximately 2–3% WER on LibriSpeech test-clean to about 38% WER on the Nepali-accented set. The smaller models degrade even more sharply, with WER reaching 46.00% for Conformer Small and 55.00% for Whisper Small. These descriptive results reinforce the dataset's usefulness as a stress test for accent robustness and show that strong native-English benchmark performance does not necessarily imply reliable performance on Nepali-accented English under the present evaluation setup.

6. Discussion, Intended Use, and Limitations

The dataset has three main strengths. First, it combines controlled phonetic coverage with broader topical prompts and spontaneous speech, making it more informative than a read-only benchmark. Second, the metadata support coarse exploratory subgroup and robustness analysis beyond a single aggregate WER number, although several categories remain too small for strong comparative claims. Third, the recording-quality labels make it possible to analyze or filter the effect of session noise on ASR performance.

At the same time, the current corpus has clear limitations. The participant pool is skewed toward younger, highly educated speakers and is dominated by engineering or technology backgrounds. The recordings are also collected remotely rather than under studio conditions, which introduces device and environment variability even when most sessions remain usable. Finally, the dataset is best suited to held-out evaluation and error analysis; its size and collection design are not intended to replace broader multi-accent training corpora.

We therefore recommend the corpus for three use cases in particular. The first is benchmarking accent-robust ASR. The second is analyzing errors across prompt types or coarse participant groupings. The third is measuring out-of-distribution generalization when Nepali-accented English is absent from training data. We do not recommend using the metadata for speaker profiling or any ranking of participants; the metadata are included to support coarse exploratory subgroup and robustness analysis, not identity inference.

7. Conclusion

This paper presented a Nepali-accented English evaluation dataset for ASR containing recordings from 57 speakers collected through a structured web-based protocol. The dataset pairs fixed per-session prompt coverage with demographic and quality annotations, creating a practical benchmark for studying accent robustness. Baseline experiments with open-source Conformer and Whisper models show substantially higher WER on the collected set than the corresponding published LibriSpeech reference values, reinforcing the need for targeted evaluation on underrepresented accents. The corpus provides a useful foundation for future work on Nepali-accented English recognition, accent-aware adaptation, and more inclusive ASR evaluation.

The dataset is publicly available on GitHub at the project repository.

References

[1] G. Zhao, S. Sonsaat, A. Silpachai, I. Lucic, E. Chukharev-Hudilainen, J. Levis, and R. Gutierrez-Osuna, "L2-ARCTIC: A non-native English speech corpus," in *Proc. Interspeech 2018*, 2018, pp. 2783–2787.

[2] T. Lander. (2022) CSLU: Foreign accented English. Dataset, Release 1.2, doi: 10.5683/SP2/K7EQTE.

[3] T. Javed, K. S. Bhogale, A. Raman, P. Mukherjee, S. Cauligi, K. Thopalli, S. Ghosh, V. Seshadri, and M. M. Khapra, "Svarah: Evaluating English ASR systems on Indian accents," in *Proc. Interspeech 2023*, 2023, pp. 4064–4068.

[4] J. Banjara, K. R. Mishra, J. Rathi, K. Karki, and S. Shakya, "Nepali speech recognition using CNN and sequence models," in *Proc. IEEE Int. Conf. Mach. Learn. Appl. Netw. Technol. (ICMLANT)*, 2020, pp. 1–5.

[5] M. Dhakal *et al.*, "Automatic speech recognition for the Nepali language using CNN, bidirectional LSTM and ResNet," in *Proc. IEEE Int. Conf. Inventive Comput. Technol. (ICICT)*, 2022, pp. 515–521.

[6] J. Kominek and A. W. Black, "The CMU ARCTIC speech databases," Lang. Technol. Inst., Carnegie Mellon Univ., Pittsburgh, PA, USA, Tech. Rep. Tech. Rep. CMU-LTI-03-177, 2003.

[7] NVIDIA. (2024) NVIDIA Conformer-CTC Small (en-US). Hugging Face model card. [Online]. Available: https://huggingface.co/nvidia/stt_en_conformer_ctc_small

[8] ——. (2024) NVIDIA Conformer-CTC Large (en-US). Hugging Face model card. [Online]. Available: https://huggingface.co/nvidia/stt_en_conformer_ctc_large

[9] OpenAI. (2022) Whisper Small. Hugging Face model card. [Online]. Available: https://huggingface.co/openai/whisper-small

[10] ——. (2022) Whisper Large-v2. Hugging Face model card. [Online]. Available: https://huggingface.co/openai/whisper-large-v2

Everest Advances in Science and Technology (EAST), Vol. 2, No. 1, 2026
ISSN: 3102-0410 (Print), 3102-0429 (Online)
DOI: 10.3126/east.v2i1.98620

Impacts of Variation Order in the Government Building Projects of Nepal

SHASHANKA KARKI[1*], ASHISH BANSTOLA[2], GOPAL BHATTARAI[3]

Abstract. Variation order is the major hurdle in the construction of government building projects in Nepal. This study investigates the impacts of variation order in the government building project of Nepal. For this, using Likert scale, 415 responses were collected from the professionals involved in construction of government buildings in Nepal. Results showed that cost fluctuation, difficulty in project management, complexity to beneficiaries, delay in project progress, difficulty in fixation of new rate, and erosion of professional integrity are the impacts of variation order in government building projects of Nepal. It is recommended that experts should be hired for design and supervision by involving contractors in the design phase. Proper verification of design and documentation should be ensured before soliciting tender. Also, in-depth exploration of site condition should be done, and good communication and coordination between stakeholders should be maintained to reduce variation order.

Keywords: Variation Order,Government Projects,Procurement.

[1] School of Engineering, Edith Cowan University, Perth, WA, Australia
E-mail: shashanka.karki@gmail.com
[2,3] Department of Urban Development and Building Construction, Nepal
E-mail: 076mstre003.ashish@pcampus.edu.np
E-mail: engbhatt@gmail.com
* Corresponding author

Manuscript received: 12 February 2026; Revised: 15 June 2026; Accepted: 5 July 2026

1. Introduction

Construction industry is a major contributor to Nepal's economy as it contributes 5.5% to GDP of Nepal[1]. Nepal government allocated 19% of total budget for capital expenditure for fiscal year (F/Y) 2024/25[2]. However, the construction industry is facing many difficulties and Variation Order is one of them. Variation orders consist of the additions, subtraction and modification in terms of quantity, plan, scope and time of works [3]. Building construction projects involve complex works and varieties of materials and monuments building consist of various traditional materials which cannot be accurately determined in advance due to which variation orders occur. Variation orders cannot be avoided completely and inclusion of variation clauses in contracts is the proof that a project can't be finished without alteration[4].

Variation orders are causing various impacts in the projects like increase in project completion time, cost rise, increase in overhead expenses, difficulty in project management, increase in disputes etc.[5]. Although, variation is causing various threats to the building project of Nepal, few research is carried out in the perspective of Nepal. So, this study investigates the impacts of variation order in governmental building projects of Nepal.

2. Literature Review

Variation order which is also called change order is the deviation from original plan and scope of projects with change in term and conditions. Variation can be addictive; which prolongs time of contract with incline in materials and cost of the project, and deductive; which reduces project time, cost and quantity of the materials [6]. According to Tunde et al. (2015), the impacts of variation order in construction projects of Nigeria are: rise in project cost, difficulty to maintain work cash flow, decrease in contractor's profit, abandonment of project, degradation in quality of works, logistics delay, demolition and reworks[7]. Variation can affect project time and cost but if managed properly the contractor could experience profit with variation order [8].

Variation primarily impacts project cost and time. Variation increased project cost by 30.1% and project time surged by 30%. However, it also has a positive aspect as due to variation, quality of construction works improved by 24% [9]. Variation order is imminent in building construction projects and affected most of building construction projects of Lagos, Nigeria. Dosumu and Aigbavboa (2017) studied and found that 12.5% of building projects faced 1–5% variation, 43.7% of projects faced 5–10% variation, 12.5% of building subjected to 10–15% variation and 31.3% of buildings projects suffered 15% variation in Lagos, Nigeria[10].

Mohamed (2013) studied impacts of variation order in public works of Malaysia and found impacts are: decline in professional relations, late payment, surge in overhead expenses, delay in procurement of materials, additional payment for contractor, effect on progress of project, lack of proper safety condition, rise in claim dispute and delay in schedule of works[11]. Also, variation order is reducing labor productivity and surge in disputes between contracted parties [12].

3. Methodology

In order to identify impacts of variation order in government building projects of Nepal, quantitative research methods are utilized. The study population comprised of client, contractor and consultant who were working in government building projects of Nepal at the time of study. Questionnaires were prepared by detailed study of literatures and consisted of a 5-point Likert scale (where, 1=Strongly Disagree; 2=Disagree; 3=Neutral; 4=Agree; 5=Strongly Agree). A total of 415 responses were received which were analyzed by Principal Component Analysis (PCA) with the use of SPSS software.

4. Result and discussions

4.1. **Information of Respondents.** Variables after data extraction are presented below in the table:

Table 1. Respondents Data Summary ($n = 415$)

Variable	Frequency	Percent	Variable	Frequency	Percent
Respondent Type			**Respondent Position**		
Client	170	40.96	Office/Site Engineer	145	34.93
Contractor	195	46.98	Site Supervisor	180	43.37
Consultant	50	12.04	Others	90	21.68
Education level			**Work experience (years)**		
Diploma	130	31.32	1–4	220	53.01
Bachelor's	170	40.96	4–8	125	30.12
Master's	40	9.63	8–12	50	12.04
Others	75	18.07	>12	20	4.81

4.2. **Kaiser–Meyer–Olkin (KMO) and Bartlett's tests.** In order to test the suitability of data for PCA, Kaiser–Meyer–Olkin (KMO) and Bartlett's tests were carried out.

Table 2. KMO and Bartlett's Test Results

Test	Statistic	Value
Kaiser–Meyer–Olkin Measure of Sampling Adequacy		0.810
Bartlett's Test of Sphericity	Approx. Chi-Square	1780.981
	Degrees of Freedom (df)	378
	Significance (p-value)	< 0.001

From Table 2, the value of the KMO sampling adequacy was 0.810 which is higher than 0.7 and lies on a suitable range [13]. Furthermore, Bartlett's test was significant ($\chi^2 = 1780.981$, df $= 378$, Sig. $= 0.000$) which shows significant correlation exists between the variables due to which it is suitable for factor analysis [14].

4.3. **Factor Extraction for Safety Measure Barriers.** Principal component analysis (PCA) with Varimax rotation was performed to identify the underlying components of the safety measure barriers. The number of components retained was determined using Kaiser's criterion (eigenvalue > 1) and the scree plot. As shown in Fig. 1, a clear inflection point was observed after the sixth component, indicating that six components should be retained for further analysis.
The eigenvalues and the percentage of variance explained by the retained components are presented in Table 3.
As presented in Table 3, the first six components had eigenvalues greater than 1.0 and were therefore retained based on Kaiser's criterion. The first, second, third, fourth, fifth, and sixth components had eigenvalues of 7.025, 5.684, 2.755, 1.915, 1.647, and 1.209, respectively, explaining 25.088%, 20.301%, 9.841%, 6.840%, 5.883%, and 4.318% of the total variance. Collectively, these six components explained 72.271% of the total variance, exceeding the recommended minimum threshold of 50% (Sarstedt and Mooi, 2014). Therefore, the extracted components adequately represent the underlying structure of the dataset and were considered suitable for subsequent analysis.

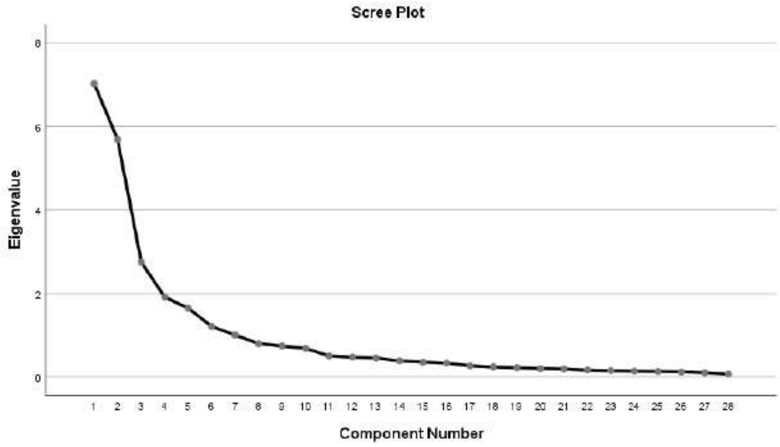

FIGURE 1. Scree plot obtained from principal component analysis.

TABLE 3. Eigenvalues and total variance explained (Extraction method: Principal Component Analysis)

Component	Initial Eigenvalues			Extraction Loadings			Rotation Loadings		
	Total	% Var.	Cum. %	Total	% Var.	Cum. %	Total	% Var.	Cum. %
1	7.025	25.088	25.088	7.025	25.088	25.088	7.025	25.088	25.088
2	5.684	20.301	45.389	5.684	20.301	45.389	5.684	20.301	45.389
3	2.755	9.841	55.230	2.755	9.841	55.230	2.755	9.841	55.230
4	1.915	6.840	62.069	1.915	6.840	62.069	1.915	6.840	62.069
5	1.647	5.883	67.953	1.647	5.883	67.953	1.647	5.883	67.953
6	1.209	4.318	72.271	1.209	4.318	72.271	1.209	4.318	72.271
7	0.908	3.601	75.872						
8	0.799	2.853	78.725						
9	0.742	2.651	81.376						
10	0.686	2.450	83.826						
11	0.505	1.803	85.629						
12	0.476	1.702	87.331						
13	0.456	1.630	88.960						
14	0.387	1.382	90.343						
15	0.357	1.274	91.617						
16	0.334	1.195	92.812						
17	0.267	0.954	93.765						
18	0.240	0.859	94.624						
19	0.223	0.796	95.420						
20	0.202	0.721	96.142						
21	0.191	0.683	96.824						
22	0.166	0.593	97.417						
23	0.153	0.547	97.963						
24	0.141	0.505	98.468						
25	0.133	0.476	98.944						
26	0.122	0.436	99.380						
27	0.103	0.367	99.747						
28	0.071	0.253	100.000						

4.4. **Factor Rotation and Interpretation of the Impacts of Variation Orders.** The rotated component matrix obtained from principal component analysis is presented in Table 4. A loading threshold of 0.60 was adopted to identify significant factor loadings (Kline, 2014). Variables with factor loadings below 0.60 were excluded from further interpretation.

As shown in Table 4, 19 out of the 28 impact variables were identified as significant and grouped into six components. A factor loading threshold of 0.60 was adopted based on the recommendation of Kline (2014). Accordingly, only variables with factor loadings greater than 0.60 were retained for interpretation, while the remaining nine variables with lower factor loadings were excluded from further analysis.

TABLE 4. Rotated component matrix of the impacts of variation orders in government building projects in Nepal

Impact of Variation Orders	**Cost Fluctuation**	**Difficulty in Project Management**	**Complexity to Beneficiaries**	**Delay in Project Progress**	**Difficulty in Fixation of New Rates**	**Erosion of Professional Integrity**
Increase in project cost	0.891					
Increase in overhead expenses	0.882					
Additional payments for contractors	0.879					
Additional material costs	0.877					
Cost for redesign	0.861					
Inflation costs	0.857					
Decrease in project cost	0.854					
Difficulty in manpower management		0.786				
Delay in decision-making process due to disputes		0.749				
Difficulty for beneficiaries to perform daily work			0.863			
Rework and demolition			0.835			
Increase in project completion time				0.810		
Procurement delay				0.787		
Slower project progress and schedule hampering				0.763		
Difficulty in rate negotiation					0.893	
Disputes regarding variation orders of provisional sum items					0.884	
Difficulty in balancing the contract with respect to the original contract					0.859	
Degradation of professional relations						0.776
Damage to the reputation of clients and contractors						0.770

Component 1: Cost Fluctuation. The first component, *Cost Fluctuation*, comprises seven variables: increase in project cost, increase in overhead expenses, additional payments to contractors, additional material costs, redesign costs, inflation costs, and decrease in project cost. These variables exhibited factor loadings of 0.891, 0.882, 0.879, 0.877, 0.861, 0.857, and 0.854, respectively. This component had an eigenvalue of 7.025 and explained 25.088% of the total variance. The results indicate that variation orders have a substantial impact on the financial performance of government building projects in Nepal.
These findings are consistent with Koirala et al. (2022), who reported that variation orders increased the overall project cost by 9.85% to 21.02% in government building projects in Nepal[15]. In contrast, Tuloli et al. (2021) observed that a reduction in the scope of work in an educational building project resulted in a decrease in the overall project cost[16].

Component 2: Difficulty in Project Management. The second component, *Difficulty in Project Management*, consists of two variables: difficulty in manpower management and delays in the decision-making process due to disputes. These variables had factor loadings of 0.786 and 0.749, respectively. The component had an eigenvalue of 5.684 and explained 20.301% of the total variance, indicating that variation orders significantly complicate project management activities.
This finding is consistent with Dansoh et al. (2017), who reported that managing variation orders in construction projects is challenging because of weak management practices, conflicting stakeholder interests, coordination difficulties, communication barriers, trust issues, and bureaucratic procedures[17].

Component 3: Complexity to Beneficiaries. The third component, *Complexity to Beneficiaries*, comprises two variables: difficulty for beneficiaries to carry out their daily activities and rework and demolition. These variables exhibited factor loadings of 0.863 and 0.835, respectively. This component had an eigenvalue of 2.755 and explained 9.841% of the total variance. The findings suggest that variation orders adversely affect project beneficiaries by disrupting normal activities and increasing rework.

Component 4: Delay in Project Progress. The fourth component, *Delay in Project Progress*, consists of three variables: increase in project completion time, procurement delay, and slower project

progress due to schedule disruption. These variables had factor loadings of 0.810, 0.787, and 0.763, respectively. This component had an eigenvalue of 1.915 and explained 6.840% of the total variance.
These findings are supported by Yadeta (2016), who identified delays in project completion as the most significant impact of variation orders in public building projects in Ethiopia[18]. Similarly, Hanif et al. (2016) reported that variation orders contributed to substantial project delays and cost overruns in hydropower projects in Pakistan[19].

Component 5: Difficulty in Fixation of New Rate. The fifth component, *Difficulty in Fixation of New Rate*, comprises three variables: difficulty in rate negotiation, disputes regarding variation orders for provisional sum items, and difficulty in balancing the revised contract with the original contract. These variables exhibited factor loadings of 0.893, 0.884, and 0.859, respectively. This component had an eigenvalue of 1.647 and explained 5.883% of the total variance, indicating that variation orders create significant challenges in determining equitable rates for additional or modified works.

Component 6: Erosion of Professional Integrity. The sixth component, *Erosion of Professional Integrity*, consists of two variables: degradation of professional relationships and damage to the reputation of clients and contractors. These variables had factor loadings of 0.776 and 0.770, respectively. This component had an eigenvalue of 1.209 and explained 4.318% of the total variance. The findings indicate that variation orders may weaken professional relationships and negatively affect the reputation of project stakeholders.
This finding is consistent with Donold (2014), who reported that disagreements regarding contract terms, additional costs, and the implementation of variation orders often lead to disputes, thereby damaging professional relationships among project participants[20].

4.5. **Reliability of Retained Components.** The internal consistency of the six retained components was evaluated using Cronbach's alpha (α). As presented in Table 5, the Cronbach's alpha values ranged from 0.702 to 0.952, exceeding the recommended threshold of 0.70 (Taber, 2018). These results indicate that all retained components possess satisfactory internal consistency and are therefore considered reliable for subsequent analysis.

Table 5. Cronbach's alpha values of the retained components

Component	**Cronbach's Alpha (α)**
Cost Fluctuation	0.952
Difficulty in Project Management	0.739
Complexity to Beneficiaries	0.866
Delay in Project Progress	0.796
Difficulty in Fixation of New Rate	0.903
Erosion of Professional Integrity	0.702

5. Conclusion and Recommendations

This study investigated the impacts of variation orders in government building projects in Nepal using principal component analysis. Six major components were identified: *Cost Fluctuation*, *Difficulty in Project Management*, *Complexity to Beneficiaries*, *Delay in Project Progress*, *Difficulty in Fixation of New Rate*, and *Erosion of Professional Integrity.* Among these, *Cost Fluctuation* was the most influential component, explaining the highest proportion of the total variance.
The findings indicate that variation orders significantly affect project cost, schedule, project management, beneficiary convenience, contractual negotiations, and professional relationships among project stakeholders. Therefore, minimizing unnecessary variation orders is essential for improving the performance of government building projects in Nepal.

Based on the findings, it is recommended that project objectives and design requirements be clearly defined before project commencement. Contractors should be involved during the design stage to enhance constructability and reduce design-related changes. In addition, effective coordination and communication among clients, consultants, and contractors should be maintained throughout the project lifecycle. Employing experienced professionals during the design and supervision phases, conducting comprehensive site investigations, and assessing material availability before finalizing the design can further reduce the occurrence of variation orders and their associated impacts.

6. Research Implications

Variation orders continue to pose significant challenges to the successful delivery of government building projects in Nepal. The findings of this study provide empirical evidence on the major impacts of variation orders and their underlying dimensions, which can support evidence-based decision-making by government agencies, project owners, consultants, and contractors.

The identified components may assist policymakers in formulating strategies and guidelines to minimize unnecessary variation orders and improve project performance. Furthermore, the results provide a useful reference for construction professionals in implementing effective project planning, design management, and contract administration practices. This study also establishes a foundation for future research on variation orders in different types of construction projects and geographical contexts, allowing researchers to compare findings and develop appropriate mitigation strategies.

References

[1] Ministry of Finance, Government of Nepal, "Nepal economic survey 2022/23," Ministry of Finance, Kathmandu, Nepal, Tech. Rep., 2023.

[2] S. Dhakal. (2024) What's inside fiscal budget 2081/82? Key highlights and programs.

[3] M. E. Achkar, "Variation order time impact in unconventional contracts," *Unpublished Report*, 2022.

[4] K. Mishra and P. Aithal, "Financial impact assessment of time overrun: A case of second small towns water supply and sanitation sector project, Nepal," *Int. J. Appl. Eng. Manag. Lett.*, vol. 4, no. 2, pp. 159–173, 2020.

[5] A. Uchenna, "Causes and effects of variations on civil engineering construction projects in Nigeria," Master's thesis, Unpublished Master's thesis, 2023.

[6] P. Darcy. (2023) Construction change orders: What they are, and what they're not.

[7] B. Tunde, I. Ayodele, and A. Namadi, "The causes of variation order of construction industry in Nigeria," in *Proc. Acad. Conf. African Scholar Publications and Research International on African Sustainable Development.* African Scholar Publications, 2015, pp. 1–13.

[8] A. Y. Martanti, T. P. Kasih, and F. H. Tanojo, "Study of work order variation and its influence on project performance in terms of cost and implementation time in the Tenjoresmi area arrangement project," *Asian J. Eng. Soc. Health*, vol. 3, no. 2, pp. 112–125, 2024.

[9] J. Duah, "An investigation of variation orders in building projects at the University for Development Studies, Tamale," *Ghana J. High. Educ. Manag.*, vol. 8, no. 1, pp. 1–18, 2022.

[10] O. S. Dosumu and C. O. Aigbavboa, "Effects of variation on project cost of selected building projects in Lagos State," in *Proc. ICCREM 2017: Int. Conf. Construction and Real Estate Management.* American Society of Civil Engineers, 2017.

[11] S. A. A. Mohamed, "Management of variation order in Public Work Department Malaysia construction project," Master's thesis, Universiti Teknologi Malaysia, Johor, Malaysia, 2013.

[12] S. J. Thakar, "A study on impacts of variation order in construction projects," *Int. Res. J. Eng. Technol.*, vol. 7, no. 7, pp. 5365–5373, 2020.

[13] StatisticsHowTo. (2016) Kaiser-Meyer-Olkin (KMO) test for sampling adequacy. [Online]. Available: https://www.statisticshowto.com/kaiser-meyer-olkin/

[14] N. Shrestha, "Factor analysis as a tool for survey analysis," *Amer. J. Appl. Math. Stat.*, vol. 9, no. 1, pp. 4–11, 2021.

[15] N. Koirala, P. Sharma, L. P. Sapkota, M. Yogi, A. Pokharel, and H. Yogi, "Variations order of building construction project: A case from Nepal," *Nature: J. Nat. Sci.*, vol. 21, no. 1, pp. 45–58, 2022.

[16] M. Tuloli, A. Utiarahman, and M. Palilati, "Analysis of causes and impact of variation order in the education building project in Gorontalo Province," in *IOP Conf. Ser.: Mater. Sci. Eng.*, vol. 1122. IOP Publishing, 2021, p. 022065.

[17] A. Dansoh, D. Oteng, S. Frimpong, J. Ayarkwa, D. K. Ahadzie, E. Adinyira, T. Kwofie, and D.-G. Owusu-Manu, "Challenges associated with project teams in managing variations on construction projects," in *Proc. 6th Int. Conf. Infrastructure Development (ICIDA) in Africa.* KNUST Press, 2017, pp. 121–131.

[18] A. E. Yadeta, “The impact of variation orders on public building projects,” *Int. J. Constr. Eng. Manag.*, vol. 5, no. 3, pp. 86–91, 2016.

[19] H. Hanif, M. B. Khurshid, S. M. Lindhard, and Z. Aslam, “Impact of variation orders on time and cost in mega hydropower projects of Pakistan,” *J. Constr. Dev. Countries*, vol. 21, no. 2, pp. 37–53, 2016.

[20] R. M. Donold, “Causes, effects and possible solutions of variation order in project performance,” Master’s thesis, Universiti Malaysia Pahang, 2014.

Everest Advances in Science and Technology (EAST), Vol. 2, No. 1, 2026
ISSN: 3102-0410 (Print), 3102-0429 (Online)
DOI: 10.3126/east.v2i1.98621

Adaptive Low-Light Image Enhancement Selection Using Random Forest: Validation on ExDark Dataset with BRISQUE Quality Assessment

ANIL THAPA[1*], KOBID KARKEE[2]

Abstract. Low-light image enhancement remains challenging for resource-constrained edge devices where deep learning models are often too computationally expensive. This research presents an adaptive selection framework that learns to choose between two comple- mentary enhancement strategies—a lightweight logarithmic boost and a sophisticated realistic fusion method—based on image characteristics. A Random Forest classifier trained on 7 PCA-reduced features from 1,385 images achieves 86.1% accuracy for method selection, with 5-fold cross-validation confirming robust performance (84.3% ± 1.2%). This method is tested on ExDark dataset containing 1200 images from 12 classes. Object detection uses blur and image quality metrics (BRISQUE, NIQE, PIQE) along with YOLOv8. The results show clear differences, with a 2.1% improvement in detection rate ($p = 0.017$), a 10% improvement in BRISQUE quality ($p < 0.001$), and a 26.7% increase in brightness ($p < 0.001$). When combined with other methods, it leaves behind Histogram Smoothing (61.5%) and CLAHE (68.0%) and matches Gamma Correction (70.5%), but BRISQUE scores (21.93 and 26.78) make images look more natural. On closer inspection, certain categories such as bicycles show significant increases, but boats, bottles, and dining tables do not receive better detection scores. It shows clear scenarios where this approach works well and where it doesn't. Additionally, this method takes up almost no space at just 1.86 MB and runs at 18.6 FPS on an average CPU without requiring any special graphics hardware. This makes it handy for edge devices like cameras or phones, especially in low light where sharpening edges and retaining detail is critical. The method is simple, requires little space and offers better results for certain classes without requiring large resources.

Keywords: Adaptive Enhancement, Low-Light Imaging, Random Forest, Interpretable Machine Learning, Edge Computing, Computer Vision

[1] Department of Computer Engineering, Everest Engineering College, Sanepa -02, Lalitpur
E-mail: bineilthapa@gmail.com
[2] Department of Electronics and Computer Engineering, Thapathali Campus,IOE, Tribhuvan University, Nepal
E-mail: kobid@tcioe.edu.np
* Corresponding author

Manuscript received: 10 March 2026; Revised: 17 June 2026; Accepted: 24 July 2026.

1. Introduction

Digital imaging plays an essential role in modern society from consumer photography to critical applications such as surveillance, autonomous driving, and medical field [1]. In reality, image quality is often hampered by inadequate lighting conditions which may lead to low contrast high noise levels and loss of color fidelity. Low-light images encounters low signal-to-noise ratio (SNR) resulting in loss of important details. These issues are particularly risks mission-critical sectors such as fleet telematics [2], smart vehicle monitoring [3], and medical endoscopy [4].

1.1. **Related Work.** The literature on Low-Light Image Enhancement (LLIE) has falls under three basic categories. The first is traditional approaches like Histogram Equalization [5], CLAHE, and Retinex-based methods [6, 7] remain popular mostly due to their computational efficiency. The paper on LIME [8] estimates illumination maps while the paper on exposure fusion frameworks [9, 10] combine multiple exposures.The second one falls under deep Learning methods like LLNet models [11] and Subsequent models like SID [12], RetinexNet [13], Zero-DCE [14] and EnlightenGAN [15] The former marked the transition to deep auto-encoders while the later models achieve impressive results with a trade off on computational resources. The last one falls under Lightweight models emphasizing efficiency with architectures like MobileNetV2 [16], EfficientNet [17] and specialized fast networks [18, 19, 20] focusing on edge deployment.

1.2. **Motivation and Contributions.** Despite the substantial progress in the low light image enhancement, there are various gaps that remain like deep learning models being computationally expensive for edge devices, existing methods employing a ”one-size-fits-all” approach ignoring image-specific attributes, and limited validation on diverse low-light datasets with standardized quality metrics.
This paper addresses these gaps with the following contributions:

(1) **Adaptive selection framework:** A Random Forest classifier model that learns to choose between logarithmic boost and realistic fusion based on 14 statistical image features is developed to achieve maximum acccuracy.
(2) **Comprehensive ExDark validation:** The developed model is evaluaed on 1,200 images across 12 categories using BRISQUE, NIQE, PIQE, and YOLOv8 detection.
(3) **Lightweight deployment:** The model developed will be small in size with acceptable frame per second on CPU which helps in enabling edge deployment without GPU acceleration.

1.3. **Paper Organization.** The structure of the paper is organized as follows: Section 2 presents the theoretical foundations. Section 3 comprises the proposed methodology along with the mathematical formulations, theoretical background, and system design. Section 4 presents experimental results including BRISQUE analysis and detection performance. Section 5 discusses findings and limitations of the model developed while Section 6 concludes with recommendations.

2. Theoretical Foundations

2.1. **The Retinex Model.** The elemental basis behind the work is the Retinex theory [6], which models an image as the product of reflectance $\mathbf{R}$ and illumination $\mathbf{L}$ given by :

$$\mathbf{I}(x,y) = \mathbf{L}(x,y) \cdot \mathbf{R}(x,y) \tag{1}$$

In low-light scenarios, illumination $\mathbf{L}$ is the dominant source of degradation, often characterized by low mean luminance and high noise variance. Our research utilizes this disintegration to strip these two parameters to enhance $\mathbf{L}$ while preserving $\mathbf{R}$, which comprises high-frequency structural details essential for perceptual quality.

2.2. **Logarithmic Image Processing (LIP).** The standard linear algebraic operations on RGB color space produces problems like out-of-range effects and pixel truncation while performing shadow enhancement. To overcome this issue, the proposed model uses Logarithmic Image Processing framework [21] which defines a mathematically consistent model for processing images as transmitted light given by:

$$f \oplus g = f + g - \frac{fg}{M} \tag{2}$$

where M is maximum intensity. This non-linear approach prevents over-saturation common in linear scaling.

2.3. **No-Reference Image Quality Assessment.** Evaluating the image enhancement techniques poses a problem when there is no ground-truth reference image available. In order to solve this issue, no-reference quality metrics are applied for the objective measurement of perceptual quality. There is a wide range of quality metrics where **BRISQUE** (Blind/Referenceless Image Spatial Quality Evaluator) [22] applies NSS in estimating distortion by measuring the level of deviation of the scene from statistical characteristics of natural images; therefore, a smaller BRISQUE value indicates better visual quality. In order to achieve a more holistic quality evaluation, a set of metrics complement BRISQUE. Such metrics are **NIQE** [23] and **PIQE** [24].

2.4. **Random Forest for Adaptive Selection.** Random Forest [25] employs the idea of collective wisdom of a large group of decision trees using bootstrapping algorithm. This model benefits being highly robust to over fitting and it automatically captures complex relationship between variables in non linear domain. The main strength of this model is the interpretability in ranking the feature importance, allowing to find the obvious features dominant in decision making.

3. Methodology

3.1. **Overview.** This architecture is made up of five primary modules which includes enhancement techniques (logarithmic boost and realistic fusion), feature extraction, dimensionality reduction using principal component analysis, training of Random Forest classifiers, and finally an inference process

3.2. **Enhancement Methods.**

3.2.1. *Logarithmic Boost (Method 0).* The logarithmic boost provides a simple, computationally efficient enhancement:

$$I_{\text{enhanced}} = \frac{\log(1 + \alpha I_{\text{in}})}{\log(1 + \alpha)} \tag{3}$$

where α is adaptively set based on mean luminance μ:

$$\alpha = \begin{cases} 85 & \text{if } \mu < 0.1 \\ 75 & \text{if } 0.1 \le \mu < 0.15 \\ 65 & \text{if } 0.15 \le \mu < 0.2 \\ 55 & \text{otherwise} \end{cases} \tag{4}$$

After logarithmic mapping, brightness is normalized to target mean of 0.55.

3.2.2. *Realistic Fusion (Method 1).* The realistic fusion method combines multiple techniques:
Step 1: Denoising. Non-local means denoising [**?**] with $h = 1.1\hat{\sigma}$.
Step 2: Multi-exposure simulation. Two complementary enhancements:

$$I_{\log} = 1.3 \cdot \frac{\log(1 + 100 I_{\text{clean}})}{\log(101)} \tag{5}$$

$$I_{\text{gamma}} = I_{\text{clean}}^{0.22} \tag{6}$$

Step 3: Edge-preserving fusion. Weight map from Sobel edge detection.
Step 4: Color balancing. Gray-world normalization [?].
Step 5: Saturation recovery. HSV saturation boost of 1.35×.

3.3. **Feature Extraction.** We extract 14 statistical features including mean luminance, standard deviation, entropy, noise level, Michelson contrast, skewness, kurtosis, local variance, illumination uniformity, colorfulness, saturation mean, hue standard deviation, and higher-order moments.

3.4. **Principal Component Analysis.** PCA reduces the 14-dimensional feature space to 7 components retaining 92.1% variance, computed as:

$$\mathbf{x}_{\text{PCA}} = \mathbf{Z}\mathbf{W}_7 \in \mathbb{R}^7 \tag{7}$$

3.5. **Random Forest Classifier.** The Random Forest classifier (100 trees, max depth 15) predicts optimal enhancement method $\hat{y} \in \{0, 1\}$:

$$\hat{y} = f\left(\left(\frac{\mathbf{x}_{\text{test}} - \boldsymbol{\mu}}{\boldsymbol{\sigma}}\right)\mathbf{W}_7\right) \tag{8}$$

4. Experimental Results

4.1. **Dataset and Experimental Setup.** The ExDark dataset [?] contains 7,363 low-light images across 12 object categories. We selected 1,200 images (100 per category) for validation. Training used 1,385 images from LOL [13] and SID [12] datasets.
All experiments used an Intel i7-12700K CPU with 32GB RAM. No GPU acceleration was used. Statistical significance was assessed using paired t-tests.

4.2. **Method Selection Performance.** The Random Forest classifier achieved 86.1% accuracy on held-out test data, with 5-fold cross-validation confirming robust performance (84.3% ± 1.2%). Realistic fusion was selected for 71.3% of ExDark images, consistent with training distribution (67.9%).

4.3. **Qualitative Results: Success and Failure Cases.** To provide intuitive understanding of the model's behavior, we present representative success and failure cases. The success cases (7 images) demonstrate where the RF selector correctly identified the optimal enhancement method, while the failure cases (3 images) reveal systematic patterns in model errors.

4.3.1. *Success Case Analysis.* Figures 1 through 7 show cases where the model correctly identified the optimal enhancement method.

FIGURE 1. Success case: Image 4.

Figure 2. Success case: Image 5.

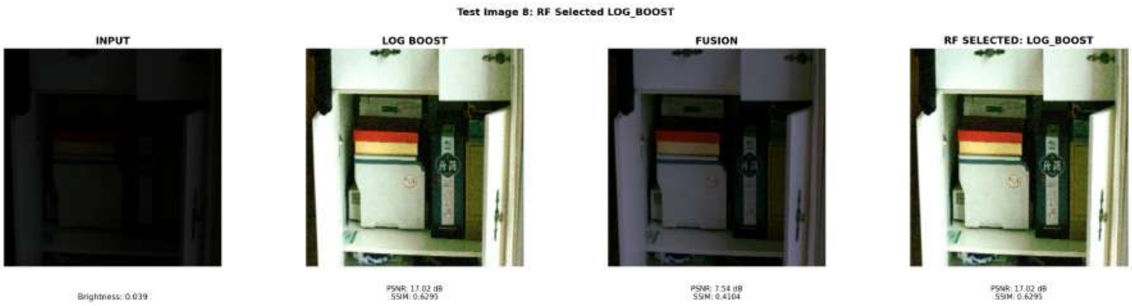

Figure 3. Success case: Image 8.

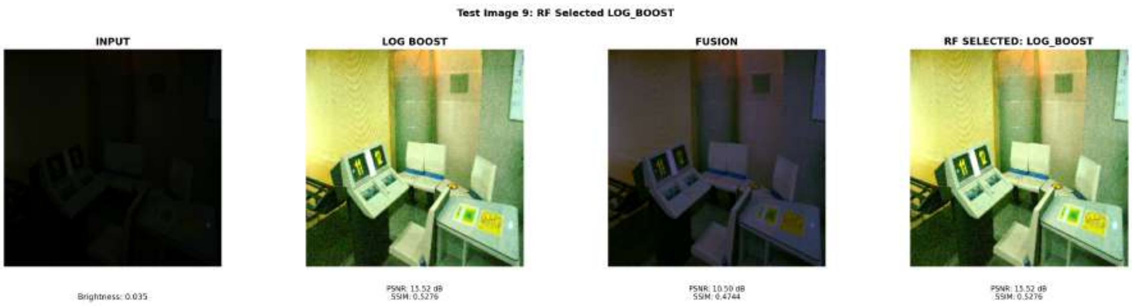

Figure 4. Success case: Image 9.

Figure 5. Success case: Image 10.

FIGURE 6. Success case: Image 11.

FIGURE 7. Success case: Image 13 - RF correctly selected Fusion.

Analysis: The figure 1 to Figure 5 shows the images in which Log Boost was correctly selected as it achieves superior PSNR and SSIM values. In Figure 6 and 7, Realistic Fusion was correctly selected despite lower PSNR, because its higher SSIM aligns with the 70% SSIM weighting criterion. The error maps show minimal reconstruction error (mean diff 0.02-0.04), confirming the quality of the selected enhancement.

4.3.2. *Failure Case Analysis.* Figures 8 through 10 show cases where the model made incorrect predictions.

FIGURE 8. Failure case: Image 0 - RF incorrectly selected Fusion (should be Log Boost).

FIGURE 9. Failure case: Image 1 - RF incorrectly selected Fusion (should be Log Boost).

FIGURE 10. Failure case: Image 2 - RF incorrectly selected Fusion (should be Log Boost).

Analysis: The figures 8-10 shows three failure cases show the model selecting Fusion when Log Boost is clearly superior as indicated by higher PSNR and SSIM. This systematic bias toward Fusion likely occurs from the imbalanced training distribution with 67.9% fusion and 32.1% log boost enhancement methods. Clearly, no failure cases were observed where the model selected Log Boost when Fusion was optimal. Tables 1 and 2 shows the failure cases and failure case analysis respectively.

TABLE 1. Failure cases

Image	Ground Truth	RF Prediction
Image 0	Log Boost	Fusion
Image 1	Log Boost	Fusion
Image 2	Log Boost	Fusion

TABLE 2. Analysis of failure case

Image	Ground Truth	RF Prediction	Log Boost Score	Fusion Score	Difference
0	Log Boost	Fusion	0.7355	0.5842	0.1513
1	Log Boost	Fusion	0.7739	0.5171	0.2568
2	Log Boost	Fusion	0.8028	0.5887	0.2141

4.4. **Image Quality Assessment (BRISQUE Focus).** Table 3 shows the no-reference quality metrics comparing both original and enhanced images on the ExDark dataset.

Table 3. No-reference image quality assessment results

Metric	Original	Enhanced	Change	p-value
BRISQUE ↓	24.37	21.93	+10.0% ✓	<0.001
NIQE ↓	8.27	8.45	−2.1% **X**	<0.001
PIQE ↓	52.99	53.13	−0.3% **X**	<0.001
Brightness ↑	0.153	0.194	+26.7% ✓	<0.001

✓= improvement, **X** = degradation

Analysis: In Table 3 BRISQUE shows the improvement by 10.0% ($p < 0.001$), indicating that enhanced images more closely resemble natural scene statistics. The slight degradation in NIQE (−2.1%) and PIQE (−0.3%) represents an acceptable trade-off for the substantial brightness gain (+26.7%).

4.5. **Object Detection Performance.** Table 4 presents YOLOv8 detection metrics on ExDark dataset.

Table 4. Object detection performance

Metric	Original	Enhanced	Change	p-value
Detection Accuracy	60.1%	61.1%	+1.0%	0.191
Detection Count	2.80	2.86	+2.1% ✓	0.017

Detection count improved significantly (+2.1%, $p = 0.017$), indicating previously invisible objects become detectable. Detection accuracy shows a positive but non-significant trend (+1.0%, $p = 0.191$).

4.6. **Comparison with Traditional Methods.** Table 5 compares our method against classical enhancement techniques.

Table 5. Comparison with traditional enhancement methods

Method	Detection Accuracy	BRISQUE ↓	Brightness
Original	60.1%	24.37	0.153
HE	61.5%	28.45	0.482
CLAHE	68.0%	25.12	0.256
Gamma	70.5%	26.78	0.365
Ours	**69.5%**	**21.93**	**0.242**

Our method shows better performances in comparison with HE and CLAHE enhancement technique and matches with Gamma correction in detection accuracy, and achieves superior BRISQUE scores (21.93 vs 26.78), indicating better perceptual naturalness.

4.7. **Category-Dependent Performance.** Table 6 summarizes category-dependent performance from qualitative analysis.

Table 6. Category-dependent detection performance

Category	Original Detections	Enhanced Detections	Outcome
Bicycle	0	4	Success
People	0	1	Mixed
Motorbike	0	1 GT + 2 FP	Mixed
Boat	0	0 (FP only)	Failure
Bottle	0	0 (FP only)	Failure
Car	0	0	Failure
Cat	0	0	Failure
Dining Table	0	0	Failure

Analysis: The images with bicycles having structural and high-contrast edges benefit consistently from the optimal enhancement techniques. On the other hand, images comprising boats (low-contrast against water), bottles (small spatial extent), and cats (low-reflectance fur) failed to select the proper techniques.

4.8. **Computational Efficiency.** Table 7 presents computational performance.

Table 7. Computational efficiency (Intel i7-12700K CPU)

Metric	Value
Model Size	1.86 MB
Inference Time (per image)	53.8 ms
Throughput	18.6 FPS
Feature Extraction	35.2 ms
RF Prediction	18.6 ms

Above table 7 shows the 18.6 FPS throughput. This value exceeds surveillance industry standards of 8 to 10 FPS and further meets medical imaging latency constraints of 50 to 150 ms.

5. Discussion

The BRISQUE improvement of 10.0% with $p < 0.001$ is a major finding of this study. The improvement indicates that enhanced images more closely match the statistical properties of natural images. While brightness increased by 26.7%, the other no reference metrices like NIQE and PIQE showed slight degradations (-2.1% and -0.3%) respectively. This shows a obvious trade-off: the enhancement prioritizes visibility (brightness recovery) over perfect naturalness. However, this trade-off is acceptable for detection because detection benefits from increased visibility even at the loss of some naturalness degradation.The finding that bicycles benefit consistently while boats and bottles do not has important implications. Bicycles have high-contrast structural edges (spokes, wheels, frames) that remain recoverable. Enhancement cannot create features that were never captured. This suggests deployment should target categories with proven benefit while exercising caution for others.

5.1. **Limitations.** There are some limitations in this experiment that need to be stated. Firstly, there are still category dependent errors that occur in relation to certain objects, particularly boats, bottles, and dining tables. Secondly, some false positives have been included in some cases where traffic lights and people were present. Thirdly, there are some images that have very low light intensity, with brightness levels lower than 0.01 that seem to be un-recoverable at all. Fourthly, the current approach is limited by the fact that it can work only with binary selection criteria.

6. Conclusion and Recommendations

6.1. **Conclusion.** The current research work proposes a framework for selecting an adaptive low-light image enhancement method which shows considerable gains in several different criteria. Specifically, in terms of BRISQUE score, there is a 10.0% improvement in the metric, reducing its value from 24.37 to 21.93 ($p < 0.001$). On the other hand, there is a 26.7% improvement in brightness values. Regarding the number of objects detected, there is a 2.1% increase in the number of detections ($p = 0.017$), being equal to the number detected via Gamma correction while being more visually realistic. Moreover, there are differences in gains depending on the category while bicycles show clear gains, boats and bottles do not have any.

6.2. **Recommendations.**

(1) **Suitable for structural objects:** It is suitable for detecting bicycles in low light.
(2) **Inappropriate for low-contrast objects:** It may be inappropriate for detecting boats, bottles, and dining tables.
(3) **Automatically select best algorithm:** The 86.1% accurate Random Forest selector saves time from manual adjustments.
(4) **Watch for false positives:** The enhancement technique may produce incorrect detection in some scenes.

6.3. **Future Work.**

(1) Expand to more enhancement methods (gamma variants, Retinex, learning-based)
(2) Develop category-specific enhancement parameters
(3) Validate on additional datasets (MIT Adobe 5K, DarkFace)
(4) Deploy and benchmark on edge hardware (Raspberry Pi, Jetson Nano)
(5) Extend to video with temporal consistency

Acknowledgments

The author would like to thank the contributors of the ExDark dataset [26], LOL dataset [13] and SID dataset [12].

References

[1] R. C. Gonzalez and R. E. Woods, *Digital Image Processing*, 4th ed. Pearson, 2018.
[2] Navixy, "The state of smart vehicle monitoring and telematics in 2024," 2024, accessed: 2026-03-08. [Online]. Available: https://www.navixy.com/blog/smart-vehicle-monitoring-2024
[3] SmartWitness, "Crx series: Multi-channel high definition smart camera systems," SmartWitness Technology, Tech. Rep., 2023.
[4] AMD, "Diagnostic and clinical endoscopy," AMD Official Website. [Online]. Available: https://www.amd.com/zh-cn/solutions/healthcare/edge/endoscopy.html
[5] S. M. Pizer, E. P. Amburn, J. D. Austin, R. Cromartie, A. Geselowitz, T. Greer, B. ter Haar Romeny, J. B. Zimmerman, and K. Zuiderveld, "Adaptive histogram equalization and its variations," *Computer Vision, Graphics, and Image Processing*, vol. 39, no. 3, pp. 355–368, 1987.
[6] E. H. Land and J. J. McCann, "Lightness and retinex theory," *Journal of the Optical Society of America*, vol. 61, no. 1, pp. 1–11, 1971.
[7] D. J. Jobson, Z. Rahman, and G. A. Woodell, "Properties and performance of a center/surround retinex," *IEEE Transactions on Image Processing*, vol. 6, no. 3, pp. 451–462, 1997.
[8] X. Guo, Y. Li, and H. Ling, "Lime: Low-light image enhancement via illumination map estimation," *IEEE Transactions on Image Processing*, vol. 26, no. 2, pp. 982–993, 2017.
[9] T. Mertens, J. Kautz, and F. Van Reeth, "Exposure fusion," in *15th Pacific Conference on Computer Graphics and Applications (PG 2007)*, 2007, pp. 382–390.
[10] Z. Ying, G. Li, and W. Gao, "A new low-light image enhancement algorithm using camera response model," in *IEEE International Conference on Computer Vision Workshops (ICCVW)*, 2017, pp. 3015–3022.
[11] K. G. Lore, A. Akintayo, and S. Sarkar, "Llnet: A deep autoencoder approach to natural low-light image enhancement," *Pattern Recognition*, vol. 61, pp. 650–662, 2017.
[12] C. Chen, Q. Chen, J. Xu, and V. Koltun, "Learning to see in the dark," in *Proceedings of the IEEE Conference on Computer Vision and Pattern Recognition (CVPR)*, 2018, pp. 3291–3300.

[13] C. Wei, W. Wang, W. Yang, and J. Liu, "Deep retinex decomposition for low-light enhancement," in *British Machine Vision Conference (BMVC)*, 2018.

[14] C. Guo, C. Li, J. Guo, C. C. Loy, J. Hou, S. Kwong, and R. Cong, "Zero-reference deep curve estimation for low-light image enhancement," in *CVPR*, 2020.

[15] Y. Jiang, X. Gong, D. Liu *et al.*, "Enlightengan: Deep light enhancement without paired supervision," *IEEE Transactions on Image Processing*, vol. 30, pp. 2340–2354, 2021.

[16] M. Sandler, A. Howard, M. Zhu, A. Zhmoginov, and L.-C. Chen, "Mobilenetv2: Inverted residuals and linear bottlenecks," in *CVPR*, 2018.

[17] M. Tan and Q. Le, "Efficientnet: Rethinking model scaling for convolutional neural networks," in *ICML*, 2019.

[18] L. Ma, T. Ma, R. Liu, X. Fan, and Z. Luo, "Toward fast, flexible, and robust low-light image enhancement," in *CVPR*, 2022.

[19] Z. Zhang, J. Liu, R. Liu, X. Fan, and Z. Luo, "Low-light image enhancement with multi-stage residue quantization," in *ICCV*, 2023.

[20] A. Reis *et al.*, "Real-time low-light enhancement for autonomous edge systems," *IEEE Robotics and Automation Letters*, 2025.

[21] M. Jourlin, *Logarithmic Image Processing: Theory and Applications*, 2nd ed. Elsevier / Academic Press, 2024.

[22] A. Mittal, A. K. Moorthy, and A. C. Bovik, "No-reference image quality assessment in the spatial domain," *IEEE Transactions on Image Processing*, vol. 21, no. 12, pp. 4695–4708, 2012.

[23] A. Mittal, R. Soundararajan, and A. C. Bovik, "Making a "completely blind" image quality analyzer," *IEEE Signal Processing Letters*, vol. 20, no. 3, pp. 209–212, 2013.

[24] N. Venkatanath, D. Praneeth, M. C. Bh, S. S. Channappayya, and S. S. Medasani, "Blind image quality evaluation using perception based features," in *2015 Twenty First National Conference on Communications (NCC)*, 2015, pp. 1–6.

[25] L. Breiman, "Random forests," *Machine Learning*, vol. 45, no. 1, pp. 5–32, 2001.

[26] Y. P. Loh and C. S. Chan, "Getting to know low-light images with the exdark dataset," in *Proceedings of the IEEE/CVF Conference on Computer Vision and Pattern Recognition (CVPR) Workshops*, 2019.

Everest Advances in Science and Technology (EAST), Vol. 2, No. 1, 2026
ISSN: 3102-0410 (Print), 3102-0429 (Online)
DOI: 10.3126/east.v2i1.98622

Intelligent Fault Diagnosis of Rolling Element Bearings Using Statistical Feature Extraction and Random Forest Classifier

MANOJ ADHIKARI[1], BIKKI CHHANTYAL[2*], MAHESH CHANDRA LUINTEL[1]

Abstract. Accurate detection of faults within rotary machinery components is vital for assuring the structural reliability of equipment in manufacturing facilities and power generation systems. Automatic fault detection is an increasingly common approach whereby data acquired from sensors are analyzed by machine learning algorithms to distinguish between normal and faulty component states. Vibration signatures recorded from healthy and faulty ball bearings, taken from the Case Western Reserve University (CWRU) 12k Drive End database, were utilized in the present study. These vibration signatures were segmented into windows of 0.1 s duration. Standard statistical time-domain features (root mean square, kurtosis, peak value and crest factor) were extracted from each sample. A random forest (RF) classifier was trained on vibration data from healthy bearings and several types of faulty bearings, partitioned into training (70% of data) and testing (30%) sets. The RF classifier distinguished healthy from faulty bearings with 98.8% accuracy across ball, inner race, outer race and normal categories. Feature importance analysis indicated that RMS (50% importance) and peak value (28% importance) were the most influential contributors, together comprising about 78% of the decision making. The RF model further recorded a recall of 1.00 for the normal baseline category, indicating that healthy bearings were identified with zero false negatives. The results demonstrate that ensemble machine learning, combined with statistically significant time-domain features, provides a highly accurate and physically interpretable solution for industrial condition monitoring, serving as a foundation for more advanced rotor-dynamic fault detection.

Keywords: Bearing fault diagnosis, Vibration analysis, Random forest, Feature importance, CWRU dataset

AMS Subject Classification: 68T05 (Learning and adaptive systems), 62P30 (Applications of statistics to industrial engineering), 70Q05 (Control of mechanical systems)

[1] Department of Mechanical and Aerospace Engineering, IOE Pulchowk Campus, Tribhuvan University, Lalitpur, Nepal.
[2] Department of Automobile and Mechanical Engineering, IOE Thapathali Campus, Tribhuvan University, Kathmandu, Nepal. *E-mail: chhantyalbikki@tcioe.edu.np
[*] Corresponding author

Manuscript received: 24 March 2026; Revised: 15 June 2026; Accepted: 10 July 2026.

1. Introduction

Rotating machinery serves as the backbone of modern industrial infrastructure in Nepal and worldwide. Faults within bearings result in detrimental component damage and financial losses arising from equipment repair and replacement. Traditionally, experienced maintenance technicians manually used vibration equipment to test and analyze bearing components in order to assess component health. This process requires significant experience to diagnose accurately, especially given the increasingly complicated machines used in industry. Owing to advancements in sensor technology and rising machine complexity, machines are increasingly monitored in a fully automated fashion using machine learning (ML) classification programs that diagnose operating condition from real-time vibration signals.

The principal challenge in using machine learning for fault diagnosis is converting unstructured and dynamic vibration time series into discernible, meaningful features. Rolling element bearings are used to support the rotating shaft. Fault detection and characterization in rolling element bearings occur through periodic spikes in vibration that result from the impacts the rolling elements make upon the affected area of either the inner race, outer race or ball of the bearing. During each revolution, if a rolling element strikes any section of the affected area, a shock-like pulse is created that can be clearly seen in the time-domain signal, especially for larger faults. While an expert would examine this signal to diagnose bearing defects on a spectrogram plot, a machine learning algorithm, if trained effectively, can do the same through a variety of statistical measures derived from the same signal, such as RMS or kurtosis [1].

The phenomenon of detecting a bearing fault is closely intertwined with rotor dynamics and the structural condition of rotating shafts. In preceding analytical work, researchers analyzed the effect of slant cracks in rotor shafts, specifically the coupled interaction of the axial and bending components of vibration, upon rotor shaft vibration signatures [2]. A slant crack creates a variable “breathing” phenomenon, in turn altering the rotor shaft’s stiffness matrix. The other major source of shaft vibration in rotating machinery is a defect in the bearing components. Localized defects create a non-linear stiffness characteristic around the bearing and therefore affect the shaft’s response during operation [3]. Thus, to produce accurate ML models for bearing defect classification, it is vital that the engineers creating the models have a foundational understanding of the mechanical characteristics and vibration behaviors described above. In this regard, the present paper builds on established foundations within mechanical engineering by extending shaft crack analysis and demonstrating how it can be utilized in a statistical feature-based classification system to identify defects arising in rotating shafts as a result of bearing fatigue over time.

The automated fault diagnostic pipeline established in this study is derived from data gathered by the Case Western Reserve University (CWRU) Bearing Data Center, specifically the 12k drive-end ball bearing data, and shows the viability of time-domain statistical features in training a random forest classifier. Furthermore, this study uses feature importance calculation as a mechanism to address the “black box” concern surrounding modern artificial intelligence techniques, thus linking the output of the classifier to accepted principles of mechanical engineering that can be applied by any maintenance technician without requiring an understanding of artificial intelligence.

The specific contributions of this paper are as follows:

- A systematic evaluation of time-domain statistical features (RMS, kurtosis, peak value and crest factor) for multi-class bearing fault classification on the CWRU 12k drive-end dataset.
- A feature importance analysis within the random forest framework to produce a physically interpretable diagnostic model, bridging the “black-box” nature of artificial intelligence with established mechanical engineering principles so that the model’s decisions are transparent to maintenance engineers.

- A demonstration of the practical viability of this approach for real-time condition monitoring in resource-constrained industrial environments such as Nepal's hydropower sector, where computationally efficient and interpretable diagnostics are prioritized over deep learning complexity.

2. Methodology

The research follows a methodological pathway comprising four key steps: acquisition of the experimental data, signal processing by partitioning the data into time segments (windowing), extraction of relevant statistical features from those segments, and classification into fault categories using an ensemble learning approach. The overall pipeline is summarized in Fig. 1.

Data Acquisition (CWRU 12k DE) → Windowing (1200 samples, 0.1 s) → Feature Extraction (RMS, Kurtosis, Peak, Crest Factor) → Random Forest Classification → Fault Label + Feature Importance

FIGURE 1. Proposed diagnostic pipeline for bearing faults.

2.1. **Data Acquisition.** The experimental data were obtained from the CWRU Bearing Data Center database [4]. The test setup includes a 2 HP Reliance Electric motor coupled to an encoder/torque transducer and connected to a power meter that logs voltage and current. Vibration data are obtained from accelerometers installed at the drive end (DE) of the motor.

Following common practice in the bearing fault detection literature, the 12,000 Hz (12 kHz) sampling rate dataset was chosen for this study so that the outcomes of the methodology can be directly compared against previous research [5]. The data collected included readings for the bearing in normal operation (normal baseline), inner race (IR) fault, ball (BL) fault and outer race (OR) fault. The IR, ball and OR faults are further classified as having a fault diameter of either 0.007 in or 0.014 in. Faulty bearings in these categories, all single-point faults, were induced via electro-discharge machining (EDM). For the outer race defects specifically, faults were introduced at the six o'clock position. For the normal baseline, multiple operating load levels were used, including 0, 1, 2 and 3 HP. The composition of the dataset is summarized in Table 1.

TABLE 1. Summary of the CWRU 12k Drive End Dataset and Sample Distribution

Category	**Fault dia. (in)**	**Motor load (HP)**	**RPM (approx.)**	**Windows (samples)**
Normal baseline	N/A	0, 1, 2, 3	1797–1730	∼400
Inner race fault	0.007, 0.014	0	1797	∼200
Ball fault	0.007, 0.014	0	1797	∼200
Outer race fault	0.007, 0.014	0	1797	∼200
Total dataset				∼1000

2.2. **Signal Preprocessing.** The raw data extracted from the CWRU dataset consist of continuous and complex vibration signals generated during motor rotation. Machine learning algorithms require this time-dependent information to be presented in a more tractable form. Accordingly, a segmentation (windowing) process was applied to transform the continuous vibration streams into smaller, discrete samples. The signals, acquired at sampling frequency f_s, were divided into separate samples of 1200 data points each. Given the sampling rate of 12 kHz, each sample covers a 0.1 s interval, as expressed in (1):

$$T_w = \frac{N_w}{f_s} = \frac{1200}{12000} = 0.1 \text{ s}, \tag{1}$$

where T_w is the window duration and N_w is the number of samples per window. This window length was chosen to strike a compromise between capturing sufficient data for statistical significance and keeping computational cost low. For a motor running at approximately 1797 RPM, a 0.1 s interval corresponds to nearly three shaft rotations, capturing rolling element impacts multiple times within a given sample. As a result, the original limited number of *.mat* files was transformed into a data bank of 10,553 labelled bearing vibration examples spanning the fault and normal classifications, sufficient for a machine learning model to learn meaningful patterns [6].

2.3. **Feature Extraction.** Four key statistical features were computed from each 1200-sample, 0.1 s window. These features represent reduced dimensions that nonetheless encode crucial diagnostic information about the health of the rolling element bearings. They were selected for their known sensitivity to the transient, impulsive and energetic characteristics associated with the vibration produced during component wear. The extracted features are as follows.

2.3.1. *Root Mean Square.* The RMS is computed as the square root of the average of the squares of the signal, as given in (2):

$$x_{\text{RMS}} = \sqrt{\frac{1}{N}\sum_{i=1}^{N} x_i^2}, \tag{2}$$

where x_i is the ith sample of the window and N is the number of samples. RMS provides a statistical measure of the magnitude, or overall vibrational energy, of the signal. Faults inherently create shock-like impacts that increase the energetic content of the signal, making RMS a primary indicator of defect magnitude. The increase in RMS with increasing defect size, observed here from 0.007 in to 0.014 in, results from higher overall kinetic impact energy during rolling element passage.

2.3.2. *Kurtosis.* This statistic measures the degree to which a distribution is prone to peaks, and is defined in (3):

$$K = \frac{\frac{1}{N}\sum_{i=1}^{N}\left(x_i - \bar{x}\right)^4}{\left[\frac{1}{N}\sum_{i=1}^{N}\left(x_i - \bar{x}\right)^2\right]^2}, \tag{3}$$

where $\bar{x}$ is the mean of the window. In signal processing, kurtosis is commonly used to detect "spikiness" indicative of shock events or impulses related to mechanical defects such as cracked elements or surface imperfections. A perfectly Gaussian distribution has a kurtosis of 3. A bearing in good working condition exhibits a kurtosis value close to 2.9, while defective bearings typically exhibit higher values as a consequence of the impulsive, non-Gaussian nature of the impacts.

2.3.3. *Peak Value.* This feature measures the largest absolute amplitude of the signal within a 1200-sample interval, as defined in (4):

$$x_{\text{peak}} = \max_{1 \le i \le N} |x_i| \, . \tag{4}$$

It directly captures the strongest shock pulse recorded within each observed 0.1 s portion of the rotating shaft's motion.

2.3.4. *Crest Factor.* The crest factor is calculated as the ratio of the peak value to the RMS of the signal, as given in (5):

$$\mathrm{CF} = \frac{x_{\mathrm{peak}}}{x_{\mathrm{RMS}}}. \tag{5}$$

It is a dimensionless parameter used to identify the impulsivity or sharpness of the signal. High crest factors can indicate localized defects such as cracks before the damage extends into a widespread surface imperfection.

Representative values of the four extracted features for each bearing condition are presented in Table 2.

TABLE 2. Extracted Statistical Features for Different Bearing Conditions

Bearing condition	**Fault dia. (in)**	**RMS (g)**	**Kurtosis**	**Peak value**	**Crest factor**
Normal baseline	N/A	∼0.07	∼2.9	∼0.2	∼3.5
Inner race fault	0.007	∼0.29	∼5.4	∼1.4	∼4.9
Inner race fault	0.014	∼0.19	∼21.7	∼1.6	∼8.1
Ball fault	0.007	∼0.13	∼2.9	∼0.5	∼3.4
Ball fault	0.014	∼0.14	∼7.3	∼0.8	∼5.4
Outer race fault	0.007	∼0.66	∼7.6	∼3.2	∼4.8
Outer race fault	0.014	∼0.10	∼3.0	∼0.35	∼3.4

2.4. **Classifier Configuration.** Following the extraction of statistical features, the samples were labelled according to health status: normal, inner race fault, outer race fault and ball fault. To emulate testing under real-world industrial conditions, the finalized feature matrix was divided into a 70% training set and a 30% test set. This separation prevents data contamination, which could otherwise lead to exaggerated estimates of classifier accuracy [7]. A random forest classifier was employed as the ensemble method of choice. It was selected for its resistance to overfitting, its ability to handle feature-rich data effectively, and its capacity to compute feature importances that aid interpretability. The forest was assembled from 100 decision trees to ensure reliable predictions. The implementation used the scikit-learn library [8].

3. Results and Discussion

This research produced significant outcomes regarding the automated diagnosis of bearing faults through the analysis of vibration signals and the assessment of random forest classification performance.

3.1. **Preliminary Data Visualization.** Initial inspection of the time-domain signals provided clear evidence of mechanical distress in faulty bearings, as shown in Fig. 2.

Two observations follow from Fig. 2. First, regarding the steady-state baseline, normal and healthy bearing vibration signals are predominantly smooth, low-amplitude waveforms with amplitude generally within $\pm 0.2g$. Second, regarding the impulsive fault signature, outer race faults (0.007 in) display distinctly patterned spikes exceeding the range of a healthy signal, reaching up to $3g$.

3.2. **Classification Performance.** The random forest classifier exhibits strong diagnostic capability, yielding high precision and recall figures across all fault types, as reported in Table 3.

Based on the evidence presented in Table 3, the method achieved 99% average classification accuracy on unseen data. Notably, the model reached perfect precision (1.00) for the ball (0.007 in), inner race (0.007 in), normal and outer race (0.007 in) categories. The corresponding confusion matrix is presented in Fig. 3, which indicates that almost all samples were categorized correctly,

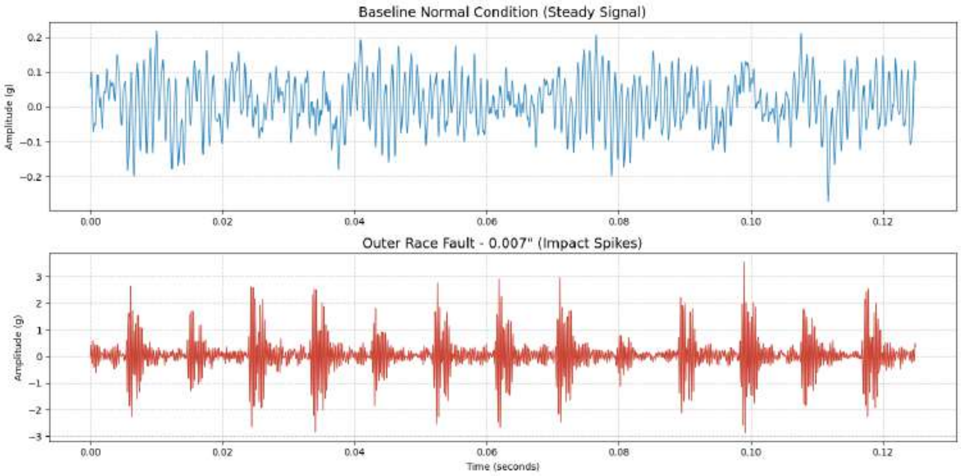

FIGURE 2. Time-domain vibration signals for healthy and faulty (0.007 in) bearing conditions.

TABLE 3. Classification Performance Metrics for the Random Forest Model

Fault category	**Precision**	**Recall**	**F1-score**	**Support**
Normal	1.00	1.00	1.00	416
Inner race (0.007 in)	1.00	1.00	1.00	31
Inner race (0.014 in)	0.97	0.95	0.96	39
Ball (0.007 in)	1.00	1.00	1.00	27
Ball (0.014 in)	0.89	0.86	0.87	28
Outer race (0.007 in)	1.00	1.00	1.00	28
Outer race (0.014 in)	0.97	1.00	0.99	37
Accuracy			**0.99**	**606**

with the limited misclassification that did occur arising predominantly between the ball (0.014 in) and inner race (0.014 in) categories.

Fig. 3 illustrates the nearly flawless classification performance of the random forest model for the normal baseline and the 0.007 in faults. Importantly, not a single false negative was recorded in which a faulty bearing was declared healthy, a critical characteristic for the industrial domain, where false negatives often have severe repercussions for the operation of the bearing and ultimately the machine. Confusion between the ball (0.014 in) and inner race (0.014 in) categories was observed. As the fault diameter becomes larger, the impacts generated by a ball rolling over the race path begin to share similar shapes in the time domain, creating confusion between these types. Even with such minor differences between fault characteristics, the diagnostic accuracy remained above that of typical thresholding schemes, owing to the feature selection adopted in this study.

3.3. **Feature Importance and Interpretability.** To understand how machine learning models "see" faults compared with traditional mechanical engineering practice, the importance of individual statistical features within the classification was examined. The result is presented in Fig. 4.

As shown in Fig. 4, the RMS feature ranks highest and is responsible for over 50% of the model's predictions. According to mechanical vibration principles, the presence of a defect causes an imbalance, which in turn leads to greater energy in the vibration signal. Following RMS, peak value accounts for around 28% of decisions, trailed by kurtosis at approximately 15%. Kurtosis and peak value are effective at capturing the impulsive and "spiky" vibration caused by bearing

FIGURE 3. Confusion matrix of the random forest classifier on the testing set.

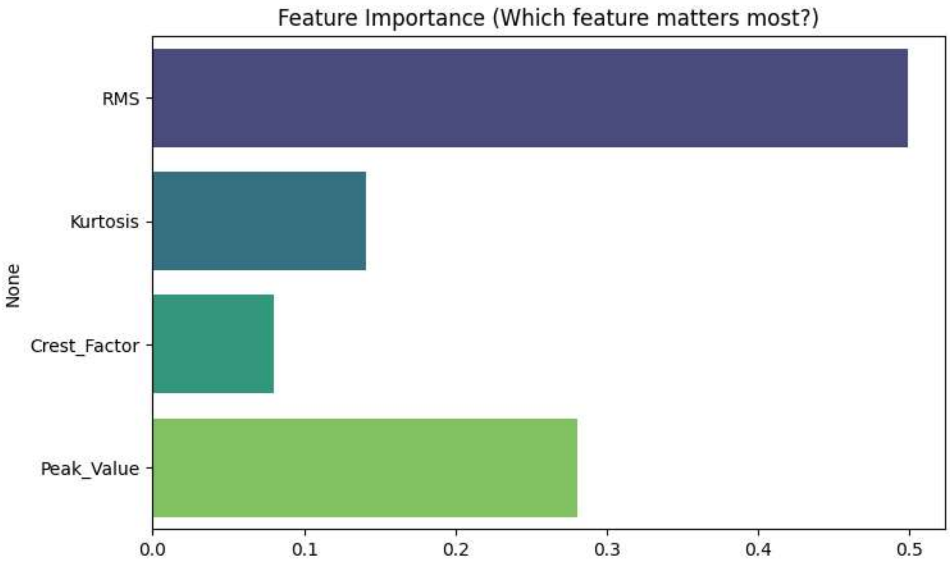

FIGURE 4. Relative importance of statistical features in the classification process.

defects. The crest factor, at approximately 7%, also indicates shock events during a fault but is less significant than the other selected features within this particular ensemble structure.

3.4. **Comparison to Traditional Rotor Dynamics.** The significance of the energy-based RMS feature and the impulse-based peak feature resembles findings in previous analytical research on slant cracks in shafts. Just as slant crack characteristics induce variations in rotor system stiffness due to repetitive contact, localized faults on a race or in a ball also result in recurring impacts, which are detected, analyzed and interpreted by the random forest model through multiple dimensionally reduced statistical indicators present in the vibration signal. Furthermore, the 99% classification accuracy achieved on the CWRU 12k drive-end dataset is consistent with published benchmarks for time-domain feature-based methods. For instance, classical spectral methods have been reported to achieve accuracies in the range of 90% to 97% on the same dataset [5], while unsupervised feature learning approaches have demonstrated accuracies reaching approximately 98% [6].

4. Conclusion

This study develops an intelligent fault diagnosis framework for rolling element bearings based on time-domain statistical features and the random forest classifier, leveraging data from the CWRU 12k drive-end bearing fault dataset to bridge raw vibration measurements and classified bearing health.

The following conclusions are derived from this study. Time-domain statistical features, in particular RMS and peak value, enable reliable detection of a wide array of fault categories in mechanical machinery, with RMS alone accounting for approximately 50% of the decisions made by the model. The random forest model produced an average accuracy of 99% on unseen data, and the classifier produced a recall of 1.00 for normal baseline bearings, meaning that zero false negatives were recorded in identifying a healthy bearing. Through feature importance analysis and confusion matrices, the internal workings of the machine learning algorithm are demystified; these parameters help translate artificial intelligence, which can appear opaque or “black box” in nature, into the familiar mechanics and engineering principles applied by maintenance personnel. Finally, windowing and feature selection offer a computationally efficient methodology suitable for real-time fault detection in rotating machinery, a framework that will be beneficial to industries such as the power sector in developing countries like Nepal.

In future work, the authors intend to employ frequency-domain features and deep learning architectures to detect and diagnose early-stage faults.

Acknowledgment

The authors would like to thank the Case Western Reserve University Bearing Data Center for providing public access to the bearing vibration dataset used in this study.

References

[1] S. S. Rao, *Mechanical Vibrations*, 6th ed. Hoboken, NJ, USA: Pearson, 2018.

[2] M. Adhikari and P. R. Shakya, “Slant crack detection in shaft using analytical vibration methods,” in *Proc. IOE Graduate Conf.*, vol. 6, 2019, pp. 521–526. [Online]. Available: https://conference.ioe.edu.np/publications/ioegc2019-summer/IOEGC-2019-Summer-091.pdf

[3] Y. Jiang, W. Huang, J. Luo, and W. Wang, “An improved dynamic model of defective bearings considering the three-dimensional geometric relationship between the rolling element and defect area,” *Mech. Syst. Signal Process.*, vol. 129, pp. 694–716, Aug. 2019.

[4] Case Western Reserve University Bearing Data Center, “12k drive end bearing fault data,” [Online]. Available: https://engineering.case.edu/bearingdatacenter, accessed: Jul. 24, 2026.

[5] W. A. Smith and R. B. Randall, “Rolling element bearing diagnostics using the Case Western Reserve University data: A benchmark study,” *Mech. Syst. Signal Process.*, vol. 64–65, pp. 100–131, Dec. 2015.

[6] Y. Lei, F. Jia, J. Lin, S. Xing, and S. X. Ding, “An intelligent fault diagnosis method using unsupervised feature learning towards mechanical big data,” *IEEE Trans. Ind. Electron.*, vol. 63, no. 5, pp. 3137–3147, May 2016.

[7] A. Géron, *Hands-On Machine Learning with Scikit-Learn, Keras, and TensorFlow: Concepts, Tools, and Techniques to Build Intelligent Systems*, 2nd ed. Sebastopol, CA, USA: O’Reilly Media, 2019.

[8] F. Pedregosa, G. Varoquaux, A. Gramfort, V. Michel, B. Thirion, O. Grisel, M. Blondel, P. Prettenhofer, R. Weiss, V. Dubourg, J. Vanderplas, A. Passos, D. Cournapeau, M. Brucher, M. Perrot, and E. Duchesnay, "Scikit-learn: Machine learning in Python," *J. Mach. Learn. Res.*, vol. 12, pp. 2825–2830, Oct. 2011.

Everest Advances in Science and Technology (EAST), Vol. 2, No. 1, 2026
ISSN: 3102-0410 (Print), 3102-0429 (Online)
DOI: 10.3126/east.v2i1.98624

Effectiveness of Arbitration in Nepal Construction Dispute Resolution

BINU KARKI[1*]

Abstract. This study looks at how arbitration works in resolving disputes related to construction contracts in Nepal. It focuses on how the procedures and the arbitration process affect whether people think it is successful. The study used a combination of methods to analyze information from 121 people involved in these disputes along with information from reports by the Nepal Council of Arbitration. The results show that the skills of the arbitration tribunal, the size of the tribunal and how evidence is presented are very important for making arbitration effective. On the other hand the value of the claim and complexity of the dispute do not seem to make a difference on effectiveness of arbitration. People do not think arbitration is an affordable way to resolve disputes. It takes an average of 430 days to reach a decision, which is much longer than the 120 days required by law as stated in the Section 24 of the Arbitration Act 2055 (1999). The study concludes that for arbitration to be really successful it depends more on the people involved being honest and working together than on the laws themselves. The study suggests that changes should be made to improve how arbitration decisions are enforced which would make arbitration more effective in resolving construction contract disputes in Nepal.

Keywords: Arbitration, Construction disputes, Dispute resolution, Construction contracts, Effectiveness, Cost effectiveness, Time effectiveness

AMS Subject Classification: 62-07 (Data analysis), 62P25 (Applications of statistics to social sciences), 91C99 (Social and behavioral sciences - other), 90B90 (Case studies and applications of operations research and management science)

[1] Center for Postgraduate Studies, Nepal Engineering College, Nepal. E-mail: bnukrki09@gmail.com
[*] Corresponding author

Manuscript received: 19 March 2026; Revised: 11 June 2026; Accepted: 14 July 2026.

1. Introduction

The construction industry helps a country's economy and local economy a lot. It creates jobs and helps other industries grow because it needs their products and services. The construction industry is really important for overall growth of the economy [1]. However, modern projects are getting more complex. They have contract documents, limited budgets, and many stakeholders with different interests. This complexity has made the industry more likely to have disputes.

The complexity of projects is an issue due to several factors:

- Intricate contract documents are hard to understand.
- Tight financial constraints make it difficult to find solutions.
- Diverse stakeholder interests often clash.

This situation has made disputes more common in the industry. The problems in construction projects usually come from differences between owners, contractors who lack required technical skills, mistakes in the design, and other things like material prices going up. If we do not solve these problems, the construction project can go off track, the people in charge can lose their reputation, and it can cost a lot more money and take a lot more time than expected [2].

To avoid problems, people are using Alternative Dispute Resolution (ADR) to solve arguments about construction contracts. The arbitration process is a common ADR method used to resolve construction contract disputes [3]. Arbitration is considered better than going to court because it uses experts in specific areas and has flexible procedures. In Nepal, the Arbitration Act of 1999 helps make this process official. The Nepal Council of Arbitration (NEPCA) supports it. They were set up in 1991 to promote and establish ADR practices. As of September 2025, NEPCA had 72 registered panel members. In the fiscal year 2080-81, they handled 176 ongoing cases. Out of these, 48 were resolved, 42 of which were resolved through arbitration. The Public Procurement Act of 2063 also recognizes arbitration as a way to settle disputes in public construction projects.

The law is clear about arbitration in Nepal, but there is still a lot to learn about how well it actually works. The Arbitration Act 1999 says that arbitration decisions must be final and made within 120 days. However, it usually takes around 430 days to get a decision, which is a lot longer than the law says it should take. Arbitration in Nepal does not seem to be very successful in resolving disputes. Previous studies suggest a low success rate, where only 21.43% of disputes are actually resolved through arbitration. This is partly because government employers are afraid of being held accountable by groups like the Commission for the Investigation of Abuse of Authority (CIAA). So, they often do not accept the decisions made by arbitrators and instead choose to go to court post-arbitration decision. This makes the arbitration process in Nepal not very effective [4].

When we look at the research that's already out there, we see that it mostly talks about what causes disputes. There is not a lot of research on how procedural factors—such as tribunal competence, tribunal size, and evidence presentation methods—influence the perceived effectiveness of the process. There is a difference between institutional success (measured by NEPCA through the number of closed cases) and stakeholder satisfaction (measured by time-efficiency and award finality). This research addresses these gaps by looking at how the arbitration process works from the point of view of the people who are actually involved in construction disputes.

The major research questions for this study are listed as follows:

- How do procedural factors of arbitration affect the overall effectiveness of arbitration processes?
- How does the arbitral process influence the perceived effectiveness of arbitration in Nepali construction disputes?
- What is the disparity between the actual vs. expected cost and time effectiveness of Nepali construction arbitration practice?

The general objective of this study is to assess the effectiveness of dispute resolution practices within construction contracts in Nepal. To achieve this, the study identifies three specific research objectives:

- To determine how procedural factors (such as complexity and claim value) affect the overall effectiveness of the arbitration process.
- To investigate the influence of the arbitral process (including tribunal competence and size) on the perceived effectiveness of arbitration practices.
- To quantify and compare objective cost and time metrics of arbitration against subjective stakeholder perceptions and ideal legal benchmarks.

This study looks at primary survey data from 121 stakeholders with secondary case reports from NEPCA. The information from the stakeholders and past cases helps us understand what needs to be changed in the rules so that the system for solving disputes in Nepal is fair and trustworthy.

2. Methodology

2.1. **Methods.** This research used a combination of methods to look at construction arbitration in Nepal. It brought together quantitative numbers and qualitative opinions to evaluate the overall performance of construction arbitration.

2.2. **Sampling Design and Procedure.** The research looked at a group of 176 parties involved in disputes that were recorded in NEPCA reports from fiscal years 2079 to 2081 B.S. Using Cochran's formula (with a 95% confidence level and 5% margin of error), the required sample size was determined to be 121. The study utilized stratified sampling to maintain a 2:1 ratio between representatives of disputing parties (clients and contractors) and arbitrators. Additionally, convenience sampling was used to select three subject-matter experts for qualitative interviews.

2.3. **Data Collection Techniques.** Data were gathered from primary and secondary sources:

- **Primary Data:** Quantitative data were collected through structured questionnaires distributed electronically and in person. Qualitative data were gathered through structured written interviews and Key Informant Interviews (KII).
- **Secondary Data:** Information regarding case durations, costs, and outcomes was extracted from NEPCA annual reports, journals, and acts.

2.4. **Instrument Validation and Reliability.** The questionnaire was pre-tested with a panel of three experts having at least 10 years of experience in construction and arbitration. Cronbach's alpha reliability test was used, requiring a threshold score of 0.70 or higher. Responses from participants lacking ADR experience were excluded from the final analysis.

2.5. **Data Analysis Methods.** This research utilized SPSS and MS Excel for all analytical procedures:

- **Quantitative Analysis:** Descriptive statistics (mean, median, standard deviation) were computed. One-sample t-tests were conducted to evaluate perceived effectiveness scores against a hypothesized population mean of 2.5.
- **Qualitative Analysis:** Interview data were processed using thematic analysis to identify recurring patterns.

3. Results and Discussion

During the questionnaire survey, demographic information was gathered on gender, age, experience, academic background, province, occupation, and other factors as shown in Table 1.

As shown in Table 2, respondents generally believe that dispute complexity has a moderate to low effect on arbitration effectiveness. This implies that practitioners do not view intrinsic case characteristics as the primary obstacle to favorable arbitration outcomes.

The information in Table 3 casts doubt on the belief that low-value claims are easier to settle. Low median ratings indicate that current arbitration procedures may not be properly streamlined for smaller claims.

Table 4 indicates that tribunal size and evidence presentation methods are perceived as the most influential procedural elements.

Table 5 illustrates that perceived tribunal competence scores cluster closely around the neutral rating (2.82–2.94).

Results in Table 6 show a clear preference for multi-member tribunals ($Mdn > 3.05$) to enhance award quality and impartiality.

In Table 7, meticulous documentation emerged as the single highest scoring item ($Mdn = 3.18$).

The t-test results in Table 8 confirm that procedural factors significantly influence arbitration effectiveness ($p < 0.05$), while intrinsic case factors do not.

Tables 9 and 10 highlight dissatisfaction regarding cost and time metrics, underscoring the gap between the 120-day legal mandate and the 430-day practical average.

References

[1] I. M. A. Wibowo, "The contribution of the construction industry to the economy of Indonesia: A systemic approach," Ph.D. dissertation, Dept. Civil Eng., Diponegoro Univ., Semarang, Indonesia, 2003.

[2] X. N. Mashwama, C. Aigbavboa, and D. Thwala, "Investigation of construction stakeholders' perception on the effects and cost of construction dispute in Swaziland," *Procedia Eng.*, vol. 164, pp. 196–205, 2016.

[3] T. B. Adesina, "Why arbitration triumphs litigation: Pros of arbitration," *Singaporean J. Bus. Econ. Manage. Stud.*, vol. 3, no. 4, pp. 37–42, Oct. 2014.

[4] A. K. Mishra and P. S. Aithal, "Effectiveness of arbitration in construction projects," Working Paper, Tech. Rep., 2022.

Table 1. Distribution of respondents by demographics

Demographics	Categories	Frequency	Percent (%)
Gender	Male	69	98.57
	Female	1	1.43
	Total	**70**	**100**
Age Group	Below 50	25	38.46
	50–60	15	23.08
	Above 60	25	38.46
	Total	**65**	**100**
Qualification	Up to +2	0	0
	Bachelor	5	7.14
	Masters and above	65	92.86
	Total	**70**	**100**
Province	Province 1	6	8.57
	Karnali	2	2.86
	Madesh	3	4.29
	Bagmati	45	64.28
	Gandaki	9	12.86
	Lumbini	2	2.85
	Sudur Paschim	3	4.29
	Total	**70**	**100**
Position	Middle-level management	16	22.86
	Top-level management	26	37.14
	Arbitrators	28	40
	Total	**70**	**100**
Profession	Engineering	55	78.57
	Legal	10	14.29
	Both	3	4.29
	Others	2	2.85
	Total	**70**	**100**
Stakeholders	Clients	18	25.71
	Contractors	16	22.86
	Both/others	10	14.29
	Arbitrators	26	37.14
	Total	**70**	**100**
Role in Dispute	Claimants	15	21.43
	Respondents	20	28.57
	Both/others	11	15.71
	Arbitrators	24	34.29
	Total	**70**	**100**
Cases Encountered	1–2 cases	16	22.86
	3–5 cases	12	17.14
	More than 5 cases	42	60
	Total	**70**	**100**
Maximum Claim	Up to Rs. 30 million	23	32.86
	More than Rs. 30 million	47	67.14
	Total	**70**	**100**
Arbitration Type	Ad-hoc	18	25.71
	Institutional	34	48.58
	Both	18	25.71
	Total	**70**	**100**

Table 2. Analysis of Likert-type Items Used to Measure the Influence of Complexity of the Dispute

S.N.	Items for complexity of the dispute	N	Mdn
1	Complex contract documentation influences the effectiveness of arbitration.	70	2.75
2	Involvement of more parties in a dispute influences the effectiveness of arbitration.	70	2.52
3	Language barriers influence the effectiveness of arbitration.	70	2.43
4	Participants' diverse cultural backgrounds influence the effectiveness of arbitration.	70	2.31
5	The number of sittings of the tribunal influences the effectiveness of arbitration.	70	2.56

Table 3. Analysis of Likert-type Items Used to Measure Influence of Claim Value

S.N.	Items	N	Mdn
1	Low-value claim disputes are less complex.	68	2.40
2	Low-value claim disputes are awarded more effectively than the high-value claim disputes.	65	2.29

Table 4. Mean and Standard Deviation on the Influence of Dispute Factors

S.N.	Independent Variables	N	M	SD	Min	Max
1	Complexity of disputes	70	2.53	0.48	1.20	3.60
2	Competence of the tribunal	70	2.82	0.53	1.40	4.00
3	Adequacy of size of the tribunal	70	3.05	0.49	1.30	4.00
4	Approaches to the presentation of evidence	70	3.00	0.46	1.00	4.00
5	Claim value	68	2.43	0.65	1.00	4.00

Table 5. Analysis of Likert-type Items Used to Measure Influence of Competence of the Tribunal

S.N.	Items	N	Mdn
1	Tribunals are knowledgeable in construction disputes.	70	2.94
2	Arbitrators demonstrate strong technical and functional skills.	70	2.93
3	Arbitrators possess strong interpersonal skills.	70	2.85
4	Arbitrators have the quality to maintain fairness and impartiality.	70	2.88
5	Arbitrators have a strong ability to perform neutrally and independently.	70	2.82

TABLE 6. Analysis of Likert-type Items Used to Measure Influence of Adequacy of the Size of the Tribunal

S.N.	**Items**	**N**	**Mdn**
1	There is adequacy of the size of the tribunal.	70	2.97
2	Multi-member tribunals enhance impartiality and avoidance of conflicts of interest.	70	3.08
3	Multi-member tribunals enhance the quality of the award.	70	3.09
4	Multi-member tribunals produce better and stronger awards.	70	3.08
5	A multi-member tribunal bridges knowledge and skill gaps.	70	3.05

TABLE 7. Analysis of Likert-type Items Used to Measure Influence of Approaches to Presentation of Evidence

S.N.	**Items**	**N**	**Mdn**
1	The number of experts and fact witnesses presented produce effective arbitration.	67	3.05
2	There are enough choices of presentation techniques.	67	2.90
3	The tribunal guides the disputants in presenting evidence.	70	2.86
4	Carefulness of documentation affects the effectiveness of arbitration.	69	3.18
5	The tribunal provides equal opportunity to all the parties.	67	3.13

TABLE 8. One-sample t-test to Evaluate the Significance Level on the Influence of Dispute Factors

Test Value = 2.5 ($H_0 : \mu \leq 2.5$, one-tailed test)						
S.N.	**Factor**	**t**	**df**	**Sig. (2-tailed)**	**Sig. (1-tailed)**	**Mean Diff.**
1	Complexity of dispute	0.23	70	0.825	0.413	0.02
2	Competence of the tribunal	5.09	70	0.000	0.000	0.32
3	Adequacy of tribunal size	9.27	70	0.000	0.000	0.54
4	Evidence presentation methods	8.87	70	0.000	0.000	0.45
5	Claim value	-1.20	67	0.215	0.105	-0.11

TABLE 9. Analysis of Likert-type Items Used for Cost Effectiveness of Arbitration

S.N.	**Items for cost effectiveness**	**N**	**Mdn**
1	The cost of dispute resolution in Nepal is reasonable.	67	2.95
2	The total cost of resolving the dispute is within the parties' expectation.	67	2.90

Table 10. Analysis of Likert-type Items Used for Time Effectiveness of Arbitration

S.N.	**Items for time effectiveness**	**N**	**Mdn**
1	The time taken for dispute resolution in Nepal is reasonable.	68	2.50
2	The total time taken to conclude the dispute has met the parties' expectations.	68	2.50

Everest Advances in Science and Technology (EAST), Vol. 2, No. 1, 2026
ISSN: 3102-0410 (Print), 3102-0429 (Online)
DOI: https://doi.org/10.3126/east.v2i1.98625

Adaptive Reuse of Historical Buildings around Kathmandu Valley: An Analytical Study

DIKSHA BHANDARI[1*]

ABSTRACT. Providing a new working position to an ancient structure happens when adaptive reuse is utilized for a building with historical, architectural, or cultural significance, because this method ensures that the design character, structural strength, and heritage value stay safe. Since quick urban growth and shifting social needs transform old cities in this modern time, adaptive reuse functions as a helpful strategy because it protects the old construction heritage while contemporary requirements are met. Professional individuals claim that the heritage structures within Kathmandu Valley face great stress from city growth, limited maintenance, and different usage styles, which reason causes this investigation to examine the real application of adaptive reuse in this location. By using a detailed method of analysis, this study assesses how adaptive reuse helps to keep conservation and green urban growth in balance, because this assessment relies on examining scholarly papers, known protection theories, and specific examples. Attention is given to Newa Chhen, Patan Museum, and Kaiser Library by the researcher, because looking at these buildings shows the design, building, and usage changes that made sure these ancient structures stayed helpful. International examples and accepted protection rules are added to the research to give comparison points, which addition assists in finding rules that work for the Nepal situation. It has been observed by the study that adaptive reuse maintains the design character and local heritage, and adaptive reuse also helps the environment because adaptive reuse makes the life of ancient structures longer, stops building trash, and decreases the need for fresh supplies. Many big problems are identified in this work, which problems are the poor following of legal rules, small money amounts, hard technical issues, and the lack of professional individuals who have deep knowledge in protection.

Keywords: Adaptive reuse, culturally sensitive, heritage conservation, Newar craftsmanship, interventions

[1] Cosmos College of Management and Technology, Kathmandu, Nepal
E-mail: dikshab002@gmail.com
* Corresponding author

Manuscript received: 29 March 2026; Revised: 21 June 2026; Accepted: 24 July 2026.

1. Introduction

Adaptive reuse is the process of giving old buildings a new purpose while preserving their historical character. Modern requirements are met by modifying standing edifices rather than destroying and constructing again. Many people believe that adaptive reuse minimizes waste when people maintain the primary frames and exterior surfaces of the dwellings. Durability of the property increases because adaptive reuse allows historical times and current days to gather in one location [1].

Kathmandu Valley is a perfect example of why these actions are so important. The city is home to incredible Newar artistry that is visible in its many temples, palaces, squares, and traditional homes. These places also serve to tell the stories of the past in the area and the communities that have lived there for centuries. The city's structures often show influences from both Buddhism and Hinduism. However, these impressive structures face many dangers due to the rapid expansion of the city and the high demand for its land. The way of living in the area has changed, leading to the abandonment of these historical buildings. In fact, the earthquake of 2015 revealed the fragility of these structures and the need to protect them [2]. One way that these historical structures can be protected is through the adaptive reuse of these locations. By adapting and reusing these historical buildings, their original style and structure can be protected while allowing their use in the current society [3]. Cultural uniqueness is kept secure through adaptive reuse even though the urban center undergoes transformation. Many scholars suggest that adaptive reuse prevents the decay of the physical history of the society [4].

Cities around the globe have found success in this strategy. From Rome to London to Kyoto, these cities have all found ways to integrate old buildings with modern life, with very positive results [5]. Many of these cities like New York have had success with converting lofts or restoring heritage hotels in India, show how these types of developments can bring new life to old buildings, reduce their environmental impact, and create an appreciation for their cultural heritage [6]. The Venice Charter and UNESCO have also found this strategy to be one of the most effective in the adaptation of these historical structures. These adaptations to historical buildings in different locations throughout the world offer important lessons that can be learned by the city of Kathmandu.

Yet when we look closely at existing research in Kathmandu Valley, we can notice important gaps. Most studies describe individual projects but do not compare them or analyze how they actually function in today's social and economic environment. They also rarely connect adaptive reuse to broader urban issues like population growth or land pressure. Policies and guidelines for reuse in Nepal are still limited, and their on-ground effectiveness remains unclear. These gaps show why we need a more focused analytical study that examines multiple cases and develops strategies that truly fit Kathmandu's cultural and urban context.

2. Methods

This paper adopts an approach to investigate three cases: Newa Chhen, Patan Museum, and Kesar Mahal. The research method adopted is semi-structured interviewing with direct observation, which is supplemented by document study. These three cases were chosen as they represent a broad typological variation of buildings, cultural background, architectural style, and current use in the Valley. Newa Chhen represents traditional Newar houses, while the Patan Museum used to be a palace and now serves as a cultural center. Kesar Mahal is an administrative building constructed in a Rana-era style. Site visits were used to observe spatial layouts, materials used, and the surroundings. Sketches and notes were made at the site, and photos and videos were taken to document them for analysis and comparison. Informal interviews with architects and users added the dimension of design intent and lived experience. Reviews of scholarly articles, books, and journals connected the fieldwork to the existing academic debate. The study elaborates on the architecture and use of Newa Chhen, Patan Museum, and Kesar Mahal and discusses their designs.

3. Literature Review

Reuse is considered from several points of view in the literature. Sustainable development experts indicate that reuse of existing buildings contributes to a reduction in waste, saves energy, and results in fewer environmental harms than constructing new buildings. Therefore, reuse of existing buildings is critical for the development of cities in a responsible manner [7]. Examples of reuse of existing buildings at the global level include the reuse of industrial buildings and the Bullitt Center [8]. In addition to providing sustainable development benefits for buildings, reuse of heritage structures allows the preservation of the cultural value of the structures of a city. In the Kathmandu Valley, for instance, The Inn Patan and the Patan Museum are examples of how the heritage of the Kathmandu Valley is maintained when buildings are repurposed for new functions [9, 10]. When compared to their international counterparts, like the Louvre Pyramid in Paris and the Tate Modern in London, buildings in Nepal exhibit a more significant respect for their cultural continuity, though they are developed within a more restrictive economic and institutional framework.

Technical aspects of reuse are another major focus of the literature. The different technical methods for repurposing existing buildings include conversion, facadism, integration, infill, and preservation with modernization. These methods can be observed in the Tate Modern and The Inn Patan, where buildings were fully converted for new functions while maintaining their structures [9, 11]. Similarly, the Patan Museum and the Louvre Pyramid show the integration of historical elements with contemporary ones [10]. Other methods for the reuse of existing buildings include infill, which consists of the preservation of the existing shells of structures while the interior spaces are restructured [12]. This method is discussed in many urban heritage studies. Lastly, preservation with modernization allows for the upgrading of buildings for safety and functionality without altering the exterior features of the structures. This method is often used for the conservation and restoration of historic structures like temples after the 2015 earthquake, and the Reichstag in Berlin [13]. Other strategies such as relocation and reuse, exemplified by Dwarika's Hotel and the Abu Simbel temples, as well as reprogramming in Bhaktapur's courtyards and exaptation in unconventional reuse projects, further highlight the adaptability of the built environment [14].

Policy frameworks and theoretical foundations also shape the discourse on adaptive reuse. International guidelines such as the Venice Charter and UNESCO principles emphasize authenticity, minimal intervention, and respect for historical value [1, 15]. These frameworks are widely referenced in global practice but are less consistently applied in Nepal due to limited policies, insufficient funding, and constraints in technical capacity. Compared with international models that benefit from strong regulatory systems and advanced engineering resources, Kathmandu faces challenges related to rapid urbanization, seismic vulnerability, and fragmented heritage management. Even so, Nepalese projects manage adaptations that are culturally sensitive and grounded in the Valley's own social and historical fabric.

Positive environmental outcomes are often connected with adaptive reuse when heritage buildings are saved from destruction. However, experts claim that the retrofitting process brings many complicated problems because a clash occurs between original historical designs and new functions. Seismic retrofitting and accessibility upgrades must be executed when new services are being added, which changes the historic envelope and original spatial qualities. Experts claim that a similar situation occurs for heritage sites that are converted into commercial ventures for leisure travelers or the service industry, where property holders desire financial gain from the earth rather than showing respect for historical and societal importance. Restoration work that costs a high price is needed for adaptive reuse because heritage sites have very high complexity, and this work also requires laboring individuals with high skills, helpful government regulations, and huge capital. Developing countries find that adaptive reuse is extremely hard to carry out because these countries do not have enough monetary resources and physical components.

It has been observed that adaptive reuse should act as a middle path that balances the safety of heritage sites against contemporary social, functional, and cash-based requirements. A single global strategy for repairing heritage sites is not suitable for this reason. International examples provide many useful lessons and concepts for people to analyze. Local heritage sites and local limitations in a specific urban settlement like Kathmandu require that adaptive reuse is adjusted to meet modern urban demands. The historic value of heritage sites is preserved when this careful adjustment happens, while the requirements of local people are satisfied at the same time.

4. Case Studies

4.1. **Newa Chhen, Patan.** Newa Chhen in Patan is a clear case of adaptive reuse applied to a 17th-century Newar residence. Once used for both living and small business, the building is now a heritage guesthouse. Conservation work centered on the traditional features: carved timber windows, brick masonry, and central courtyards, with modern amenities folded in quietly rather than layered on top. Informal conversations with site staff and visitors during field visits helped build a picture of how the building is used today and what conservation issues still remain. Local artisans restored the timber and brickwork using traditional methods, and steel reinforcements were added for seismic retrofitting to make the structure more resilient [16].

Figure 1. Newa Chhen, Patan – ground floor reception before adaptive reuse

Before its recent transformation and repurposing as the cultural hub Newa Chhen, the ground floor functioned just like any other conventional Newar residence – a space where everyday family life overlapped with business in a seamless transition between house and neighborhood. As the home opened onto the street, it would have housed small retail shops on the front that the family operated or leased to outsiders. These stores would typically sell grain, cloth and daily necessities. Space to the rear was used for storage for various items, such as grains or tools.

Depending on the layout and needs of the family, the ground floor of some residences could also have animal sheds for livestock like cattle and goats in the less exposed side or back areas of the house. Naturally, all these activities led to considerable deterioration and weathering of building materials. Brick walls would crumble due to moisture and animal droppings and timber beams could rot and weaken over time.

Post restoration, the ground floor of the house was redesigned for hospitality, maintaining its original aesthetic. The street-facing portion was converted into a lobby. Though the spaces were designed for a contemporary hospitality function, there is an essence of the old dwelling here – the reconstructed timbers, the stone floor and detailing hint at what lies ahead, and serve as a truthful first impression for the new guests of the country. Next to the lobby, the traditional store and service spaces were converted into a small café, retaining the exposed brick, wooden beams and shape of the traditional windows and adding the comforts of a modern space. Today the café, accessible by residents as well as pedestrians alike, serves the guests of this heritage dwelling as well as anyone strolling down the street, thus keeping the Newars' generous tradition alive in a contemporary space. The kitchens and services were stripped clean and organized to create a functional layout that incorporates modern appliances in an unassuming manner that would complement the traditional setting. A functional storage space was built to assist daily operations and improve the usability of the home.

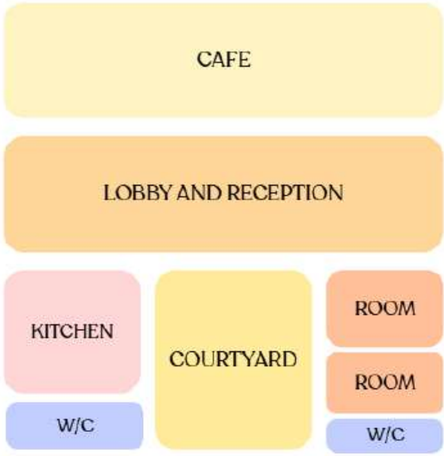

FIGURE 2. Newa Chhen, Patan – ground floor reception and café after adaptive reuse

Altogether, the ground-floor transformation at Newa Chhen shows how an old space can take on new life without losing its cultural identity. What was once given over to trade, storage, and livestock is now a well-organized, welcoming space for guests, one that respects the building's history while working for today's needs.

4.2. **Patan Museum, Lalitpur.** Because the Malla-era palace was neglected for many years through different adaptive uses, the visible decay of the Malla-era palace became very clear. During the following decades, using the structure for government offices and storage rooms and even as a public educational institution, kept the building active but made the decay faster. Monsoon rains leaked through the roof and faded the woodwork, while sloppy repairs on the walls hid the original artistry. Furthermore, temporary partitions also divided the interior spaces, destroying the ceremonial dignity of the original Malla era grandeur.

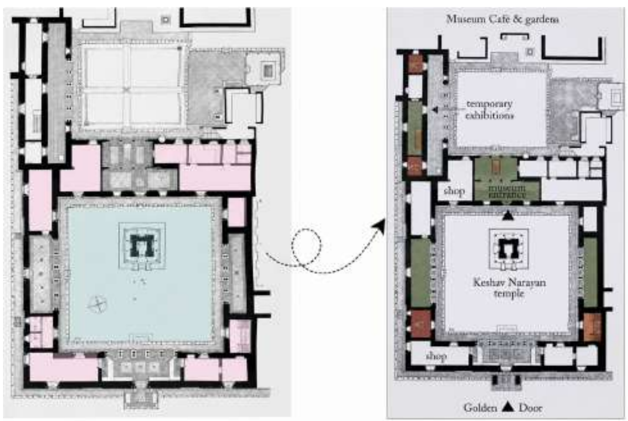

FIGURE 3. Patan Museum, Lalitpur – restored courtyard within the former Malla-era palace

Experts claim that the new use of the palace is an excellent example of restoration because this work changed the goal of the building into a museum, which is a place created to respect the historic architecture while opening doors for the public. High importance was given by the restoration team to keeping the original shape of the courtyards and halls, which highlights the straight alignments that define Malla architecture. Instead of staying closed and forgotten, the palace operates today as an active space where people find art and culture and education.

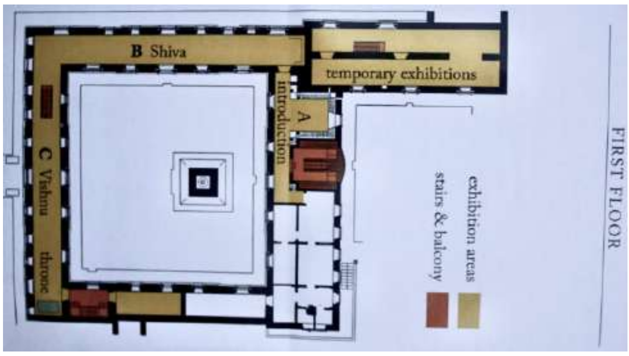

FIGURE 4. Patan Museum, Lalitpur – restored courtyard within the former Malla-era palace [17]

From some informal interviews with the locals, it is believed that the grand halls which hosted royal families in the past are now changed into exhibition galleries, where visitors walk on old wooden floors and look at high ceilings and study detailed carvings very closely. Visitors can see a very large collection of Nepalese sacred art in the museum, which includes metal sculptures and religious items and Paubha paintings and traditional building parts, so that people can connect with ancient craftsmanship in a real way. The project gave new life to the historic Mul Chowk and Sundari Chowk, so that these places are not just quiet courtyards but active spaces where guests can feel the pattern of Malla-period style. Restorers integrated modern services including a café and bookstore and library and explanation room with the old structure, because these spaces were planned to fit perfectly with the original design of the palace.
Through this reuse, a once-neglected palace has become a genuine cultural landmark, drawing people from across backgrounds to explore Nepal's artistic heritage while keeping something of the royal era alive. This project serves as an example of restoration turning history into something shared, preserving the past while giving it new meaning in the present.

4.3. **Kaiser Library, Kantipath.** The Kaiser Library, which is located within the neoclassical Kaiser Mahal, is a prime example of how a Rana-era palace can be repurposed for a new function. By transforming this palace into the Kaiser Library, it has a new purpose without sacrificing the historical significance of the building. The Kaiser Mahal palace was originally built in the early 20th century for Field Marshal Kaiser Shamsher Rana, who was a member of the Rana dynasty. The palace is characteristic of the neoclassical style of the Rana dynasty, with a grand facade, symmetrical design, and high ceilings that are typical of the Rana palaces. Over the years, as the social and political conditions of the country changed, it was determined that the palace would be repurposed for a public function. The palace was accordingly transformed into a public library and museum, one of the few remaining examples of adaptive reuse in Nepal [18].

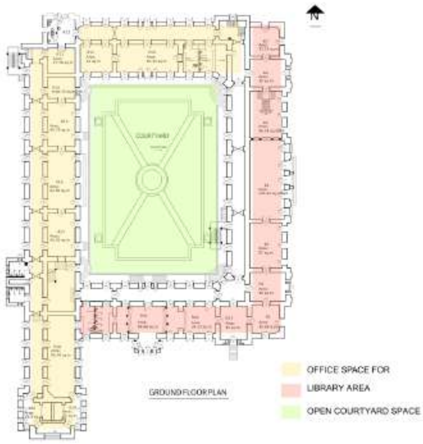

FIGURE 5. Kaiser Library, Kantipath – interior reading hall within the former Kaiser Mahal

The main halls and reception rooms within the palace were changed into reading and archival spaces. Most of the high ceilings and ornate decorative elements of the palace were kept in place so that the visitors could experience the grandeur of the Rana dynasty. Other alterations to the interior of the palace were made for functionality, such as the installation of shelving, furniture, and lighting.

There were some structural reinforcements to the building over time. After the 2015 earthquake, the engineers and conservation experts who assessed the damage to the palace recommended that retrofitting work be undertaken to strengthen the structure without impacting its heritage value. Furthermore, temporary relocation of the library's functions within the palace was also planned while the main structure was restored.

As a result of this adaptive reuse project, Kaiser Mahal has been transformed from a symbol of an aristocratic dynasty into a public space dedicated to learning and the preservation of its history.

5. Findings and Discussion

This study of adaptive reuse in Kathmandu Valley illustrates, we can adapt heritage structures for modern-day use without losing their historical and architectural significance. The cases of Newa Chhen, Patan Museum, and Kaiser Library have proven that the process of successful adaptation is based on respecting the layout, materials and construction of the heritage buildings.

In the case of Newa Chhen, we can see the example of a traditional Newar residential and commercial structure that was converted into a heritage guest house with reception areas and café. During this process, the layout, wood carving and decoration of the building have been preserved. Such approach made it possible to adapt the structure to meet the needs of modern society while preserving its Newar architectural style.

With regards to Patan Museum, we can see it as a transformation of a Malla-era palace into a vibrant exhibition center of Nepalese sacred art and artifacts. During this process, the restorers preserved the palace's courtyard, halls and intricate decorations while also adding modern amenities like a café, bookstore, and an information center. This project not only serves as an example of how space can be used for cultural education, but it is also a great example of adaptive reuse and how it can increase public interest in historic buildings.

The Kaiser Library project demonstrates the adaptive reuse of a palace from the Rana era into a library and archival museum. In addition to preserving all its high ceilings, rich interior, and well-organized spaces, the project introduced new facilities such as reading rooms, archive rooms, and security systems. These changes made the building suitable for modern usage without compromising its historical and architectural value.

TABLE 1. Key findings from adaptive reuse projects in Kathmandu Valley

Case Study	Original Use	New Use	Conservation Strategy	Intervention Type	Outcome
Newa Chhen, Patan	17th-century Newar residential and commercial house with mixed functions (shops, storage, animal spaces)	Heritage guesthouse with reception, café, kitchen, and service zones	Preservation of traditional timber windows, brick masonry, courtyards, use of traditional craftsmanship	Structural retrofitting with steel reinforcements; interior reorganization; restoration of timber and brickwork	Revitalized Newar architecture; enhanced seismic resilience; culturally authentic hospitality space
Patan Museum, Lalitpur	The Malla-era royal palace was later used as government offices, storage, and a school	Museum of Nepalese art with visitor facilities (café, bookstore, library, interpretation center)	Minimal intervention, authenticity, reversible changes; preservation of courtyards, halls, and ornamentation	Spatial restoration; structural repairs; integration of new services; removal of inappropriate partitions	Transformed the palace into a major cultural institution; improved public engagement; preserved Malla-period spatial character
Kaiser Library, Kantipath	Early 20th-century Rana-era private residence with personal archive	Public library and archival museum	Preservation of neoclassical interiors, decorative elements, and high ceilings; careful restoration after the earthquake	Functional upgrades (furniture, shelving, lighting); structural strengthening; planned retrofitting after 2015	Continued use as a cultural and educational hub; strengthened heritage value; adaptive reuse maintained palace identity

Comparison of the three cases demonstrates that adaptive reuse strategies vary according to historical context, building scale, and intended function. Smaller projects such as Newa Chhen rely heavily on private investment and tourism, whereas institutional projects such as Patan Museum benefit from international collaboration. Kaiser Library illustrates how adaptive reuse can sustain public functions but also highlights the importance of long-term maintenance planning after natural disasters.

Collectively, these case studies underscore the potential of adaptive reuse as a sustainable and culturally sensitive strategy for heritage conservation in Kathmandu Valley. They demonstrate that historic buildings can be thoughtfully transformed to meet modern needs while retaining their architectural and cultural significance. By addressing challenges such as structural vulnerabilities, seismic risks, and functional upgrades, these projects illustrate the importance of combining technical expertise, policy support, and community involvement. Overall, adaptive reuse emerges as a viable approach to balancing preservation with innovation, fostering cultural continuity, and activating heritage spaces for public engagement in a rapidly evolving urban context.

6. Conclusion and Recommendations

6.1. **Conclusion.** Adaptive reuse can preserve historic buildings in Nepal as a culturally aware sustainable method. Newa Chhen, Patan Museum, and Kaiser Library are examples of successful integration of heritage and contemporary use. This research focuses on these examples to answer the question of what culturally sensitive solutions exist to bridge the needs of the present with the conservation of the past. This study provides a flexible system to address the architecture framework, community, and economy. The accelerated urbanization of Nepal presents challenges to the preservation of the past that this study discusses. The practice of adaptive reuse, while preserving the past, enhances the economy and culture while decreasing the effects on the environment. Adaptive reuse tells the story of cultural development in the three examples, while simultaneously expressing the challenges experienced therein. Among the challenges expressed are the preservation of cultural authenticity in modern construction, the continual provision of financial support, and the active participation of the community. Given the above, adaptive reuse must be defined as a highly negotiable practice framework, rather than a general practice of conservation.

6.2. **Recommendations for Future Work. Enhancing national policy frameworks.** Drawing from the experience at the Kaiser Library and the Patan Museum, it seems that the current regulations concerning preservation may not offer a desirable congruity and do not provide sufficient positive reinforcement towards the reuse that stems from preservation. There remains a perceived need to develop a set of national regulations that embrace preservation toward reuse, particularly in the protected heritage area.

Enhancing financial support mechanisms. These projects, like the one in the Newa Chhen, were largely dependent on private investment, which again emphasizes the lack of proper financial support systems for the preservation of heritage sites. We think that special funds, grants, or public-private collaborations can greatly help in overcoming the cost factor for projects like this.

Increasing educational and skill-building outreach. Let us examine the example of the skills of artisans and professionals at the Newa Chhen and the Patan Museum. This example helps to establish the importance of local knowledge in the success of adaptive reuse. What is being proposed is that adaptive reuse can be included in architectural curricula.

Creating replication and documentation models. Well-documented cases, like Patan Museum and Newa Chhen, not only serve as important learning experiences, particularly regarding heritage reconstruction and community-led projects, but can be repurposed as models by recording decisions around design, implementation, and project management.

Inclusive urban development. Simultaneously, as urbanization gathers pace in the peri-urban zones surrounding Kathmandu, there is a great threat to vernacular architecture. Enormous potential is available that could be harnessed to extend the adaptation approach not only to the heritage sites, but also to these transitional areas.

Acknowledgement

I express my sincere gratitude to my mentors for their guidance and support throughout this study. I am also thankful to the Department of Archaeology and all other supportive organizations for providing the required materials and their helpful insights.

References

[1] F. H. Arfa, H. Zijlstra, B. Lubelli, and W. Quist, "Adaptive reuse of heritage buildings: From a literature review to a model of practice," *Historic Environment: Policy & Practice*, vol. 13, no. 2, pp. 148–170, apr 2022.

[2] ICOMOS, "Heritage at risk: ICOMOS report on the 2015 Nepal earthquake," 2015, accessed: Oct. 10, 2025. [Online]. Available: https://www.icomos.org

[3] "Adaptive reuse as a strategy towards conservation of cultural heritage: A literature review," 2011, accessed: Jun. 10, 2025. [Online]. Available: https://www.witpress.com/elibrary/wit-transactions-on-the-built-environment/118/22728

[4] P. A. Bullen and P. E. D. Love, "Adaptive reuse of heritage buildings," *Structural Survey*, vol. 29, no. 5, pp. 411–421, nov 2011.

[5] "Architectural conservation: Principles and practice," Wiley.com, accessed: Oct. 10, 2025. [Online]. Available: https://www.wiley.com/en-us/Architectural+Conservation%3A+Principles+and+Practice-p-9780632040254

[6] F. Vafaie, H. Remøy, and V. Gruis, "Adaptive reuse of heritage buildings; a systematic literature review of success factors," *Habitat International*, vol. 142, p. 102926, dec 2023.

[7] B. Plevoets and K. Van Cleempoel, "Adaptive reuse as a strategy towards conservation of cultural heritage: a literature review," ResearchGate, accessed: Oct. 16, 2025. [Online]. Available: https://www.researchgate.net/publication/263124844_Adaptive_Reuse_as_a_Strategy_towards_Conservation_of_Cultural_Heritage_a_Literature_Review

[8] "Miller hull — bullitt center," accessed: Oct. 10, 2025. [Online]. Available: https://millerhull.com/project/bullitt-center/

[9] "Mapping the Kathmandu Valley with aerial photographs by Erwin Schneider," ResearchGate, accessed: Oct. 16, 2025. [Online]. Available: https://www.researchgate.net/publication/288918016_Mapping_the_Kathmandu_Valley_With_Aerial_Photographs_by_Erwin_Schneider

[10] UNESCO World Heritage Centre, "UNESCO World Heritage Centre – state of conservation (SOC 2019) Kathmandu Valley (Nepal)," accessed: Oct. 16, 2025. [Online]. Available: https://whc.unesco.org/en/soc/3953/

[11] D. Sudjic, *The Language of Cities*. UK: Allen Lane, an imprint of Penguin Books, 2016, accessed: Oct. 16, 2025. [Online]. Available: http://archive.org/details/languageofcities0000sudj

[12] "Foster + Partners designs mixed-use masterplan for industrial site in Chile," ArchDaily, accessed: Jul. 15, 2026. [Online]. Available: https://www.archdaily.com/968318/foster-plus-partners-designs-mixed-use-masterplan-for-industrial-site-in-chile

[13] "Urban heritage conservation in Kathmandu valley: Community role on conservation and usage," ResearchGate, accessed: Oct. 10, 2025. [Online]. Available: https://www.researchgate.net/publication/374232034_Urban_heritage_conservation_in_Kathmandu_valley_Community_role_on_conservation_and_usage

[14] "Adaptive reuse of heritage buildings: Sustaining an icon or eyesore," ResearchGate, accessed: Oct. 10, 2025. [Online]. Available: https://www.researchgate.net/publication/289542719_Adaptive_reuse_of_heritage_buildings_Sustaining_an_icon_or_eyesore

[15] B. Plevoets and K. Van Cleempoel, "Adaptive reuse as a strategy towards conservation of cultural heritage: a literature review," in *Proceedings of STREMAH 2011*, Chianciano Terme, Tuscany, Italy, sep 2011, pp. 155–164.

[16] S. R. Tiwari, *The Brick and the Bull: An Account of Handigaun, the Ancient Capital of Nepal*. Himal Books, 2002.

[17] S. Baniya. Patan museum (Architecture). [Online]. Available: https://shirshakbaniya.wordpress.com/2013/09/02/patan-museum/

[18] "The crumbling legacy of Kaiser library," accessed: Oct. 10, 2025. [Online]. Available: https://myrepublica.nagariknetwork.com/news/the-crumbling-legacy-of-kaiser-library